Inauguraldissertation

zur Erlangung der Doktorwürde
der
Fakultät für Physik
der Universität Bielefeld

vorgelegt von
Diplom-Physiker Marc Löllmann
aus Zell/Mosel

Tag der mündlichen Prüfung: 24.06.2010

Conformational Dynamics of Polypeptides and the Folding of Miniproteins studied by Fluorescence Spectroscopy

Gutachter:

Prof. Dr. Markus Sauer

Prof. Dr. Andreas Hütten

Abstract

Protein folding describes the process in which an unstructured amino acid chain folds into a three dimensional protein structure depending on the amino acid sequence. The transition from the amino acid chain to the folded protein is not fully understood yet because many circumstances besides the chain sequence influence this transition.

Fluorescence correlation spectroscopy was used to investigate the conformational dynamics of different model systems from highly flexible polypeptides to those that exhibit secondary structure elements like protein turns. We looked at the temperature and viscosity dependence of the end-to-end contact formation. It was found that glutamine rich peptides show a significant internal friction and activation enthalpy. Furthermore it showed that the local flexibility of protein turns is very dependent on the amino acid sequence.

A further part was to look on the influence of the salt bridge on the folding of the tryptophan cage miniprotein. The observation was that the salt bridge is essential for the high stability of the tryptophan cage.

The last part concentrates on the question how organic osmolytes influence the loop closure of peptides and the folding of the tryptophan cage. Our results show that intrinsically unstructured peptides are not influenced by osmolytes but glutaminerich peptides and the tryptophan cage are. We were able to show that a high concentration of a stabilizing osmolyte is able to compensate the loss of the salt bridge in the tryptophan cage.

Einführung

Proteinfaltung beschreibt den Prozess in dem eine unstrukturierte Aminosäurekette in eine dreidimensionale Proteinstruktur faltet und zwar in Abhängigkeit von der Aminosäurensequenz. Der Übergang von der Aminosäurekette zum gefalteten Protein ist noch nicht vollständig verstanden da viele weitere Einflüsse neben der Aminosäurensequenz die Faltung beeinflussen.
Fluoreszenz Korrelations Spektroskopie wurde benutzt um die Konformationsdynamik von verschiedenen Modellsystemen wie sehr flexible Polypeptide bis hin zu Proteinturns die eine Sekundärstruktur zeigen zu untersuchen. Die Abhängigkeit der End-zu-End Kontaktformation der Peptide von der Temperatur und der Viskosität wurde betrachtet. Wir fanden, dass glutamindominierte Peptide eine hohe Interne Reibung und Aktivierungsenthalpie zeigen. Desweiteren zeigte sich, dass die lokale Flexibilität von Proteinturns stark von der Aminosäuresequenz abhängig ist.
Ein weiterer Teil der Arbeit beschäftigte sich mit dem Einfluss der Salzbrücke auf die Faltung des Tryptophan Cage Miniproteins. Wir konnten beobachten, dass die Salzbrücke ein essentieller Teil für die hohe Stabilität des Tryptophan Cage darstellt.
Der letzte Teil der Arbeit konzentrierte sich auf die Fragestellung wie organische Osmolyte die End-zu-End Kontaktformation von Peptiden und die Faltung des Tryptophan Cage beeinflussen. Unsere Ergebnisse zeigen, dass intrinsisch unstrukturierte Peptide nicht von Osmolyten beeinflusst werden, dass jedoch glutamindominierte Peptide und der Tryptophan Cage beeinflusst werden. Wir konnten zeigen, dass eine hohe Konzentration von stabilisierenden Osmolyten in der Lage sind den Verlust der Salzbrücke im Tryptophan Cage zu kompensieren.

Contents

Chapter 1

Introduction

The first steps of protein folding are the loop closure of parts of the polypeptide chain in order to enable side groups to interact. It could be a rate limiting step which depends on the amino acid sequence and length. Loop closure kinetics occur in a time range from several nanoseconds to microseconds depending on the loop size and sequence [Buc05]. Via the loop closure the polypeptide chain is able to explore the conformational space and eventually find the native state of the protein. So a slow loop formation hinders the folding of the protein to the native state in the first steps. Therefore it is essential to understand the effects that determine the speed of the loop closure. Intrinsically unstructured fully flexible peptides of Glycine-serine repeats are understood very well and serve as model peptides for the investigation of the fastest loop closure dynamics [KFB$^+$03] [NLDS07] [Hud01] [LEH00]. It is known, that Glycine-serine peptides behave as is predicted by polymer theory. The scaling law was measured with various methods and follows power law dependence for a length of approximately 10 amino acids or more [Buc05].

The reason that the spontaneous unfolded $\Leftrightarrow$ native state transition occurs is the Gibbs free energy. Therefore protein folding is driven by thermodynamics and has to be examined in this regard. The Gibbs free energy ΔG is divided into two parts, the enthalpic ΔH and entropic parts ΔS with $\Delta G = \Delta H - T\Delta S$ where T denotes the temperature of the system. This can give insights to the nature of the loop closure and protein folding kinetics and if these can occur spontaneously [vH84]. In this regard there are two major factors that influence

the protein folding kinetics. These are on one side the backbone to solvent interaction and on the other side the intramolecular side chain interactions which are often the cause for the hydrophobic effect. It is assumed that the hydrophobic effect is responsible for the folding of proteins into the native state [RFBM06]. Additionally the Arrhenius activation energy gives insights on the energy barrier that the amino acid chain has to cross in order to establish the loop or secondary structure elements that are the building blocks of the native state of the protein [Arr89]. Both the Gibbs free energy and the Arrhenius activation energy define the energy landscape of every step in the folding pathway. So every folding step has to be investigated if one wants to draw an accurate picture of the energy landscape of the folding pathway.

The method that was used to investigate the topics mentioned above was for the most part fluorescence correlation spectroscopy (FCS) [MEW74] [KB02] in conjunction with photoinduced electron transfer (PET) between the oxazine dye MR121 and the amino acid tryptophan [MEW74] [KB02] [Lak06].
In FCS, as well as in fluorescence spectroscopy in general, fluorescent dyes are used as probes. They are excitable by light. Here we use lasers that emit in the optical range for this purpose. After excitation the dye usually emits a photon to go back to the ground state which is called fluorescence. From there it could be excited again until it diffuses out of the focus or gets destroyed. The advantage of this method is that the time resolution is high because it is only limited by the fluorescence lifetime of the dye. It is mostly in the range of a few nanoseconds. Furthermore besides of attaching the dye to the sample of interest fluorescence spectroscopy is a noninvasive technique. Because dyes are usually small in comparison to samples like proteins they do not influence the dynamics of the sample. To use a dye in this manner it has to offer some specific properties. It should be very photostable which means, that it is not easily destroyed by absorbing light and can go through the excitation-emission cycle often. Additionally the quantum yield QY has to be reasonably high. The QY is the ratio between emitted photons versus absorbed photons. Modern dyes have QY that are in a range of about 60 % to 90 %. But the emission of light is not the only possibility to relax to the ground state again. It can cross from the singlet state into the

triplet state. This transition is forbidden by the selection rules of transitions in a molecule because the spin of the electron performing the transition has to switch signs. Therefore the probability for this transition is low and the lifetime of the triplet state is high and in the region of microseconds to even seconds or minutes. If the dye then relaxes to the ground state again by emitting a photon this is called phosphorescence. The dye is not excitable in the triplet state anymore and so is essentially useless for fluorescence spectroscopy like FCS in the time it stays in the triplet state. So dyes with a low triplet probability are beneficial for FCS. Additionally the triplet transition is dependent on the excitation power and so most of the time FCS measurements are performed with relatively low excitation powers. Another option to relax to the ground state opens up for the dye if it is in contact with a quencher molecule like tryptophan. If one of the molecules can act as an electron donor and the other one as an electron acceptor then an electron transfer can occur. At first the electron of the dye is excited and shifted to a higher energetic state. Then one electron of the tryptophan ground state may occupy the now free ground state of the dye. This is possible because the tryptophan ground state is energetically higher than the dye ground state. The excited electron of the dye relaxes to the ground state of the tryptophan. In this way the excitation energy is dissipated without the emission of a photon and so the fluorescence is effectively quenched. Because this electron transfer is initialized by the absorption of a photon this process is called photoinduced electron transfer (PET) [Neu02] [Lak06].

Lasers are a powerful light source because they can excite dyes specifically at a given wavelength and at high intensities. Furthermore the detection system has to be sensitive. Usually so called avalanche photodiodes (APDs) are used optimized for sensitivity setups. If one then combines these qualities with the confocal principle one is able to detect even single dye molecules in the detection volume. This principle uses a pinhole to limit the detection volume to a small space, usually in the order of one femtoliter. Single molecule spectroscopy (SMS) is a powerful tool to investigate subpopulations of a given sample that would be averaged out in the ensemble level [Wei99]. Furthermore one is able to sort out subpopulations that are of interest and could then look at specific properties of this subpopulation. This obviously would not be feasible on the ensemble level

without some means for sorting the molecules. Additionally one is able to look at one molecule and monitor it over a specific period of time by adding immobilization techniques [Ha01] [KLL$^+$04].

FCS was first introduced in 1974 by Magde and coworkers. It takes advantage of the fact that fluctuations cause a correlation signal that separates the signal from the background. Each process that causes a periodic fluctuation in the fluorescence of the dye shows up in the correlation function as a periodic signal. If the fluctuation belongs to a statistical two state transition the signal will be an exponential decay. If the time constants of this decay are different enough they can be characterized via FCS. Examples are the free diffusion through the detection volume and the triplet rate of the dye that can be easily distinguished via FCS. The technique was not widely used at the early stages. It had a renaissance when better detectors, dyes and excitation light sources were introduced and the confocal principal applied. This was done by Rigler et al [RK93] and published in 1993. This enabled the scientists to use FCS on the ensemble level which opened up many new options for investigations. Today FCS is a standard technique in many laboratories and can even be purchased as a commercial instrument. If one wants to investigate loop closure dynamics of short peptides a time resolution of less than 10 nanoseconds is needed. The limiting factors are the dead time of the detectors and the time resolution of the photon counting device. The first issue can be addressed by using two detectors and cross-correlating them. The second issue was addressed by installing a fast photon counting device into the measurement setup (the DPC230 correlator from Becker & Hickl). The time resolution with these improvements was then 165 picoseconds. This is enough to measure the antibunching characteristic of a dye that lies in the time range of its lifetime, so usually around two nanoseconds. Antibunching is the phenomenon that a dye can never emit two photons at the same time. So there is always a specific time that the dye needs to emit a second photon. And the fastest possibility to do so is the fluorescence lifetime which denotes the time a dye needs to go through the excitation emission cycle. With this fast measurement setup we were able to measure loop closure dynamics in the time range of less than ten nanoseconds with a much greater accuracy.

Anfisen et al showed in 1961 that only the sequence of the amino acid chains determines the native state of the protein [HA61]. If one would exactly know the energy landscape of a given amino acid sequence one would be able to predict the process of folding into the native structure of the resulting protein. This is the goal of the research in the field of protein folding. Knowledge of this coverage would enable scientists and physicians to directly design pharmaceuticals with specific functions or to cure diseases that are caused by misfolding or building of amyloid-like fibrils (see below).

Glutaminerich peptides are of special interest because it is known that glutamine repeats in proteins can be responsible for causing aggregation into amyloid-like fibrils. This can cause neurodegenerative diseases like Huntingtons [SSS$^+$99]. The glutamine repeats are assumed to be stiff and thus slow down the protein folding procedure considerably. Large strands can cause the aggregation of the protein into the amyloid-like fibrils by forming intermolecular h-bonds similar to β sheets. These then can build deposits which may be the cause for the diseases. Another cause for diseases can be the misfolding of proteins. The protein then does not fold into the native state but rather in a state that is metastable but not necessarily the minimum of the energy funnel, where the fully functional native state would end up. The function of the protein is then hindered or even vanished in the misfolded state. One example of this are the so called prion-diseases that are solemnly caused by the misfolding of a prion protein. Famous diseases of this class are bovine spongiform encephalopathy (BSE) or the Creutzfeld-Jacop Disease but there are many more [CNJ05].

One further interesting part of a protein is the so called β-turn. These are short amino acid sequences (usually 4 to 6 long) that are the essential bond in β-sheet secondary structures. They enable the backbone chain to turn and kink so that the mostly globular structure of a protein may fold. It is possible, that some β-turn structures act as a folding promoter by inducing the kink or turn into the backbone chain by themselves. In this work we investigated the thermodynamic values of a specific β-turn sequence via van´t Hoff analysis and determined the Arrhenius Activation Enthalpy. Furthermore a considerable internal friction contribution was found.

But not only the loop size and the amino acid chain sequence have an influence

on the folding dynamic of a protein. So called organic osmolytes can have a great influence on the thermodynamic values that are involved in the process. They can for example lower or rise the Gibbs free energy of the participating states [BR08]. In most cases the organic osmolytes lower or rise the energy of the native state considerably and do not change the initial state that much. So they are able to shift the balance towards the native or the unfolded state. Osmolytes, that favor the unfolded state are called denaturants whereas osmolytes, that favor the native state are called protecting osmolytes. Osmolytes are known throughout nature because they are further able to influence the size of the cell for example and are helpful in stress response. Nice examples are sharks. They have a big amount of urea in their cells, which is a strong denaturant. To enable protein folding despite the high urea concentration they also have a large amount of trimethylamine-N-oxide (TMAO) in their cells which is a protecting osmolyte. Obviously TMAO is able to fully counter the effects of urea which is impressively shown in White Sharks for example.

Organic osmolytes influence the protein folding by changing the solvent quality. This principle is known from polymer dynamics. Water is a rather poor solvent for most peptide chains. Therefore the peptide chain tries to reduce the peptide solvent interaction which is called the hydrophobic effect. Because of this a native state of a protein is favored over the unfolded state because the mostly globular structure reduces protein solvent interactions. Denaturants like urea shift the solvent quality to a good solvent for peptides. This then leads to a weakening of the hydrophobic effect and a shift to the unfolded state. TMAO on the other hand reduces the solvent quality and so leads to favoring the native state of the protein. Responsible for this is the solvent backbone interaction, or, in more detail, the h bonding network of the backbone with the solvent [RFBM06].

This work is a contribution to the subjects that are presented above. We investigated the energy landscape of the loop closure dynamic of glutamine rich peptides. We found that they are not fully flexible like Glycine-serine peptides. They have a significant internal friction contribution to the loop closure formation. This means, that not only the peptide solvent interaction limits the speed of the loop closure. Intrachain interactions also hinder the loop closure and pose an additional resistance to the formation of the loop which slows down the rate with

which this happens and is indicated by a high Arrhenius Activation Enthalpy. Another point was to look at the temperature dependence of the dynamics. The outcome was that they behave like similar Glycine-Serine peptides. Overall this means that the glutamine side groups have a great influence on the thermodynamic potentials of the loop closure dynamics of these peptides. Furthermore it was found that TMAO significantly speeds up the loop closure of glutamine rich peptides whereas it has no effect on Glycine-serine peptides. This indicates that loops of glutamine rich peptides might have some sort of secondary structure. If this assumption holds, than guanidine hydrochloride, which is a strong denaturant like urea, should influence the glutamine rich peptides. But this effect was not found in our data and the glutamine rich peptides behaved like the Glycine-serine peptides in regards to guanidine hydrochloride.

One further part of this work concentrated on the investigation of the folding of the so called Tryptophan Cage (TC). It is a miniprotein that consists of a sequence of 20 amino acids that exhibit secondary structure. It has a C-terminal α-helix followed by a 3_{10}-type helix and at the N-terminal part a polyproline II helix. It is one of the fastest folding proteins with a folding time in the microsecond range. The name is derived from the fact that the side chain of the tryptophan residue is embedded in the hydrophobic core in the middle of the native structure and so is shielded against the solvent. It was engineered by Neidigh et al in 2002 who wanted to make a fast folding, stable model protein [NFA02]. Because of the intrinsic tryptophan residue it is suitable for photoinduced electron transfer techniques (see below). Extensive studies have been done on it and it was found that it folds via an intermediate state [DNS05]. Furthermore computer simulations were done that tried to predict the role of the salt bridge that is located between the residues nine and sixteen. Three partly contradicting predictions were made that ranged from a speeding up due to the salt bridge over no influence at all to a rate limiting step caused by the salt bridge [Zho03] [PNG07] [JB06]. In this work we addressed this topic by investigating a TC mutant that substitutes the arginine residue at position 16 with a glutamine residue. This effectively removes the salt bridge as does a measurement of the original TC at a pH of 3. Our results show clearly that the removal of the salt bridge decreases the stability of the TC considerably. Furthermore measurements were done of the TC and its

mutant in different concentrations of TMAO. As mentioned above TMAO is able to stabilize proteins and speed up their folding procedure. With our technique we are able to distinguish simple viscosity effects from stabilizing effects of the osmolyte. We found that TMAO significantly increases the stability of the original TC and that TMAO is able to counter the removal of the salt bridge and stabilizing it to the extent of the original TC.

Chapter 2

Theoretical background

2.1 Photophysical properties of organic dyes

In this section the emission and absorption of light in organic dyes and the photophysical properties of this system will be discussed.
If an electron descents from an excited state to the ground state by emitting a photon this process is generally called Luminescence. One can now differentiate two cases of Luminescence and the state from which the electron descents to the ground state is deciding the sort of Luminescence. If the electron is in a so called singlet state before emitting the photon, then the spins of the electrons in the excited and in the ground state are antiparallel. This is called a coupled electron pair. The transition is then spin allowed and happens very fast in a dimension of tens of nanoseconds.[Lak06]
If the electron spins are parallel the excited state is a so called triplet state and the electron pair is not coupled. The transition is spin forbidden and the lifetime of a triplet state is in the order of milliseconds to seconds and so is quite slow. The transition in the first case is called fluorescence and in the second case is called phosphorescence. In the following sections only fluorescence will be discussed.
Fluorescent dyes in general consist of a delocalized π-electron system. Figure (2.1) depicts the oxazine derivative dye MR121 that is used for this work. It has a high photostability and the likelihood of a spin skip is low, so that MR121 populates the triplet state rarely. These properties are beneficial for the methods

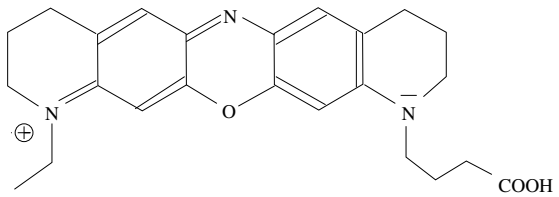

Figure 2.1: This figure shows the structure of the oxazine dye MR121. The delocalized π-electron system is positioned all over the dye. Water solubility is high due to the separated charges.

that are used for this work.

2.1.1 The Jablonski Diagram of organic dyes

To illustrate the processes of absorption and emission of light the so called Jablonski Diagram is used. It has a wide variety of applications and forms and is named after Professor Alexander Jablonski. Figure (2.2) shows a typical Jablonski Diagram that is used to illustrate absorption and emission of light. In this diagram the first three electronic singlet states are called S_0, S_1 and S_2. In every state in the Jablonski Diagram the dye can be in a multitude of vibrational energy levels exemplary depicted with 0, 1 and 2 for the S_0 ground state. The internal conversion is a very fast process (10^{-12} seconds or less) and is the reason that almost all electronic transitions take place from the respective vibrational ground state. Higher vibronical states are not populated because the energy at room temperature is too low to populate them. Absorption and Emission is depicted as vertical lines in the diagram. They take place in approximately 10^{-15} seconds which can be seen as instantaneous regarding the position of the nuclei. This is a basic principal and is called the Franck Condon Principle (see 2.1.2).
Once absorption of light took place the fluorophore has several options to relax to the ground state S_0. The typical lifetime of an excited state S_1 or S_2 is in the nanosecond range. If fluorescence occurs, then the dye relaxes directly from the excited state to the ground state S_0. In the case of intersystem crossing the spin of the excited electron flips and it changes to the first triplet state T_1. From there it can relax back to the ground state S_0. Due to the spin forbidden flip the lifetime of the triplet state is significantly higher than that of the singlet states.

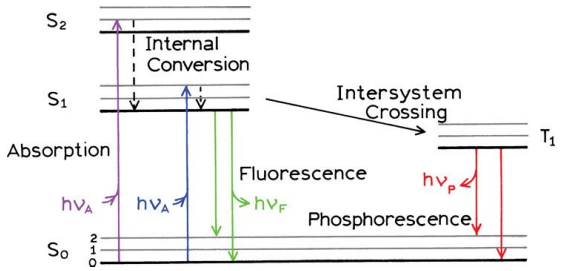

Figure 2.2: A typical Jablonski Diagram for the absorption and emission of light. The colored arrows denote the absorption or emission of light. $h\nu_A$ stands for the absorbed photons and $h\nu_F$ denotes the fluorescence photons. The photons of the phosphorescence are depicted as $h\nu_P$. S_0, S_1 and S_2 are the singlet states of the fluorophore and T_1 is the triplet state. The lighter grey lines are the vibrational levels where the internal conversion reduces the state into the respective ground state on a fast timescale. Intersystem crossing is an alternative way to dissipate the absorbed energy but it is spin forbidden. The electron has to flip its spin in order to populate this state. This makes this path less probable than fluorescence [Lak06].

This process is called phosphorescence and the lifetime of it is in the range of milliseconds to seconds. MR121 has a low intersystem crossing rate which is favorable for the methods used in this work because the dye cannot be excited to a singlet state as long as it is stuck in the triplet state and so does not show fluorescence in this time period.

2.1.2 The Franck Condon principle

The Franck Condon Principle may be reduced into one sentence that includes the main message of it: *The electron transition is much faster than the movement of the molecular nuclei because of their much greater mass.* After the transition the atomic nuclei are affected by a changed force field and have to adapt to it. The new force field is a result of the changed electron configuration after the transition. The adaption of the atomic nuclei to the new force field results in a new equilibrium position that is usually further away of each other than in the ground state. The reason for this is that in the excited state the non-binding

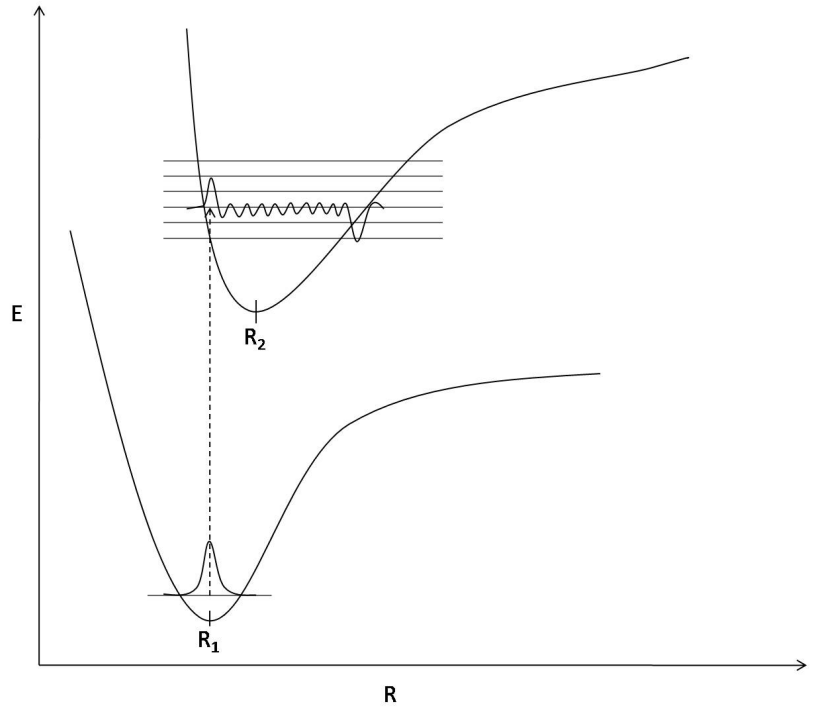

Figure 2.3: A typical transition after the absorption of a photon. The Y-axis denotes the energy of the electron and the X-axis stands for the distance between the atomic nuclei in the molecule. The horizontal lines are the vibrational states that the electron can occupy. In this figure the dashed line represents the transition of the electron after excitation. The vibrational states of the atomic nuclei are depicted too [Atk02].

molecular orbitals are stronger than in the ground state. Figure (2.3) shows a typical transition after the absorption of a photon. The transition is shown as a dashed line and is exactly vertical which is the Franck Condon Principle in essence. Important for the transition are the vibrational states of the distance of the atomic nuclei. They are depicted in figure (2.3) for the vibrational states that are part of the transition. In the ground state the atomic nuclei are in equilibrium and thus the maximum likelihood of the distance is in the middle of the vibrational state. The probability of the transition is the highest into the excited state where the likelihood of the distance for the atomic nuclei is greatest. Adjacent vibronical states are possible too but the probability for a transition into these states is lower. The potential of the excited state is in general

displaced to the right because the non-binding molecular orbitals are occupied. Until now the description of the Franck Condon Principle was a classical one. If one considers quantum mechanics the overlap integral determines the probability for a transition from the ground state to the excited state [Atk02].

2.1.3 Absorption and emission of light and the Stokes Shift

The procedure of fluorescence shows some general characteristics that are common to almost all fluorophores. By looking carefully at the Jablonski Diagram (figure (2.2)) one can observe that the fluorescent light appears to have a lower energy as the absorbed light. The most common cause for this loss of energy is the very rapid decay of the vibrational states after absorption of light in higher excited vibrational states. Furthermore the fluorescent light mostly decays into excited vibrational states of the S_0 ground state which then further relax to the zero ground state. Additionally the fluorophore can exhibit further Stokes Shifts due to solvent effects, excited states reactions or energy transfer. [Lak06]
One further observation concerning fluorescence is that the emission spectrum of the fluorophore is independent of the excitation wavelength. The reason of this is that the energy that is in excess of the energy needed to excite the fluorophore is rapidly dissipated and the fluorescence light is emitted from the lowest vibrational S_1-state.
One further attribute of the absorption and emission of light is that the absorption spectrum and the emission spectrum follow the mirror image rule. Therefore the emission spectrum is an exact mirror image of the absorption spectrum. The reason is that the exactly same states are involved in the transition and that the vibrational states are similar in the S_0 and S_1 states.

2.1.4 Quantum yield and fluorescence lifetime

The fluorescence lifetime and the quantum yield of a fluorophore are two important characteristics of a dye.
In order to derive the quantum yield we take a look at the Jablonski Diagram (figure (2.2)). To simplify we only consider the emissive rate Γ and the nonra-

diative rate k_{nr} without looking at the vibrational levels. The nonradiative rate k_{nr} unifies all mechanisms to depopulate the excited state. The quantum yield Q relates the number of photons that are emitted as fluorescent light to the energy that is dissipated in another way. Since both rates depopulate the excited state the quantum yield is given by:

$$Q = \frac{\Gamma}{\Gamma + k_{nr}} \ . \tag{2.1}$$

[Lak06] The quantum yield can be close to one if the nonradiative rate is small ($k_{nr} \ll \Gamma$). Because of the Stokes Shift the energy yield is always less than one. The fluorescence lifetime τ is the average time the fluorophore remains in the excited state since the emission of light is a random process. In general the lifetime of fluorophores is in the order of nanoseconds. MR121 has a fluorescence lifetime of 1.82 ns [DNS05] . It is given by:

$$\tau = \frac{1}{\Gamma + k_{nr}} \ . \tag{2.2}$$

2.1.5 Photon antibunching

Photon antibunching is a phenomenon that appears if one looks at single photon emitters [TWV$^+$02]. For a single emitter it is impossible to emit a photon directly after one photon has been emitted previously. This means that the minimum time an emitter needs to emit a second photon is the fluorescence lifetime. This is the time the emitter needs to circle trough one cycle of absorption and emission of light. This leads to the effect that the emitted photons are spaced from each other by a characteristic timescale and so do not bunch which leads to the term antibunching.

As it is a statistical process which accounts for a fluctuation in fluorescence it can be monitored by FCS if the time resolution of the measurement system is fast enough (see section 2.2.2) [lM96]. Rigler et al measured the antibunching behavior of Rhodamine 6G in solution with FCS. They saw that it is dependent from the excitation intensity I and the absorption cross section σ of the dye. They derived the following equation to describe the correlation function $G(\tau)$ for the antibunching effect:

$$G(\tau) = 1 + \frac{1}{N}(1 - \exp[-(k_e + k_d) \cdot \tau)]) \ . \tag{2.3}$$

Here N denotes the average number of molecules in the detection volume. The excitation rate k_e and the decay rate of the excited state k_d characterize the antibunching effect of a two state system like the singlet fluorescence of dyes. The first one can be derived from the excitation intensity I and the absorption cross section σ by $k_e = I \cdot \sigma$ [lM96].

2.1.6 Photoinduced electron transfer

The quenching of the emission of light is a procedure that can have several causes [Lak06][Neu02]. Quenching means that the nonradiative rate k_{nr} is greater than the radiative rate Γ ($k_{nr} \gg \Gamma$) and therefore the energy of the absorption of light is dissipated without emitting a photon. Photoinduced electron transfer (PET) is one method for quenching the fluorescence of a dye. PET in general is a concept that is found in many aspects of science and has some striking applications like the photosynthesis of plants or photovoltaic devices. In this work PET is used to effectively quench MR121 upon contact with the amino acid tryptophan.
PET occurs when a complex between an electron donor D and an electron acceptor A is formed. The exited charge transfer complex can then go to the ground state without emitting a photon. Therefore the electron from the Donor D transfers to the acceptor A. Then, one electron from the acceptor ground state transfers to the donor and the acceptor relaxes to the ground state. An excited fluorophore can be either the electron donor or acceptor. The direction of the electron transfer is determined by the redox potentials of the participating states and so the exited species is not always the electron donor. In this case MR121 in the excited state acts as the electron acceptor and the amino acid tryptophan is the electron donor when the MR121/Tryptophan complex is formed.

To decide if PET occurs one has to consider the free energy of the electron transfer ΔG^0_{CS}. The Rhem Weller equation estimates the free energy change for PET and is given by:

$$\Delta G^0_{CS} = E_{ox} - E_{red} - E_{0,0} + \Delta G^0_{coul} \ , \tag{2.4}$$

with

$$\Delta G^0_{coul} = \frac{-e^2}{\epsilon_s d} \ . \tag{2.5}$$

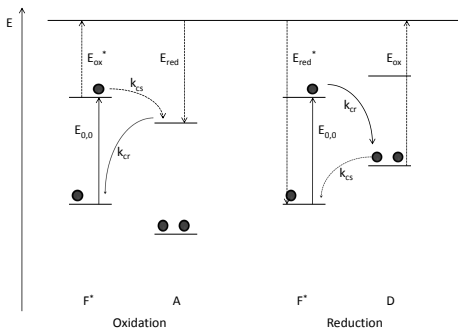

Figure 2.4: Simplified PET diagram between an excited fluorophore F^* and an electron donor D or acceptor A respectively. The charge separation and recombination rates are depicted as k_{cs} and k_{cr}. The oxidation potential and the reduction potential are depicted as E_{ox} and E_{red} respectively. The transition between the S_0 and S_1 is denoted as $E_{0,0}$. The electrons that do the transition are the filled circles.

Here E_{ox} denotes the oxidation and E_{red} the reduction potential of the PET process. $E_{0,0}$ describes the transition energy of the transition between the S_0 and S_1 state in the fluorophore. ΔG^0_{coul} is the Coulomb potential of the charge separated state and gives the attraction of the charges after electron transfer. In this equation e stands for the electron charge and d describes the distance between the charges and ϵ is the dielectric constant of the solvent which shields the charges.

The Rhem-Weller equation is a basic description of the energies involved in the PET process. But it gives a good first estimation of the free energy change. For a more comprehensive analysis of the PET process kinetic and quantum mechanical effects have to be considered too.[Mar93][Was88]

In this work the PET mechanism that occurs between Tryptophan and MR121 is used to induce fluctuations in the fluorescence of the dye that can be monitored by FCS (see (2.2.2)). The characteristic timescales that then show up in FCS measurements are directly connected to the conformational changes of the sample (see (3.3))

2.2 Measurement methods

The topic of this section is the theoretical backgrounds of the measurement methods that were used for this work. The first subsection describes the standard methods of measuring the absorption and emission spectra on the ensemble level. The second subsection describes the principles and theory of fluorescence correlation spectroscopy (FCS).

2.2.1 Fluorescence absorption and emission measurements

For this work standard ensemble methods were used to characterize the samples and measure melting temperatures on the ensemble level.
To get reproducible results the concentration c of each sample has to be determined. The tool for doing so is derived from the Lambert-Beer law:

$$c = \frac{E}{\epsilon \cdot d} \ . \tag{2.6}$$

Here E denotes the extinction of the intensity that is given by $E = \log \frac{I}{I_0}$ with I as the measured intensity and I_0 as the initial intensity. The thickness of the sample is given by d and ϵ donates the molar extinction coefficient.
By using temperature dependent measurements the melting temperature T_m of a protein can be determined if a quenching of the fluorescence intensity I occurs upon folding or unfolding. In this work the following equation was used:

$$I = A_1 - \frac{A_2 - A_1}{1 + 10^{(T_m - T)\,p}} \ , \tag{2.7}$$

with A_1 and A_2 as the bottom and top asymptote respectively. The temperature of the system is given by T and p stands for the slope of the sigmoidal curve.

2.2.2 Fluorescence correlation spectroscopy

Unlike ensemble methods, fluorescence correlation spectroscopy (FCS) is a technique that observes single molecules or small groups thereof. It can be performed in solution and with free diffusing molecules. Because of this the examined molecules can be observed over a great period of time due to new sample molecules diffusing steadily into the measurement area. FCS is based upon the

observation of the fluctuation of the fluorescence intensity of a dye. The origin of these fluctuations can be manifold. All have in common the fluctuation caused by entering and leaving the detection volume. Furthermore photophysical processes or quenching of the dye by quencher molecules can be observed with FCS over a broad range of timescales. All of this makes FCS a powerful tool to study dynamics of biological samples. To make the working of FCS vivid, imagine a fluorescent molecule freely diffusion through the detection area. As soon as it enters the fluorescent molecule begins to emit a photon burst. The length of this burst is then determined by the average time the molecule stays in the detection area. If it is diffusing fast the photon burst will be short and for a bigger, slower moving molecule the photon burst will be longer. In general the fluorescent molecule will not suffer photobleaching because the time it travels in the excitation volume is shorter than the photobleaching time constant. But mostly the fluorescent molecule will undergo a triplet excitation and so be nonfluorescent for short time periods when inside the detection volume. FCS is able to distinguish between the diffusion fluctuations and the triplet fluctuations in the intensity of the fluorescent molecule because of the different timescales of these processes. Fluorescence fluctuations can occur through numerous processes in quite different timescales. As long as these timescales are shorter than the diffusion time of the system of interest FCS is able to detect them. This gives this technique its broad applicability.

FCS was first introduced in the early 1970s by Webb and coworkers[MEW74]. They recognized the power of this technique in observing fluctuations of the fluorescence of dyes. Even under equilibrium conditions the reaction that causes the fluctuation is still proceeding in both directions. But in the early FCS studies the measurements were not free from problems. The signal to noise ratio was unfavorable due to several reasons. The number of molecules was large, the intensity of the laser for the excitation of the molecules varied, the quantum yield of the used dyes was quite low and the detectors were inefficient. Because of all these problems FCS was not widely used for approximately 20 years. In the 1990 the technical advance lead to stable lasers, high quantum yield fluorophores and efficient avalanche photo detectors (APDs). Most of these devices were commercially available and so FCS was now a widely applicable tool for the analysis of

many different tasks.

The mathematical derivation of the autocorrelation function is no trivial task[KB02]. To do this first consider an ideal solution of a fluorescent material. The local concentration is then given by $C(r,t)$. The average concentration $\bar{C} = \langle C(r,t) \rangle$ and the local variance $\delta C(r,t) = C(r,t) - \bar{C}$ are then two important variables for describing a solution. The material at hand is able to diffuse freely through the solution and it is allowed to undergo chemical reactions or other procedures that alter the fluorescent properties. The relaxation of $\delta C(r,t)$ is then given by:

$$\frac{\partial \delta C(r,t)}{\partial t} = D\,\nabla^2 \delta C(r,t) + K\,\delta C(r,t)\ . \tag{2.8}$$

Here D denotes the diffusion constant and K is a coefficient that is given by the reaction rate and the equilibrium constant of the material. The first term of equation (2.8) describes the diffusion of the fluorescent material and the second term describes the changes in the fluorescence properties of the fluorescent material.

A further important property for deriving the correlation function is the light intensity $I(r)$ that is responsible for the excitation of the fluorescent material. It is dependent on the exact light pathway and the measurement setup. Let us here assume that the number of detected photons $n(t)$ is directly dependent on the light intensity $I(r)$. It then follows:

$$n(t) = \Delta t \int d^3r \cdot I(r)\, Q\, C(r,t)\ , \tag{2.9}$$

with Q as the product of the absorption cross-section and the quantum yield of the fluorescent material and therefore reflects the fluorescence properties of it. For deriving the correlation function light fluctuations of the light source such as shot noise are neglected because they are generally uncorrelated and do not distribute to the correlation function.

The variance of the number of photons $\delta n(t)$ of the mean value $\bar{n} = \langle n(t) \rangle$ is given by:

$$\delta n(t) = n(t) - \bar{n} = \Delta t \int d^3r \cdot I(r)\, Q\, \delta C(r,t)\ . \tag{2.10}$$

Now a fluorescence correlation experiment is performed and then the correlation function $G(t)$ is given by averaging over the product of the photon fluctuation

over time. Normalization is then done via the square of the average photon number $\bar{n}^2$:

$$G(t) = \frac{1}{\bar{n}^2\,T}\sum_{i=0}^{T-1}\delta n(t')\,\delta n(t'+t) = \frac{1}{\bar{n}^2\,T}\sum_{i=0}^{T-1}(n_i-\bar{n})(n_{i+m}-\bar{n})\ . \tag{2.11}$$

In this equation T stands for the total number of measurement intervals Δt ($T\cdot\Delta t$ gives the total duration of the experiment) and t is defined via the delay channel m of the correlator with: $m = t/\Delta t$. The number of photons that are detected in the measurement time $t' = i\,\Delta t$ and $t'+t = (i+m)\,\Delta t$ are given by n_i and n_{i+m} respectively.

By using the ergocity of the system it is possible to formulate equation (2.11) as an ensemble average:

$$G(t) = \frac{1}{\bar{n}^2}\,\langle\delta n(0)\,\delta n(t)\rangle\ . \tag{2.12}$$

With equation (2.10) then follows:

$$G(t) = \frac{(\Delta t)^2\cdot Q^2}{\bar{n}^2}\iint d^3r\,d^3r'\,I(r)I(r')\ \langle\delta C(r,0)\,\delta C(r',t)\rangle\ . \tag{2.13}$$

Therefore the correlation function of the intensity fluctuation is a convolution of the auto- or crosscorrelation of the concentration fluctuations and the excitation profile of the experiment.

To solve the integral of equation (2.13) the Fourier transformation $\delta\tilde{C}(q,t)$ of $\delta C(r,t)$ is used and it follows:

$$\frac{\partial\delta\tilde{C}(q,t)}{\partial t} = -D\,q^2\,\delta\tilde{C}(q,t)\ . \tag{2.14}$$

From this differential equation then follows:

$$\delta\tilde{C}(q,t) = \delta\tilde{C}(q,0)\cdot\exp(-D\,q^2\,t)\ . \tag{2.15}$$

Furthermore from the Fourier transformation of $\langle\delta C(r,0)\,\delta C(r',t)\rangle$ follows:

$$\langle\delta C(r,0)\,\delta C(r',t)\rangle = (2\pi)^{-3/2}\int d^3q\cdot e^{iqr'}\left\langle\delta C(r,0)\,\delta\tilde{C}(q,t)\right\rangle\ . \tag{2.16}$$

Together with equation (2.15) holds:

$$\langle\delta C(r,0)\,\delta C(r',t)\rangle = (2\pi)^{-3/2}\int d^3q\cdot e^{iqr'}\cdot e^{-D\,q^2\,t}\left\langle\delta C(r,0)\,\delta\tilde{C}(q,0)\right\rangle\ . \tag{2.17}$$

By using the Fourier transformation back the result is:

$$\begin{aligned}\langle \delta C(r,0)\, \delta C(r',t)\rangle = (2\pi)^{-3} \int d^3q \cdot e^{iqr'} \cdot e^{-D\,q^2\,t} \\ \cdot \int d^3r'' \cdot e^{iqr''} \langle \delta C(r,0)\, \delta C(r'',0)\rangle \ .\end{aligned} \tag{2.18}$$

Two molecules at different positions in the detection volume can be considered uncorrelated because the correlation length is much smaller than the distance of the molecules. With this in mind equation (2.18) simplifies to:

$$\langle \delta C(r,0)\, \delta C(r',t)\rangle = (2\pi)^{-3}\bar{C} \int d^3q \cdot e^{-iq(r-r')} \cdot e^{-D\,q^2\,t} \ . \tag{2.19}$$

Equation (2.19) enables us to simplify equation (2.12) and do the integration. It follows:

$$G(t) = \frac{(\Delta t)^2 \cdot Q^2}{(\bar{n})^2} \int d^3q\, \tilde{I}^2(q)\, \bar{C} \cdot e^{-D\,q^2\,t} \ , \tag{2.20}$$

with $\tilde{I}^2(q) = (2\pi)^{-3/2} \int d^3r \cdot e^{iqr}\, I(r)$ as the Fourier transform of $I(r)$. Then equation (2.9) simplifies to:

$$\bar{n} = (2\pi)^{-3/2} \tilde{I}(0)\, Q\, \bar{C} \ . \tag{2.21}$$

In general FCS measurements are done on confocal setups (see chapter (XX)) and therefore the intensity profile $I(r)$ can be approximated as a 3D Gaussian profile which leads to:

$$I(r) = I_0 \cdot \exp\left(-\frac{2x^2}{\omega_x^2} - \frac{2y^2}{\omega_y^2} - \frac{2z^2}{\omega_z^2}\right) \ . \tag{2.22}$$

In this equation ω_x, ω_y and ω_z denote the maximum width of the profile in the respective direction. The Fourier transform of $I(r)$ then holds as follows:

$$\tilde{I}(q) = \frac{\tilde{I}_0\, \omega_x\, \omega_y\, \omega_z}{8} \cdot \exp\left(-\frac{\omega_x^2\, q_x^2}{8} - \frac{\omega_y^2\, q_y^2}{8} - \frac{\omega_z^2\, q_z^2}{8}\right) \ . \tag{2.23}$$

The correlation function $G(t)$ can be described as follows with the help of equations (2.21) and (2.23):

$$G(t) = \frac{(2\pi)^3}{\bar{C}} \int d^3q \exp\left(-\frac{\omega_x^2\, q_x^2}{4} - \frac{\omega_y^2\, q_y^2}{4} - \frac{\omega_z^2\, q_z^2}{4} - D\,t(q_x^2 + q_y^2 + q_z^2)\right) \ . \tag{2.24}$$

The next step considers the effective detection volume $V = \pi^{3/2}\omega_x\omega_y\omega_z$ and the diffusion time along the corresponding spacial dimensions that is given by $\tau_{D_x} = \frac{\omega_x^2}{4D}$ (and analogous in the y and z direction. Equation (2.24) then derives as follows:

$$G(t) = \frac{1}{\bar{C}\,V}\left(1+\frac{t}{\tau_{D_x}}\right)^{-1/2}\left(1+\frac{t}{\tau_{D_y}}\right)^{-1/2}\left(1+\frac{t}{\tau_{D_z}}\right)^{-1/2} . \tag{2.25}$$

In a confocal setup the dimensions in the z direction are in general much larger than in the x and y direction and because of this the last contribution in equation (2.25) can be neglected. So two dimensional diffusion can be regarded. For the sake of simplicity for the derivation of the correlation function the diffusion becomes further constrained to one dimensional diffusion. It then follows:

$$G(t) = \frac{1}{\bar{N}}\left(1+\frac{t}{\tau_D}\right)^{-1/2} , \tag{2.26}$$

where $\bar{N}$ denotes the average number of particles in the detection volume V for a given average concentration $\bar{C}$.
To end this derivation of the correlation function a few further considerations have to be done. Therefore equation (2.8) will be expanded by looking at photophysical and chemical processes and by assuming a constant flow through the detection volume. Equation (2.8) then looks like this:

$$\frac{\partial\delta C(r,t)}{\partial t} = D\,\nabla^2\,\delta C(r,t) + K\,\delta C(r,t) + \Gamma\,\delta C(r,t) + V\vec{(r)}\,\nabla\,\delta C(r,t) , \tag{2.27}$$

where Γ is the emission rate of the fluorescent material and $V\vec{(r)}$ denotes the flow speed in the solution. By deriving the autocorrelation function $G'(t)$ from equation (2.27) it follows:

$$G'(t) = \frac{1}{\bar{N}}\,G(t)\cdot\exp\left(-G(t)\,\frac{t^2}{\tau_f^2}\right) . \tag{2.28}$$

The characteristic diffusion time for the flow in the detection volume is given by τ_f^2. $G(t)$ is then given by:

$$G(t) = \left(1+\frac{t}{\tau_D}\right)^{1/2}\left(1+K\cdot\exp\left(\frac{-t}{\tau}\right)\right) . \tag{2.29}$$

The parameter K stands for the ratio between fluorescent and nonfluorescent molecules in the detection volume and τ is the relaxation time for the molecule from the fluorescent to the nonfluorescent state. The average diffusion time of the molecule is given by τ_D.
Equations (2.28) and (2.29) are the basic functions for fluorescence correlation spectroscopy measurements and are the tools to derive measurement variables like photophysical properties, diffusion constants or quenching kinetics. For Details on how we fitted the measurement data see section (3.3).

2.3 Thermodynamic Methods

2.3.1 Arrhenius analysis

The Arrhenius equation is now more than 120 years old and still continues to play a major role in analyzing classical studies of kinetics [Men69]. It was first discovered empirically by Hood [Hoo78] and then later van´t Hoff and Arrhenius [vH84][Arr89] showed that it is consistent with the theory of thermodynamic. It enables us to characterize a temperature dependent rate constant $k(T)$ via two empirical parameters, namely the activation energy E_a and a pre-exponential factor A:

$$k(T) = A \cdot \exp\left(\frac{-E_a}{k_B\,T}\right) \ . \tag{2.30}$$

Here T is the temperature of the system and k_B is the Boltzmann constant. The activation energy is usually interpreted as the height of the energy barrier that has to be overcome for a particular reaction (see figure (2.5)). This viewpoint is generally correct but it oversimplifies the matter. The equation examines macroscopic effects and has to be adjusted if one looks at microscopic procedures, for example with energy or velocity dependent cross-sections. One has to distinguish between the probability of a reaction and the activation energy which are generally not the same. The probability of the reaction is given by parameters like the velocity of the molecules (temperature) or the reaction cross section for example. In contrast to that the activation energy is a macroscopic value.

One can combine the Arrhenius equation with the Gibbs energy of activation ΔG_a via:

$$E_a = \Delta G_a = \Delta H_a - T\Delta S_a \ , \tag{2.31}$$

where ΔH_a denotes the activation enthalpy and ΔS_a stands for the activation entropy. Combined with equation (2.30) one obtains:

$$k(T) = A \cdot \exp -\frac{\Delta H_a}{k_B T} \exp \frac{\Delta S_a}{k_B} \ . \tag{2.32}$$

In this work the simple picture of the activation energy is used and the data is shown in the so called Arrhenius plot where the slope of the plot denotes the activation enthalpy ΔH_a if one plots $\ln(k(T))$ versus $1/T$. The y-intercept of the Arrhenius plot includes the activation entropy ΔS_a but one cannot distinguish it from the pre-exponential factor A in general. The following equation specifies this circumstance:

$$E_a = k_B\, T^2 \frac{d\, \ln k(T)}{d\, T} = -k_B \frac{d\, \ln k(T)}{d(1/T)} \ . \tag{2.33}$$

To distinguish the activation energy part that is purely dependent on the solvent viscosity from the activation energy that origins in the system at hand, the reaction rates in this work are being multiplied with the solvent viscosity before taking the logarithm. Therefore we can examine the activation energy independently of the solute that is responsible for the change in solvent viscosity. If one examines a specific reaction in the way shown above one has to keep in mind that the rate under investigation is usually not linearly dependent of the temperature. This only applies in a given temperature range. All measurements done in this work showed sufficient linearity to evaluate the Arrhenius activation energy.

2.3.2 Van´t Hoff analysis

Not only the rate constant is temperature dependent the equilibrium constant K is also temperature dependent[Atk02]. To describe this, the van´t Hoff equation

can be used [vH84]. It is an expression for the slope of a plot of $\ln K$ versus the inverse temperature $1/T$:

$$\frac{d \ln K}{dT} = \frac{\Delta H_r}{R T^2} \ . \tag{2.34}$$

If one combines equation (2.34) with the Gibbs Free Energy $\Delta G_r = \Delta H_r - T \Delta S_r$ one can obtain insight into the thermodynamic process of the reaction at hand. It then can be written in the following form:

$$R T \ln K = -\Delta G_r = \Delta H_r - T \Delta S_r \ . \tag{2.35}$$

In these equations ΔH_r stands for the standard reaction enthalpy and ΔS_r is the standard reaction entropy. If one now has a plot that is essentially linear one can fit it with $lnK = U + m T^{-1}$. Here U stands for the Y-intercept of the van´t Hoff plot and m denotes the slope of the linear graph. By multiplying these values with the universal gas constant one can derive ΔS_r from U and ΔH_r from m. From these values one can then calculate ΔG_r via the equation given above. From a thermodynamic point of view the Gibbs reaction energy denotes the work that is done from the system to the surrounding. It can be a measure for the spontaneity of a reaction. If ΔG_r is negative, the reaction happens spontaneously.

2.4 Circular dichroism

Circular dichroism (CD) is a technique that measures the difference between the absorbance of left-handed and right-handed circularly polarized light. CD measurements are done in the UV region of the light spectrum, usually in the range of 190 nm to 300 nm [Buc05][Can80].

Proteins show two regions where CD can be observed. The first one is the so called amide region, where the amide bonds of the protein absorb the light dichroically. It is located in the far UV range (170 - 250 nm). Aromatic side chains also absorb in this region and contribute to the amide region CD signal.

In the near UV (250 - 300 nm) the aromatic rings of the amino acid sidechains dichroically absorb the light. Disulfide bonds also contribute in this spectral region.

From these different spectral regions it is possible to derive different kinds of

information about the folding structure of a protein. The far UV range reports on the backbone of the protein and can be used to characterize the secondary structure. Particularly the α-Helix secondary structure shows strong, well defined contributions in the CD absorbance in this region. Other secondary structures are less well defined but the content of secondary structure in a protein can be calculated from a CD spectrum in the far UV range.

The near UV range reports on planar aromatic residues. If they are rotating freely like in unfolded domains or in the unfolded state, their contribution to the CD spectrum is zero. But if the protein is in a folded structure the aromatic residues are fixed in the structure of the protein and therefore one is able to check if a protein is properly folded in the native state. The CD spectrum in the near UV is then like a fingerprint for the structure of the respective protein but it cannot be calculated and assigned to specific amino acid sidechains.

There are two possibilities to record CD data. The first one is to measure the difference ΔA in absorbance of left- and right-handed circularly polarized light (A_l,A_r respectively) via $\Delta A = A_l - A_r$. The second possibility is to use the ellipticity Θ_{obs} in degrees. The last one is a historical value. The ellipticity is defined as: $\tan\Theta = \frac{E_r - E_l}{E_r + E_l}$ where E stands for the magnitude of the electric field vector of the right- and left-circularly polarized light respectively.

With the differential molar circular extinction coefficient $\Delta\epsilon = \epsilon_l - \epsilon_r$ and the molar ellipticity $[\Theta]$ both possibilities to measure the CD data can be converted to molar values via $[\Theta] = 3300 \cdot \Delta\epsilon$. One has to pay attention to the units of the concentration standards $[\Theta]$ and $\Delta\epsilon$. These possibilities of recording the CD data are just historical conventions and are different means to express the same data.

In this work CD measurements were used to study the melting temperature of Tryptophan Cage and its mutant without a dye label by looking at the appearance of the α-helix for the respective temperatures (see figure (2.7) for Tryptophan Cage structure). This was done to compare this data to the data with a dye label to see if the dye influences the Tryptophan Cage folding.

2.5 Theory of polymer dynamics

This section discusses the theory of polymer dynamics. In this work, the end to end contact formation dynamic is in the focus of interest. Extensive work has been done on unstructured, fully flexible peptides with Glycine-serine repeats. The length dependence has been studied and it could be shown that they behave like a Gaussian chain with the so called extended volume effect. To achieve end to end contact, the polymer chain has to undergo conformational changes that are hindered by sterical repulsion of the chain itself and the solvent viscosity. Furthermore the dependence of the amino acid sequence can be investigated to see if side chains influence the end to end contact dynamic. For example glutamine rich peptides or protein turns are interesting sequences in this regard. The following subsections discuss the different models of polymer dynamics [Buc05].

2.5.1 The freely jointed chain

An ideal polymer can be described as a three-dimensional random walk. It consists of n segments of the length l with uniformly distributed angles at every joint. The chain is then fully described with the $n+1$ position vectors $\vec{R}_i$ of the chain segments. Alternatively, the chain could also be described by the n vectors $\vec{r_i}$ of the chain segments. As the vectors are independent of each other, the expected value $\langle \vec{r_n} \cdot \vec{r_m} \rangle = 0$. The expected value $\langle r^2 \rangle$ of the end to end distance of the chain is then given by:

$$\left\langle r^2 \right\rangle = n \cdot l^2 \ . \tag{2.36}$$

The end to end vectors of the freely jointed chain are a normal variable.
In the alternative Gaussian Chain model, the lengths of the chain segments follows a Gaussian distribution and the end to end distance vectors follow a Gaussian distribution too. Equation (2.36) also applies in this case.
Both models describe the global properties of the chain accurately but the local structure is described inaccurately.

2.5.2 Persistence length

If the angle between two adjacent segments is not freely selectable, then the expected value $\langle \vec{r_n} \cdot \vec{r_m} \rangle$ is nonzero for $n \neq m$. But the expected value asymptotically goes to zero for long chains. This implies, that the chain is not as flexible as the freely jointed chain because every segment is influenced by his neighboring segment. This increases the end to end distance and equation (2.36) does not apply anymore. The increase of the end to end distance can be interpreted as the stiffness of the chain. This leads to the following equation for the expected value:

$$\left\langle r^2 \right\rangle = C_n \cdot n \cdot l^2 \tag{2.37}$$

where C_n is a value that describes the stiffness of the chain. For short chains C_n rises with decreasing chain length because the segments orient themselves preferably in one direction. For long chains ($n \to \infty$) C_n approaches a constant value. So in the limit for long chains, the end to end distance rises proportionally to the number n of new segments in analog to the freely jointed chain. The rise of the distance per segment with the value C_∞ is greater than in the freely jointed chain case. Therefore C_∞ is the average number of segments that point in the same direction. So for a freely jointed or Gaussian chain C_∞ equals one and for stiff chains, this value is greater than one.
By defining a value $b \geq l$ which lets the chain behave like a freely jointed chain one gets the number of segments that can move together without noticing the stiffness of the chain. The value b is called the Kuhn Length. The maximal chain length r_{max} is unperturbed by this definition and is calculated via $r_{max} = n \cdot l = n' \cdot l$ with $n' \leq n$. The Kuhn Length can be derived as follows:

$$b = \frac{\langle r^2 \rangle}{r_{max}} = \frac{C_\infty n l^2}{r_{max}} = C_\infty l \ . \tag{2.38}$$

From the Kuhn Length the persistence length l_p can be derived quite easily via $b = 2 \cdot l_p$. It denotes how far a finite chain can be continued in one particular direction. The persistence length is a characteristic parameter in the wormlike chain model. In this model the chain consists of an isotropic rod that is flexible over the whole length of the chain. This is in contrast to the freely jointed chain

where only the joints are flexible. It applies:

$$l_p = (1 + C_\infty)\frac{l}{2} \ . \tag{2.39}$$

2.5.3 Sterical repulsion of polymer chains

In a real chain the segments are not allowed to overlap each other. Additionally each segment has a finite dimension which enlarges the end to end distance. Flory et al approximated this as follows:

$$\sqrt{\langle r^2 \rangle} \propto l \cdot n^\nu \ , \quad \nu = 0.59 \ . \tag{2.40}$$

So this effect comes to bear for long chains mainly. Furthermore the end to end distance of real chains depends from circumstances like solvent properties or the temperature of the system. Despite of this it is possible to approximate global chain characteristics with statistical models in a satisfactory manner.

2.5.4 The Langevin equation

The energy landscape of intramolecular diffusion is complex. The Langevin equation describes the influence of the solvent on the motion of the chain. The molecules of the solvent transfer energy to the polymer chain by colliding with it because of their Brownian motion. At the same time the solvent molecules hinder the chain motion by friction. The Langevin equation describes this motion but it only applies if the relaxation time of the solvent fluctuations is significantly shorter than chain motion:

$$\ddot{x} = M^{-1}\frac{\partial U(x)}{\partial x} - \gamma\dot{x} + M^{-1}F_{fluc}(t) \quad . \tag{2.41}$$

Here M denotes the mass of the polymer, x is the reaction coordinate, $U(x)$ stands for the energy of the system and γ links the system to the solvent and is called friction coefficient. In real systems γ is given by the solvent viscosity. $F_{fluc}(t)$ describes a random force that is produced by the thermal movement of the solvent. It is given by:

$$\langle F_{fluc}(t) \rangle = 0 \qquad \langle F_{fluc}(t) \cdot F_{fluc}(t') \rangle = 2k_B T \gamma M \delta(t - t') \ . \tag{2.42}$$

This resembles a Gaussian noise with a δ-function as correlation function.
In this regard the internal friction contribution, that might be present in some end to end contact formation dynamics has to be incorporated into equation 2.42 via adding the factor σ. But as can be seen in section 2.6 this model does not hold for most internal friction dynamics. So internal friction is not a friction in the direct meaning of it. De Gennes proposed to view it as a fastest possible end to end contact time and so a lower barrier. For further explanation of this topic see section 2.6.

2.5.5 The length dependence of end to end contact formation

Szabo, Schulten and Schulten investigated the length dependence of the end to end contact formation of a Gaussian chain that is diffusion controlled. This theory is called the SSS-theory [Sza80]. They looked at the end to end contact formation as an event of diffusion on a potential surface. The model was an exponential decay model. It was found that the contact formation rate $k_{contact}$ scales with the length n of the polymer in the following matter:

$$k_{contact} \propto n^{-3/2} \ . \tag{2.43}$$

This equation holds for an ideal freely jointed Gaussian chain. If one now adds the effect of excluded volume the exponent in the SSS model becomes $k'_{contact} \propto n^{-1,8}$ [Buc05]. For the Glycine-serine repeating peptides was found that the exponent $a = 1.7 \pm 0.1$. This shows that Glycine-serine peptides behave like Gaussian chains with excluded volume and that the end to end contact formation is diffusion controlled. This finding was reproduced with our method which enabled us to use Glycine-serine peptides as model systems for intrinsically unstructured fully flexible peptides [NLDS07].

2.6 Protein folding and internal friction

The folding of proteins is a wide field that progressed rapidly in recent years due to the development of new techniques. Especially it is now possible to probe

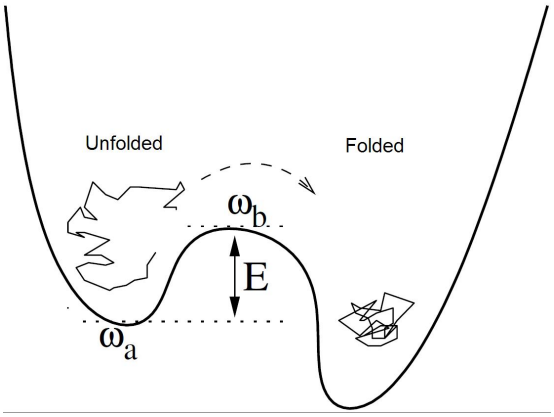

Figure 2.5: Two state model for the diffusional transition from the unfolded to the folded state by barrier crossing without an intermediate [Kra40]. The roughness of the energy landscape is given by ω_a and ω_b respectively. E stands for the Arrhenius Activation Energy and shows the height of the energy barrier.

the folding of a protein in timescales down to microseconds or even faster. It is known, that some proteins fold in this time range and that the formation of secondary structures like alpha helices can occur even faster [EMH$^+$00]. By reaching such fast timescales for folding one can ask where the limit is [Hag05]. The diffusional motion of the polypeptide chain is the intuitive reason for a fastest time limit. But this limit would be very fast and it is known that some proteins fold much slower. The internal interactions in the polypeptide chain result in a slower speed limit. This is called the Internal Friction of the system. In this work it is shown that glutamine and asparagine rich polypeptides show a significant internal friction contribution to their loop closure kinetics.

The dynamics of protein folding is often described in a two state, barrier crossing model (figure(2.5)). In this model the molecule crosses an energy barrier E in a one dimensional diffusion. The energy barrier divides the unfolded from the folded state. Because the motion of the polypeptide chain is heavily damped by the friction to the solvent the driving force of the barrier crossing is the Brownian motion. Because the transition state is very short lived and therefore can be omitted the reaction rate theory of Kramers is better suited to describe this process [Kra40]. Then the average rate k of the diffusion of the particle

across the energy barrier of height E is given by:

$$k = \frac{\omega_a \omega_b}{2\pi\gamma} \exp\left(\frac{-E}{k_b T}\right) . \tag{2.44}$$

Here ω_a and ω_b denote the curvature of the energy landscape, k_b is the Boltzmann constant and T stands for the temperature of the system. γ is the fractional drag coefficient of the Langevin equation of the motion of the particle. One can now interpret γ as arising from the dynamic viscosity of the system η_s and then Kramers theory predicts (see equation (2.44)) that $k \propto 1/\eta_s$ holds [Kli97].
It is reasonable to assume that the upper speed limit of the protein folding is set by the diffusional search of the chain through all possible configurations that is driven by the Brownian motion. The folding cannot be any faster. The simplest case of folding would be a reconfiguration of disordered polypeptides or the end to end contact formation. Several groups measured the loop formation rate of short unstructured polypeptides and the fastest loop closure rate has been reported to be in the order of 10 ns and depends on the number of residues in the polypeptide chain. So far no protein is found that folds nearly as fast as this. The limit is approximately 10 to 100 times faster than the fastest miniproteins. This leads to the question if some other process slows down the folding speed of proteins. A reasonable candidate for this process is the so called internal friction.
The first observation of an effect that hints at an Internal Friction has been done by Ansari and coworkers in 1992 [AJH$^+$92]. They studied the relaxation time $(1/k)$ for the conformational relaxation of sperm whale myoglobin. They found that the relaxation time showed a linear behavior as expected by a kramerslike barrier crossing. But they also observed that the y-intercept did not vanish if the viscosity of the system goes to zero (figure(2.6)). One can then interpret this finding in the way that the simple antiproportional behavior of the inverse rate to the solvent viscosity has to be extended to:

$$k^{-1} = \eta_s + \sigma . \tag{2.45}$$

In this equation σ is an extra term that represents an internal viscosity that has to be added to the solvent viscosity as an offset which dampens the folding of the protein considerably. As a consequence such an addition should be detectable in most protein folding studies as the additional internal viscosity should always

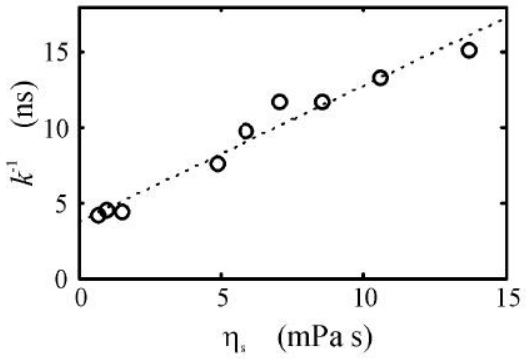

Figure 2.6: Relaxation time $(1/k)$ for the conformational relaxation of sperm whale myoglobin, following photodissociation of a heam ligand depicted against the viscosity of the solvent (Ansari 1992). The dashed line to the horizontal axis indicates $\sigma \approx 4.1 mPAs$ for this relaxation time as a value for internal friction.

be present. But most studies, especially for big proteins, show no significant σ. There have been numerous theoretical studies that tried to find the source of the internal viscosity. No consistent model for the internal viscosity could be proposed and the cause of the internal viscosity is strongly dependent on the exact nature of the folding process [Man85].
If one considers that a homopolymer without secondary structure folds in a specific time τ_s into its equilibrium configuration which is the random coil one can find that τ_s is viscosity controlled by the solvent. De Gennes then proposes that internal friction adds a solvent independent time τ_0 to the folding time and it follows []:

$$\tau = \tau_s + \tau_0 \ . \tag{2.46}$$

It then still holds from equation (2.44) that $\tau_s \propto \eta_s$ and then by measuring the folding time of a given process in dependence of the solvent viscosity. By extrapolating the linear behavior the y-intercept then directly indicates τ_0. This approach predicts the same viscosity dependencies as equation (2.45) but the interpretation is completely different. The internal friction of the polypeptide chain does not induce a viscosity but rather an additional limit to the folding time. So not only the solvent viscosity implies a limit but the interchain interactions give a solvent viscosity independent limit too. The actual mechanism behind the τ_0

value have to be looked at for every system specifically because no consistent model for the cause of the internal friction could be proposed. In this view the finding that some protein show no internal friction contribution in the folding measurements is consistent because in this cases the τ_0 is then small and the internal friction limit is much faster than the limit generated by τ_s [Hag05].
It is known that unstructured poly GS peptides show no internal friction contribution in their end to end contact formation dynamics. So a polypeptide chain poses no limitation on the protein folding in regards of internal friction. If for a given system an internal friction contribution arises the reason for this have to be interchain or sidechain interactions. One has to investigate the specific reason for a given sample if it shows an internal friction contribution. The causes of this phenomenon are not fully understood yet. There is no microscopic theory of internal friction to the knowledge of the author. Possible reasons for internal friction could be intramolecular rejections of charged side groups or steric repulsions for the formation of secondary structure. The opposite case is known for example in the folding of the Tryptophan Cage miniprotein. Here a salt bridge speeds up the folding. If the side groups would be equally charged the folding would be slowed down considerably or even be impossible.

2.7 Tryptophancage folding properties

The so called Tryptophan Cage miniprotein was designed in 2002 by Neidigh and coworkers [NFA02]. It is a 20 residue protein that exhibits secondary structure elements and is more than 95% folded in water under physiological pH. It also is a fast folding protein that makes it a good model protein to investigate protein folding under various different conditions and to try to understand the basic principles of protein folding. The Tryptophan Cage follows a hierarchical folding structure via an intermediate state under equilibrium conditions that extends the proposed two state folding mechanism. The intermediate state has the form of a molten globule with preformed secondary structures [NDS05]. There exists a salt bridge between the residues 9 and 16. This intermediate speeds up the folding of the Tryptophan Cage. The conformational flexibility in the denatured state is high [NDS05].

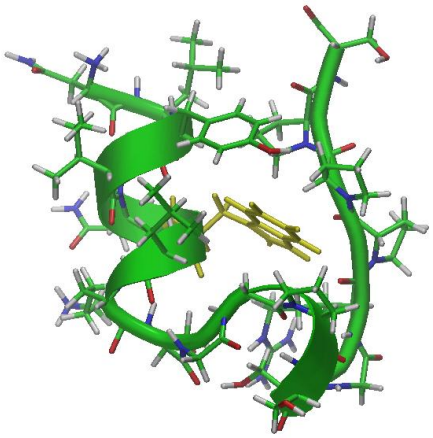

Figure 2.7: The Tryptophan Cage miniprotein. It exhibits secondary structure elements that are in particular a proline rich structure element and a α-helical structure that tightly encapsulate the hydrophobic tryptophan residue at the core of the miniprotein. The Protein Database code is 1L2Y. It has the amino acid sequence: NLYIQ WLKDG GPSSG RPPPS. The backbone is depicted in green.

There have been three theoretical studies that examine the folding behavior of the Tryptophan Cage in detail with a close look at the salt bridge and the influence it has on folding.
Zhou et al reported in 2003 about the folding of the Tryptophan Cage by using a high parallel replica exchange molecular dynamics model in explicit solvent. In their study the salt bridge stabilizes the intermediate states and thus is responsible for the fast folding of the Tryptophan Cage [Zho03].
In the study of Paschek et al a replica exchange model was used too. They propose that the salt bridge influence on the folding is small because they found internal water molecules in the Tryptophan Cage that stabilizes the native state via hydrogen bonds [PNG07].
Juraszek et al proposed in 2006 that the salt bridge is formed early in the folding process and does not have an influence on the intermediate state and that water molecules are strongly bound to the Tryptophan Cage. These exhibit the major influence on the folding process because in the last step of folding the water molecules are expulsed and this is the limiting step. They used the so called transition path sampling technique in their studies [JB06].

2.8 Beta turn properties

Reverse turns are an important secondary structure motive in proteins. They connect β-sheets or other secondary structures in the protein by forming a side chain reversal and are responsible for the globular structure of a protein. Without turns a protein would be a rod like structure of helices and sheets. Turns can have an active or a passive role in protein folding. Active turns have a stable structure on their own as a peptide and so are able to promote folding by inducing their structure into the amino acid chain. Passive turns just enable the protein to reverse the backbone. So turns with a structure in their peptide form are interesting as an object for studying the end to end contact formation dynamics because they might not be purely viscosity controlled. Additionally an internal friction contribution might be present.

The categorization of turns is difficult because there exist many different structures and sequences for turns [MG08]. They are generally defined as a region in the protein or peptide where a change in the direction of the backbone occurs. The categorization of turns is by no means trivial because they appear in many different lengths and sequences [MG08]. The most prevalent turns are the β-turns. Additionally there exist α- and γ-turns. A further class of turns are well defined loops, such as the Ω-loops. The modern classification of turns depends on the length of the chain, the position of the stabilizing h-bond and the preferred angles Φ and Γ of the turn [MG08]. The β-turn is the most common form of turns and here the h-bond occurs between the i and $i+3$ residue, so it consists of 4 amino acids generally. If a β-turn is flanked by two β-strands it makes up the basic unit of a β-sheet [MG08].

An interesting turn sequence is the DDATKT-sequence. It is part of the B3 domain of the immunoglobulin binding protein G from Streptococcus. This sequence is reported to be a nucleation site for the folding of the C-terminal β-hairpin [SZO$^+$09]. This implies an active role in the folding of the protein.

We decided to study this turn sequence because there are many investigations on the structure of turns but there are no investigations of the loop closure dynamic

yet. We introduced a mutation at position two where the second aspartic acid was exchanged to proline. The goal of the study was to see if we can shed light on the properties of β- turns and see how the turn sequence influences the loop closure behavior. We assumed that the proline residue introduces a kink into the turn sequence and that should speed up the loop formation rate. Furthermore we wanted to investigate if our method is able to measure the dynamics and thermodynamic values of β-turns as they are small and the loop formation is fast.

2.9 The influence of osmolytes on protein folding

The thermodynamics of protein folding is a complex field [BR08]. A protein is in the equilibrium between its unfolded and native state under any circumstance. This equilibrium is being influenced by the addition of cosolvents to the solvent. One class of cosolvents are the organic osmolytes that can be found in nature in many different organisms and functions. They can be differentiated into two groups, namely protecting and denaturing osmolytes. Urea is an example of a denaturing osmolyte and these classes of osmolytes shift the equilibrium towards the unfolded state. Protecting osmolytes like trimethylamine N-oxide (TMAO) act in the opposite direction by shifting the equilibrium towards the native state. Figure (2.8) shows exemplary the structure of urea and TMAO.
The driving force of the spontaneous unfolded $\rightleftharpoons$ native transfer is a gradient in the Gibbs free energy of the relevant states. In figure (2.9) the influence of osmolytes on the Gibbs free energy is depicted.

There are two paradigms for the theoretical description of protein folding as a special case and to describe thermodynamic processes in general.
The first one is called the energy ledger approach and was introduced by Kauzmann. He models folding as a two state process and it then follows for the equilibrium constant K:

$$K = \frac{[N]}{[U]} \ , \tag{2.47}$$

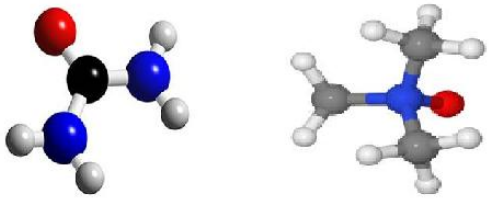

Figure 2.8: The structure of the organic osmolytes urea (left) and TMAO (right). The following colorcoding was used in this picture: white stands for hydrogen, blue depicts nitrogen, black or grey respectively is the color for carbon and red is oxygen.

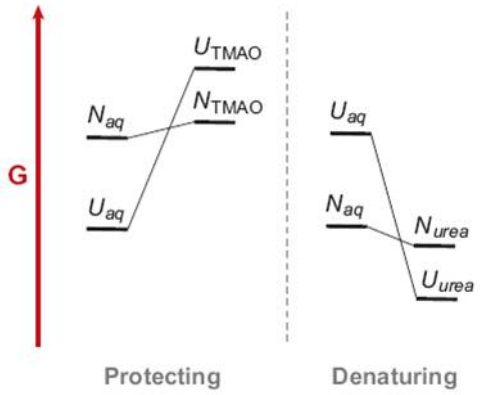

Figure 2.9: The influence on the Gibbs free energy G of protecting and denaturing osmolytes. The initial state is not changed by the organic osmolytes. They change significantly the final state of one or the other conformation. TMAO as a protecting osmolyte, raises the Gibbs Free Energy of the unfolded state over the Gibbs Free Energy of the native state and so favors the native state. Urea is an example of a denaturing osmolyte and lowers the Gibbs free energy of the unfolded state below the level of the native state. This results in a favoring of the unfolded state in presence of denaturing osmolytes. In both cases the unfolded state is influenced much more than the native state.

with $[N]$ and $[U]$ denote the respective population of the unfolded and the native state. It then follows for the Gibbs free energy $\Delta G_{U\to N}$ for the folding transition:

$$\Delta G_{U\to N} = -R\,T\,\ln K\ , \tag{2.48}$$

where R is the universal gas constant and T stands in for the temperature of the system. The energy ledger approach then summarizes all contributions to derive the Gibbs free energy of the folding process. In the case of protein folding the entropy $T\,\Delta S_{U\to N}$ favors the unfolded state and the enthalpy $\Delta H_{U\to N}$ favors the native state. It then follows:

$$\Delta G_{U\to N} = \Delta H_{U\to N} - T\,\Delta S_{U\to N}\ . \tag{2.49}$$

In equation (2.49) the resulting Gibbs free energy is a small difference between two large opposing contributions. In this approach one then has to investigate the single contributions of the system at hand individually and then summarize over all contributions to obtain the resulting energy of the transition. This is a major weakness of the energy ledger approach because small errors or miscalculations of one of the contributions may lead to incorrect predictions. Furthermore a difficulty of the energy ledger approach is that it is often hard or even impossible to investigate all contributions to the resulting energy individually.

Another paradigm to specifically describe protein folding is the so called Stimulus Response model. This approach is used by the most studies that investigate transitions between different states including this work. In this approach one introduces a perturbation to the system and then tries to intuit what is responsible for the answer of the system. Possible perturbations are a change in temperature or pressure, mutations in the amino acid sequence, organic osmolytes et cetera. If one then systematically changes the perturbations one can obtain insights into the system by looking at the different responses. Complementary investigations are of great value for this approach because it enables the scientist to look at a transition from different angles.

The two paradigms are of opposite type because the energy ledger approach is a reductive bottom up and the stimulus response approach is an inductive top down method [Hag05].

2.9.1 Protein folding and solvent quality

The term of solvent quality is defined in polymer science and defines the character of a solvent with the nouns good or poor in respect to the solvent character. As amino acid chains are essentially polymers this description of solvents can be applied for protein folding. In this picture the contributions to the Gibbs free energy can be classified by the solvent protein interaction. The unfolded ensembles radius of gyration decreases in a poor solvent and increases in a good solvent. So solvent protein interactions are enhanced in a good solvent whereas the intramolecular interactions are enhanced in a poor solvent. As water is a rather poor solvent for proteins the native state is preferred because it decreases the accessible surface area and so the solvent protein interaction. Organic osmolytes act in a way that they change the solvent quality. A denaturing osmolyte increases the solvent quality and so the preferable solvent protein interaction changes the contributions to the Gibbs free energy in favor of the unfolded state. A protecting osmolyte decreases the solvent quality and in the now poor solvent the intramolecular interactions are preferred and therefore the native state gets energetically favorable.

Chapter 3

Materials and methods

This section describes the materials and methods that were used for this work in detail. Also the distributors are named that procured working materials.

3.1 FCS setup

The measurement setup consists of a standard inverse confocal microscope. As excitation source serves a HeNe Laser with an emission maximum at 632.8 nm. The collimated excitation beam is then coupled into the objective (62x, NA 1.4, Zeiss, Jena, Germany) by a dichroic beam splitter (645DLRP, Omega Optics, Brattleboro, USA). The fluorescence of the sample is collected by the same objective and projected on the active area of two avalanche photo diodes (AQR-15-FC, PerkinElmer, Dunberry, Canada). To clean the signal, it is filtered through a band-pass filter (650RDF50, Omega Optics, Brattleboro, USA) and it is splitted by a cubic non-polarizing beamsplitter (Linos, Göttingen, Germany). To apply the confocal principle, the fluorescence light is focused on multimode optical fibers with a diameter of $\sim 100\ \mu m$. The reason to use two APDs is to circumvent the dead times and afterpulsing of the devices. The detector signals were recorded and cross-correlated by the DPC-230 (Becker & Hickl GmbH, Berlin, Germany (see 3.2)). The time resolution of this setup is 165 ps. Temperature control was achieved by a custom-built objective heater that is connected to a water bath. Figure (3.1) shows a schematic view of the setup. This method of building an FCS setup has proven to be robust and easy to adapt to new tasks. For example

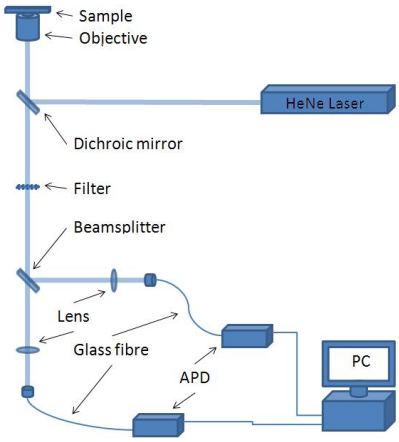

Figure 3.1: Schematic view of the FCS measurement setup that was used in this work. The excitation source is a HeNe Laser that emits at a wavelength of 632.8 nm in its maximum. The laser light is focused to the sample via an oil immersion objective with a numerical aperture of 1.4. This objective also collects the fluorescence light and it is then focused on glass fibers to apply the confocal principle. As detectors are two avalanche photo diodes (APDs) used. The signal is cleaned by filters and correlated by the DPC-230 single photon counting card. The dichroic mirror is used to separate the laser light from the fluorescence and the beamsplitter splits the fluorescent light with a 50:50 ratio.

an adaptation to a two color setup is easily done by changing the beamsplitter to a dichroic mirror. Chromatic aberrations are unproblematic because every detector has its own lens and pinhole (via the glass fiber).

3.2 DPC-230

The DPC-230 is a 16 channel photon correlator provided by Becker & Hickl GmbH. It is able to do photon correlation down to 165 ps because it is able to record absolute photon times with this time resolution. So even antibunching measurements are possible because it is in a time range of a few nanoseconds. It has 16 Low Voltage Transistor Transistor Logic (LVTTL) input channels for SPADs and 4 Constant Fraction Discrimination (CFD) inputs for PMTs. Autocorrelation is possible on all channels and crosscorrelation between all pairs of

Figure 3.2: The DPC-230 module. It is a single slot PCI module with operating software for Windows 2000, NT and XP. It has 16 LVTTL inputs and 4 CFD inputs and is able to record absolute photon times with time tags.

channels. It is a handy device because it is a single-slot PCI module with operating software for Windows 2000, NT and XP.
If one wants to use such a module for fluorescence measurements and FCS in particular, one has to look at the connection of the APDs to the module carefully. It is necessary to adjust the cable length of respective APDs to the input channel because of electronic effects that might occur by matching some APDs to respective input channels. One has to find the right combination of APD, cable length and input channel for undisturbed FCS measurements. To see if the detectors are connected correctly one has to do a cross correlation between both detectors, in both directions. So one has to correlate detector one to detector two and vice versa. If the connection is incorrect, one of the correlation curves will break down at short timescales and deviate from the other correlation curve. Only if both correlation curves are identical within the noise the connection to the detectors has the right combination of cable length and input channel. This process usually takes a while because to see this discrepancy one has to correlate the dye signal for at least 15 minutes to be able to see the difference in the correlation curves.

After matching the cable lengths to the input channels one is able to do FCS measurements over a time range of picoseconds to even hours. The data acquisition and handling happens online via the so-called First In First Out (FIFO) procedure. Single photon timetraces can also be obtained for post processing of the data. The DPC230 correlator card is able to perform many different methods simultaneously. For example it is possible to perform a Time Correlated Single

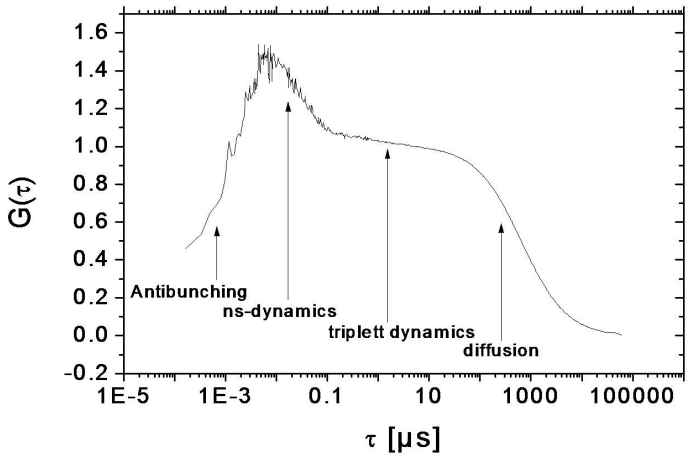

Figure 3.3: Typical FCS curve of MR121-$(GS)_5$-W in the measurement buffer on the described setup (see (3.1) and (3.6)). The correlation function $G(\tau)$ is depicted against the lagtime τ. The arrows indicate the respective mechanism that lead to the exponential decay in the correlation function. The loop closure dynamics of peptides usually lies in the ns time range whereas the folding dynamic of the TC has a longer relaxation time, closer to the triplet dynamic.

Photon Counting (TCSPC) at the same time as a FCS measurement. This makes this device very useful and versatile.

3.3 The PET-FCS method

This section describes how the photoinduced electron transfer (PET, see (2.1.6)) of MR121 and the amino acid tryptophan is combined with Fluorescence Correlation Spectroscopy (FCS, see (2.2.2)).
As mentioned above FCS detects fluctuations of fluorescence on various timescales. One is able to determine the characteristic timescales and ratios of a process that leads to the fluctuation. Figure (3.3) shows a measured FCS curve with the setup that was detailed above of MR121-$(GS)_5$-W in the standard measurement buffer of this work (see (3.6)). The autocorrelation function is then fitted with the following model that is derived from the standard FCS formalism (see (2.2.2)) and

modified to include all fluctuations that occur in the system:

$$G(\tau) = \frac{1}{N}\frac{1}{\left(1+\left(\frac{\tau}{\tau_D}\right)\right)} \cdot \left(1 + K\exp\left[-\frac{\tau}{\tau_{exp}}\right]\right) \cdot \left(1 + T\exp\left[-\frac{\tau}{\tau_{tr}}\right]\right) \cdot \left(1 + A\exp\left[-\frac{\tau}{\tau_{AB}}\right]\right) \ . \tag{3.1}$$

Here N denotes the average number of fluorescent molecules in the detection volume and τ_D is the average diffusion time of the fluorescent molecules through the focus. The exponential terms in this equation describe the different causes of the fluctuation of the fluorescence that FCS is sensitive for. The first two parameters K and τ_{exp} describe the conformational fluctuations that cause the quenching of the dye by the amino acid tryptophan (see (2.1.6)). The parameters T and τ_{tr} are the fitparameters for the triplet behavior of the dye that causes statistical off times of the dye when it performs an intersystem crossing (see (2.1.1)). The last exponential term describes the antibunching of the dye with the parameters A and τ_{AB} (see (2.1.5)). Together with equation (2.3) it follows that $\tau_{AB} = \frac{1}{k_e+k_d}$ and that our fitting parameter A should have the value $A \approx -1$. With this equation the measured data can be fitted and it is then possible to extract on (k_+) and off (k_-) rates of the dye via:

$$K = \frac{k_+}{k_-} \qquad \text{and} \qquad \tau_{exp} = \frac{1}{k_+ + k_-} \ . \tag{3.2}$$

In this instant, the parameter K is called equilibrium constant and τ_{exp} is called relaxation time. These rates then translate to the model picture seen in figure (3.4) for the end to end contact formation rate k_+ and dissociation rate k_- for the loop formation of a peptide.

In the case of the Tryptophan Cage (TC, see (2.7)) the rates k_+ and k_- are interpreted in another way. As can be seen in figure (2.7) the tryptophan is embedded in the middle of the folded protein and shielded from the surrounding. So in the folded state, the dye fluoresces freely whereas in the unfolded state the tryptophan is able to get into contact with the dye via peptide chain dynamics and so quenches the fluorescence. So the rate k_+ is in this case the unfolding rate and k_- denotes the folding rate. Another interesting value that can be calculated is the fraction of folded TC molecules F_f via:

$$F_f = \frac{k_-}{k_+ + k_-} = \frac{1}{K+1} \ . \tag{3.3}$$

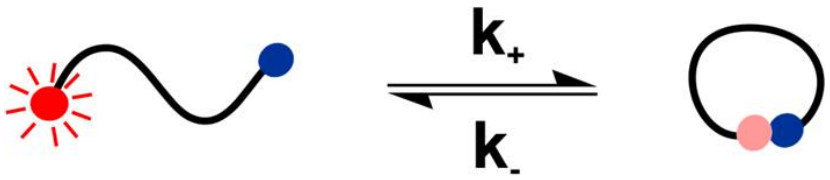

Figure 3.4: The loop formation and dissociation of a peptide translate to the measured on and off rates k_+ and k_- respectively in the manner shown here. The red dot stands for a fluorescent dye and the grey dot is the quenched dye. The blue dot represents the quencher molecule.

3.4 CD measurements

CD measurements were done with a Jasco J-810 Circular Dichroism Spectropolarimeter. The wavelength range was from 180 nm to 350 nm over a temperature range of 10°C to 60°C. Samples were prepared as shown in section (3.6) with one difference: the buffer concentration was reduced to 10 mM to suppress background signal. And of course the samples were the unlabeled Tryptophan Cage and its mutant the TC(R16Q).

3.5 Ensemble methods

Ensemble measurements were performed in commercially available equipment. For the absorption measurements a Perkin Elmer Lambda 25 UV/Vis spectrometer was used. Ensemble fluorescence was measured Varian CARY Eclipse spectrometer. The measurements were performed in glass cuvettes with an optical path length d of 1 cm and a capacity of 1 ml. The concentration was typically in the range of 10^{-5} to 10^{-6} molar. The concentration c can be determined by measuring the optical extinction $E = \log \frac{I}{I_0}$ (where I is the measured intensity and I_0 is the reference intensity) and with the help of the following equation:

$$c = \frac{E}{\epsilon \cdot d} \, . \tag{3.4}$$

In this equation ϵ stands for the molar extinction coefficient of the dye. If one performs temperature dependent measurements with the method presented here and evaluates the data with the help of equation 2.7 one has to bear in mind the

following. One has to measure a heating and cooling cycle for all samples to make sure that no irreversible effects occur at high or low temperatures. Furthermore one has to try and measure as far a temperature range as possible. The reason for this is to make sure that the asymptotes can be fitted. If the sigmoidal curve is incomplete fitting of the melting temperature is inaccurate.

3.6 Sample preparation

All measurements were done in a buffer solution of phosphate buffer at a pH of 7.2 with a concentration of 100 mM. Additionally the buffer contained 50mM NaCl and 0,3 mg/ml Bovine Serum Albumin (BSA). BSA is used to suppress glass surface interactions of the sample. To alter the viscosity of the solvent, sucrose was added to a concentration of up to 40% weight per volume. The resulting viscosity of the solution was calculated with the help of the sucrose calculator by Roberto Gilli (Association Andrew van Hook, 1997). It is known, that sucrose does not interact with polypeptide chains and it does not induce structure, too [MKK05]. The organic osmolytes GdHCl and TMAO were added up to a concentration of 400 mg/ml (see figure (2.8)). The resulting viscosities of these solutions were measured by using a Haake falling ball viscosimeter. The sample concentration for FCS measurements was approximately 1 nM and in the ensemble experiments the concentration used was approximately 1 μM.
All samples were modified with the dye MR121 via standard NHS-Ester chemistry. Purification was done via a reversed phase HPLC (Agilent 1100 Series).
All chemicals were purchased by Sigma and MR121 was kindly provided by K.H. Drexhage. The Tryptophan Cage samples and the peptides were purchased from Byosyntan.

The presented buffer system was not the only buffer that was tested for the measurement system. It showed to be the one that interferes the least with the reporter system or the sample.
The buffer pH of 7.2 is necessary because the reporter system is sensible to changes in pH. Due to the fact that TMAO and GdHCl do influence the pH of a solution one has to counteract this effect by adding HCl or NaOH respectively

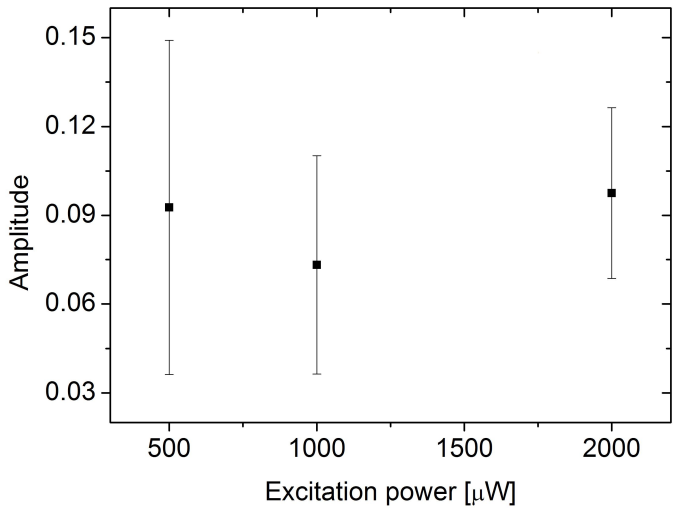

Figure 3.5: The amplitude of the fitted contribution to the FCS curve is shown against the excitation power. The measured peptide was the MR121-$(GS)_9$-W in a concentration of 3M TMAO and 0.05 % Tween20. It shows that the process recorded here does not origin in the triplet photophysics of the dye. The source of this contribution is indeed the TMAO Tween20 interaction.

until the pH has again a value of 7.2. Furthermore the concentration of salt ions has to be controlled because protein folding and peptide dynamics may be influenced by the ion concentration. BSA is added to make sure that no sample molecules adhere to the surface. The BSA molecules adhere to the surface and so counteract the positive charge of the surface which then makes it much less likely for the charched samples to adhere to the surface.
The first buffer solution contained 0.05 % Tween20. It serves the same purpose as BSA. Unfortunately in conjunction with TMAO it shows quite strong influences on the reporter system. This can be seen by an additional contribution to the FCS curve if both TMAO and Tween20 are present in the solution. At first glance this contribution looked like an unusually high triplet contribution. To confirm this, a measurement with the MR121-$(GS)_9$-W peptide was done in a concentration of 3M TMAO and 0.05 % Tween20 at three different excitation powers. If this contribution origins from the photophysics of the dye the amplitude of the curve should increase. One can see in figure (3.5) that the amplitude

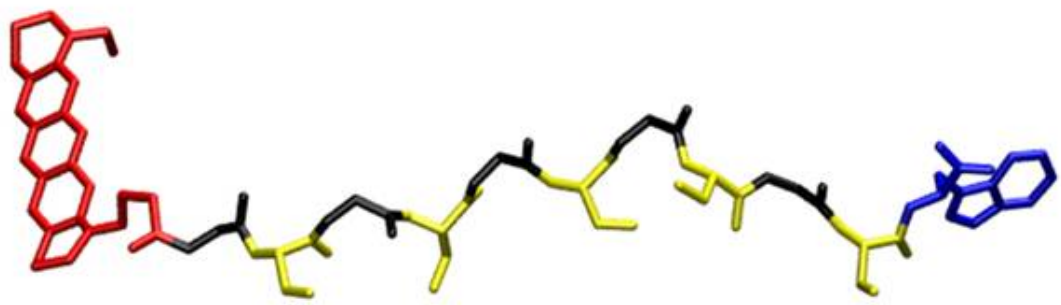

Figure 3.6: The MR121-$(GS)_5$-W peptide as an example for an intrinsically unstructured, fully flexible peptide. The MR121 is depicted in red. Glycine is black, Serine is yellow and Tryptophan is blue.

is independent from the excitation power. This shows that this contribution does not origin in the photophysics of the dye and that the TMAO Tween20 pair somehow interfered with the reporter system. After changing from Tween20 to BSA the contribution to the FCS curve vanished.

3.7 Samples

This subsection lists the samples that were used in this work.
As reference for intrinsically unstructured, flexible peptides MR121-$(GS)_n$-W with $n = 2, 3, 5, 7, 9$ were used (see figure (3.6)). They have been widely used as model system and are well understood [KFB+03] [NLDS07] [Hud01] [LEH00]. As glutaminerich peptides the sequences MR121-$P_3Q_6P_3$-W and MR121-$P_3N_2Q_2NYP_3$-W. Their respective structures are depicted in figure (3.7) and (3.8). Polyglutamine structures cause glutaminerich proteins to aggregate. To check if the glutaminerich peptides aggregate too, measurements with and without tris(2-carboxyethyl)phosphine (TCEP, suppresses aggregation) were compared and no measurable influence was detected which leads to the conclusion that the glutaminerich peptides do not aggregate.
One further sample that was investigated in this work are the so called β-turns (see 2.8). We chose two different sequences for our measurements. The first one

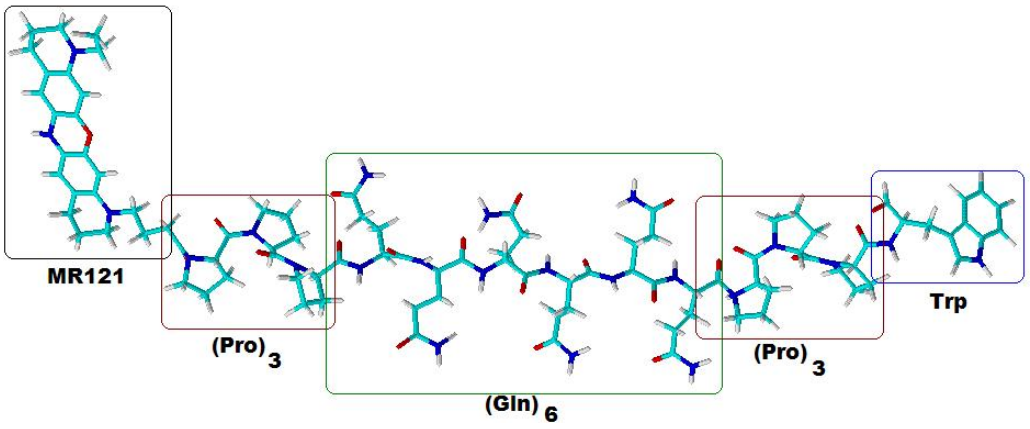

Figure 3.7: The glutaminerich peptide MR121-$P_3Q_6P_3$-W. Here Pro and P stand for the amino acid proline, Gln and Q are glutamine and Trp and W are the abbreviations for tryptophan. It was made with the ACD ChemSketch Freeware [ACD09].

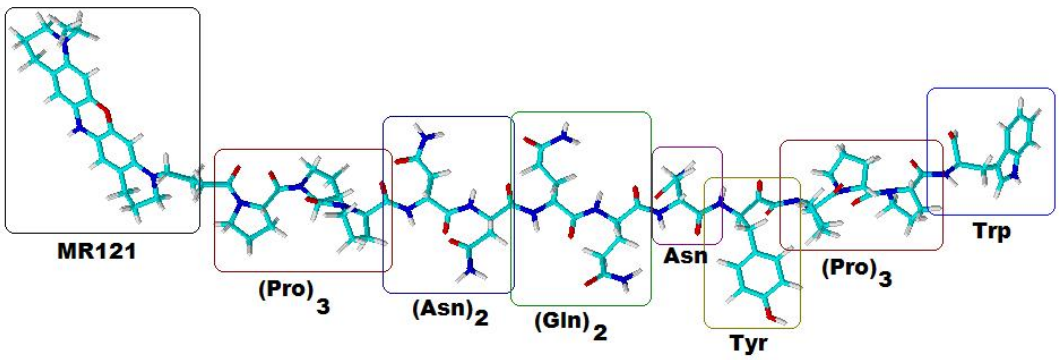

Figure 3.8: This peptide qualifies as glutaminerich because the amino acid asparagine is similar to glutamine. The sequence is MR121-$P_3N_2Q_2NYP_3$-W. Here Pro and P stand for the amino acid proline, Gln and Q are glutamine and Trp and W are the abbreviations for tryptophan. Additionally Asn and N depict asparagine and Tyr and Y stand for tyrosine. The structure was made with the ACD ChemSketch Freeware [ACD09].

is the MR121-DDATKT-W sequence and in the second sequence the second aspartic acid (D) is exchanged for a proline residue.
For the Tryptophan Cage (TC) measurements several mutants to the original TC sequence were used. The structure of the TC is depicted in figure (2.7). As reference sequences the following two mutated sequences were used. The first one is a fragment of the TC which includes the Amino acids 1 to 11. This fragment does not have a secondary structure and serves as a control for the unperturbed quenching mechanism. Another mutant that was used to monitor the influence of the folding on the dye without tryptophan is the TC(W6F) mutant where the tryptophan (W) at position 6 (the only W in the TC sequence) is exchanged for a phenylalanine. So the dye is not quenched even in the unfolded TC state. Furthermore the mutant TC(R16Q) was studied. This mutation of the arginine at position 16 for glutamine removes the salt bridge of the TC.

All samples were labeled with MR121 via standard NHS-ester chemistry. It was done in a carbonate buffer solution at pH 8.3. The incubation time was approximately 12 hours at room temperature. Purification of the labeled sample was done with the help of a reversed phase high pressure liquid chromatography (HPLC, Agilent Technologies, Waldbronn, Germany) with a hypersil-ODS column. The labeling of the glutaminerich peptides proved to be a challenge. At the first tries with the method detailed above we saw no product. But we then looked more careful at the output measurements of the HPLC. The answer was that the peak of the product was hidden in the peak of the free dye. This problem could be solved by applying a longer gradient. With a gradient of 60 minutes instead of 20 minutes the product peak was separated enough from the peak of the free dye to enable us to collect the product.

Chapter 4

Results and discussion

4.1 Characterization of the reporter system

The first imperative step is to characterize the reporter system and make sure that all artifacts are known and suppressed if possible.
In figure (4.1) one can see an example of a FCS curve measured with the setup shown in section (3.1). It shows a bimolecular measurement of MR121 and tryptophan as a quencher with the corresponding fit as outlined in section (3.3). The measurement took 30 minutes. On the right hand side in figure (4.1) one can see the residuals of the fit and that they are randomly distributed. We did longer measurements up to 6 hours. An example is shown in figure (4.2). One can see that the noise is reduced significantly and therefore the residuals are much smaller than in figure (4.1). The noise is also dependent on the concentration of the sample. The optimal measurement range for our setup is 10 to 20 molecules in the detection volume. This corresponds to a concentration of approximately 10^{-9} molar. The reason for the oscillation at long timescales is the drift of the objective and therefore the focus over the long measurement time.
As presented in section (3.3) the FCS measurements always show a contribution in the FCS curve that origin from the photophysical properties of the dye, in this case, the triplet transition. This contribution is dependent on the excitation power. The first test was to determine if the fitting of the conformational fluctuations is influenced by the magnitude of the triplet fluctuation. To do this the inverse contact formation rate ($1/k_+$) and the inverse dissociation rate $1/k_-$ of

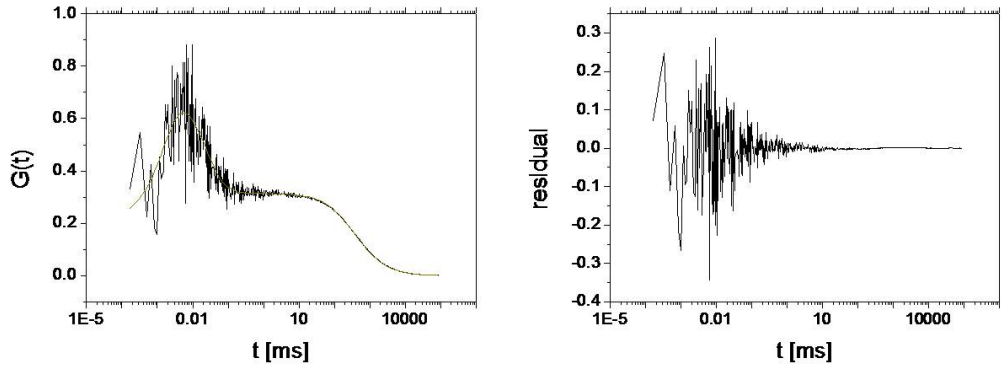

Figure 4.1: This figure shows on the left hand side the FCS curve of a bimolecular measurement of MR121 and tryptophan as a quencher that took 30 minutes. The fit is depicted in yellow that was performed as explained in section (3.3). On the right hand side are the residuals of the fit depicted.

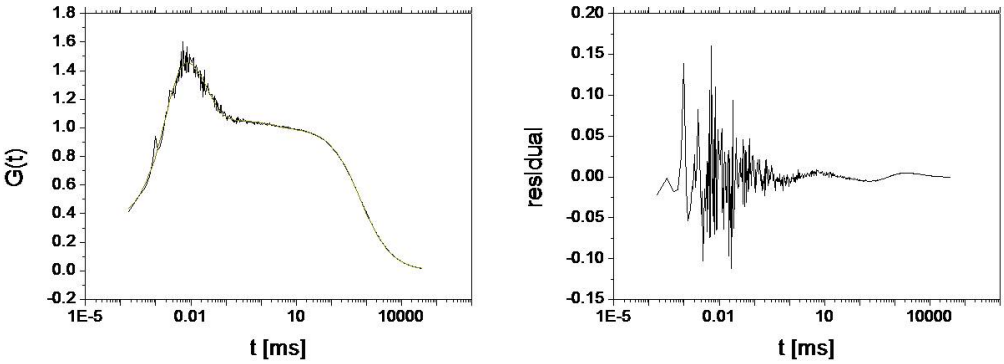

Figure 4.2: This figure shows the FCS curve of a measurement of MR121-$(GS)_{12}$-W that took 6 hours. The corresponding fit is depicted in yellow that was performed as explained in section (3.3). On the right hand side one can see the corresponding residuals of the fit.

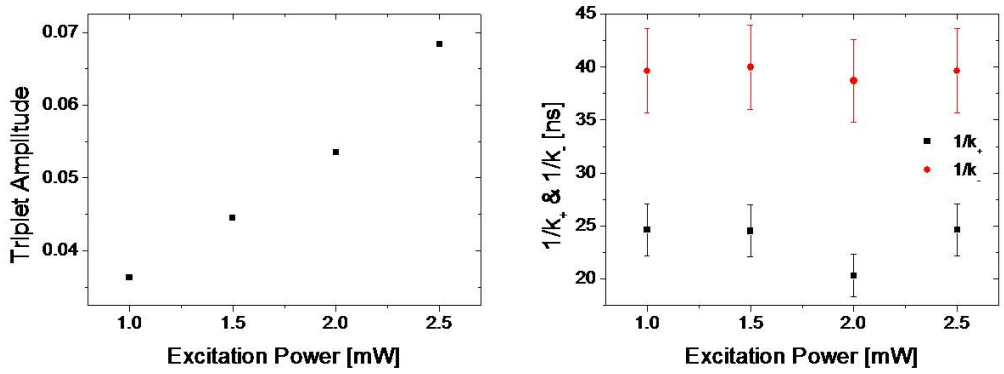

Figure 4.3: For these plots the MR121-$(GS)_5$-W peptide was measured at different excitation powers. The triplet transition is dependent of the excitation power and the triplet state gets more populated for higher excitation powers. This can be seen on the left hand side where the triplet amplitude is plotted against the excitation power. The amplitude is a measure for the population of the triplet state in the dye. On the right hand side are plotted the inverse loop closure rate $1/k_+$ and the inverse dissociation rate $1/k_-$ against the excitation power. The rates were obtained via FCS (see (3.3)).

the MR121-$(GS)_5$-W peptide was measured at several different excitation powers since the triplet transition rises for greater excitation powers. One can see in figure (4.3) that $1/k_+$ and $1/k_-$ is independent of the excitation power within the error bars. Additionally one can see in figure (4.3) that the triplet amplitude raises with rising excitation power. We used an excitation power of 1 mW as a standard value for the measurements shown here if not noted otherwise.
A next step was to look at the antibunching behavior of the dye and if the reporter system is able to measure it. The amplitude A of the exponential decay should yield $A \approx -1$ and the decay time τ_{AB} is composed of the excitation rate k_e and decay rate k_d of the excited state of the dye by $\tau_{AB} = \frac{1}{k_e+k_d}$. The excitation rate is dependent on the absorption cross section of the dye and the excitation intensity and the decay rate of the excited state is considered to be constant if the excitation wavelength does not overlap with the emission band to exclude stimulated emission. The last condition is not met in our setup so no further predictions on the excitation and decay rate can be made for this system. But in

our measurements the amplitude A yielded an average value of $A = -0.85 \pm 0.15$ which is in agreement with theory (see (2.1.5)) [lM96]. The antibunching of the dye defines the time resolution of the measurement setup. The correct reflection of the antibunching shows that the time resolution of our setup lies in the order of a few nanoseconds.
As was shown previously our reporter system is able to report on end to end contact formation rates correctly [NLDS07]. We compared therefore the obtained rates to the ones other groups found with different techniques [KFB$^+$03] [Hud01] [LEH00]. With the modification of the FCS setup, namely the fast photon counting device DPC-230, we had to do this comparison again and it showed that the new setup was able to reproduce our own data nicely.

4.2 Internal friction and the thermodynamic values of peptides

This section is about the limiting factors of the loop formation of peptides. As is already known, fully flexible, structureless poly Glycine-serine peptides are only limited by the viscosity of the solvent [NLDS07] [KFB$^+$03]. It is also known that Glycine-serine peptides do not show an internal friction contribution and the thermodynamic values like the activation enthalpy are known [NLDS07]. We now studied glutaminerich peptides to see if they are also only diffusion limited in their loop formation and to shed some light on the fact why they are prone to aggregation in glutaminerich proteins. We investigated if glutaminerich peptides show internal friction and looked at their thermodynamic values.

4.2.1 Internal friction of glutaminerich peptides

At first we investigated the dependence of the loop formation kinetic from the temperature and the viscosity of the solvent. Both glutaminerich peptides (see 3.7) were measured from 10°C to 50°C in solutions between 10% (weight/volume) sucrose and 40% (w/v) sucrose. Figure (4.4) shows the effect that sucrose has on the FCS curve of the MR121-$P_3Q_6P_3$-W at a temperature of 20°C. One can

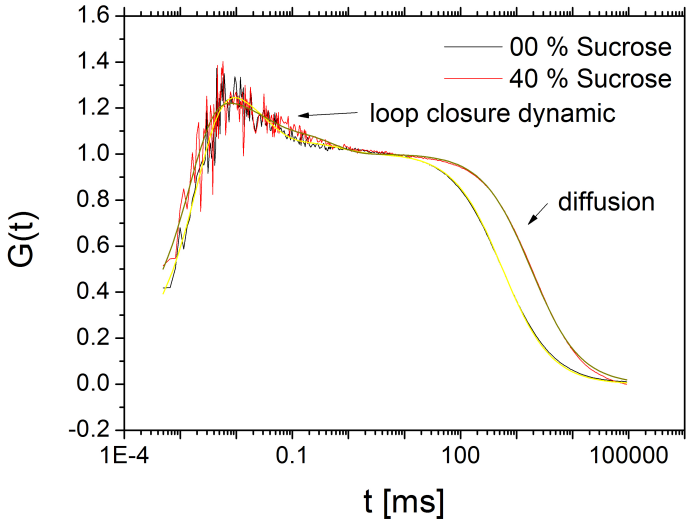

Figure 4.4: This figure shows examples of FCS curves of the MR121-$P_3Q_6P_3$-W in different sucrose solutions. The measurement was done at 20°C and the yellow lines denote the fits that were done as explained in section (3.3).

see that the diffusion time is clearly shifted to a longer diffusion time due to the higher viscosity of the sample. Furthermore one can see that the amplitude K and the relaxation time τ_{exp} are clearly influenced by the sucrose which leads to the different loop closure and dissociation rates as shown below.

Figure (4.5) shows the temperature dependence of the MR121-$P_3Q_6P_3$-W peptide as example FCS curves. One can see the small change in the diffusion time due to the change in viscosity of the solvent. Furthermore the changes to the amplitude K and the relaxation time τ_{exp} can be seen here too. The MR121-$P_3N_2Q_2NYP_3$-W peptide shows similar FCS curves.

In figures (4.6) and (4.7) one can see the results of these measurements. The errorbars origin from the standard deviation of at least 3 independent measurements. The lines in these figures are linear fits through the datapoints. The Y-intercept of these fits corresponds to the internal friction of the loop formation kinetic of the respective peptide (see 2.6). One can observe that the linear fits move downwards and the Y-intercepts decreases. For a temperature of 50°C the glutaminerich peptides behave similar to the MR121-$P_3(GS)_3P_3$-W peptide at 20°C which has a length of 13 amino acids and therefore is a good comparison

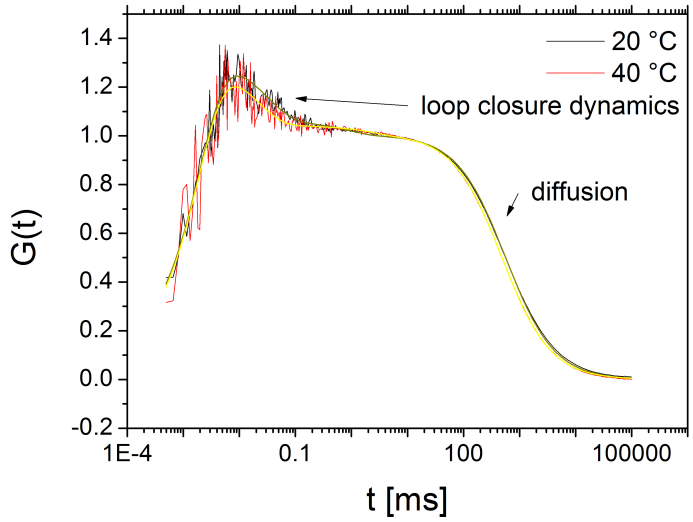

Figure 4.5: This figure shows examples of FCS curves of the MR121-$P_3N_2Q_2NYP_3$-W at two different temperatures. The yellow lines denote the fits that were done as explained in section (3.3).

to the glutaminerich peptides which also have a length of 13 amino acids. This shows that at this temperature the glutaminerich peptides behave like unstructured, fully flexible amino acid chains.

Figure (4.8) shows the Y-intercepts of the linear fits from the measurements presented above. In addition to the glutaminerich peptides the Y-intercepts of the MR121-$P_3(GS)_3P_3$-W were depicted for a better comparison. The lines are linear fits for visualization purposes only. The error bars are the errors computed by the linear fits of above. Both glutaminerich peptides show a significant internal friction contribution to the loop formation kinetic which decreases linearly with higher temperatures. One can observe that the internal friction contribution has a value of zero within the error bars for a temperature of 50°C which corresponds to the observation from above where one could see that the glutaminerich peptides at 50°C behave similar to unstructured peptides at 20°C. This is true for poly (GS) peptides of various lengths (see [KFB$^+$03] [NLDS07]).

Another value that can be studied is the dissociation rate of the tryptophan-dye complex k_-. It can be evaluated exactly as the loop closure rate k_+, as can be seen above. An example of the dissociation rates in sucrose for two temperatures

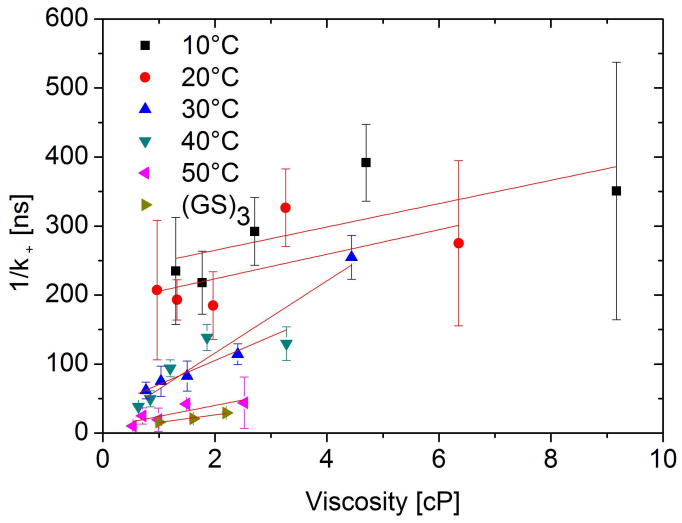

Figure 4.6: The inverse loop formation rate $1/k_+$ of the MR121-$P_3N_2Q_2NYP_3$-W measured in sucrose solutions from 10% (w/v) to 40% (w/v) for different temperatures. The lines denote linear fits through the datapoints. The error bars origin from the standard deviation of at least three independent measurements. The triangles pointing right denote the exact same measurement with the MR121-$P_3(GS)_3P_3$-W peptide.

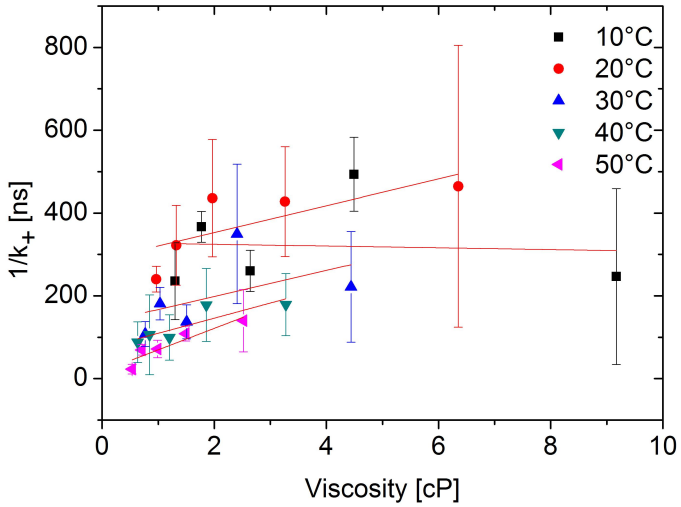

Figure 4.7: This figure depicts the same measurement as in figure (4.6) for the MR121-$P_3Q_6P_3$-W peptide. It shows the inverse loop formation rate $1/k_+$ in dependence of the viscosity of the solvent and for different temperatures (10% to 40% (w/v) Sucrose in the solution to alter the solvent viscosity). The lines denote linear fits through the datapoints and the errorbars origin from the standard deviation of at least three independent measurements.

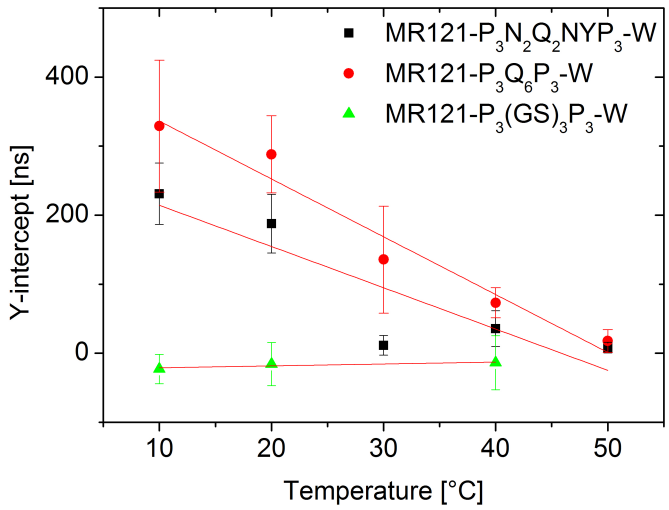

Figure 4.8: This figure shows the Y-intercepts from the linear fits of figures (4.6) and (4.7). The errorbars origin in the errors of the linear fits of the inverse loop formation rate $1/k_+$ versus the viscosity of the solvent (see figures (4.6) and (4.7)).

can be seen in figure (4.9). One can clearly see the linear dependence of the data and that a significant Y-Intercept exists. Figure (4.10) shows all Y-Intercepts of the dissociation rate. One can see that the influence is much smaller as in the case of the loop closure rate. Additionally it seems to be the case, that the internal friction for the dissociation rate follows a similar linear trend as the loop formation rate and decreases with rising temperature.

The Y-intercepts for the loop closure rate k_+ and dissociation rate k_- both decrease with higher temperatures. This indicates a temperature dependent internal friction for both rates. The internal friction is significantly smaller for the dissociation rate of both glutaminerich peptides. In a microscopic picture this may indicate stiff peptides because the dissociation is hindered less than the loop closure. Higher temperature then leads to a behavior that is more like fully flexible peptides.

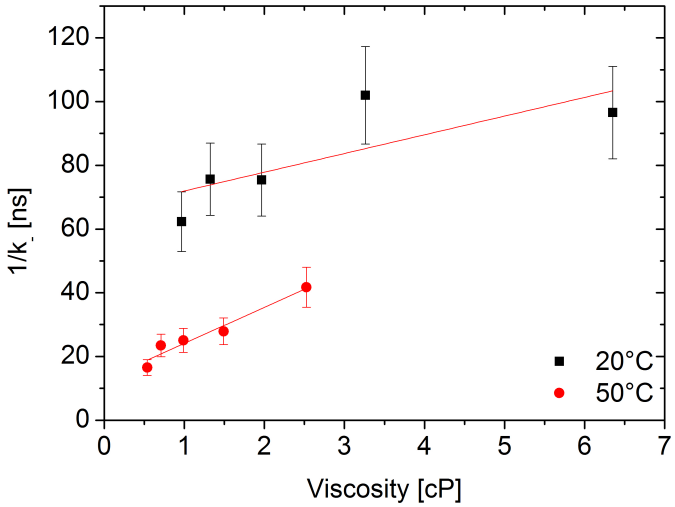

Figure 4.9: This figure shows examples of the inverse dissociation rate of MR121-$P_3Q_6P_3$-W at two temperatures in sucrose. The solid lines are linear fits through the data points from which the Y-intercept represents the internal friction.

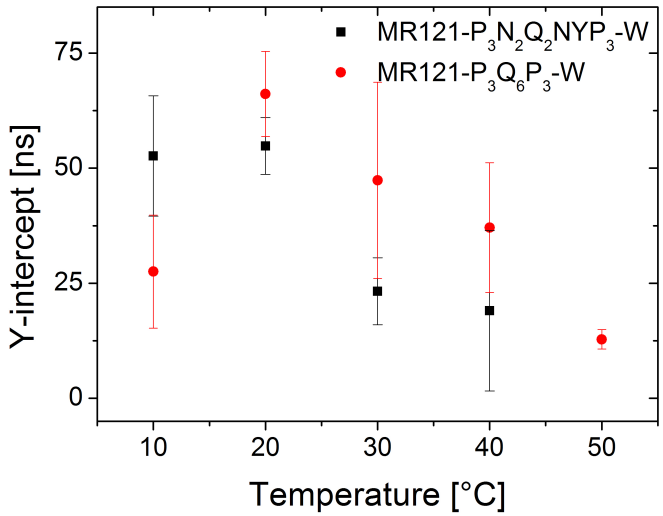

Figure 4.10: Here one can see the Y-intercepts of the inverse dissociation rate $1/k_-$ for both glutaminerich peptides. The error bars origin from the linear fits of the inverse dissociation rate $1/k_-$ versus the viscosity of the solvent.

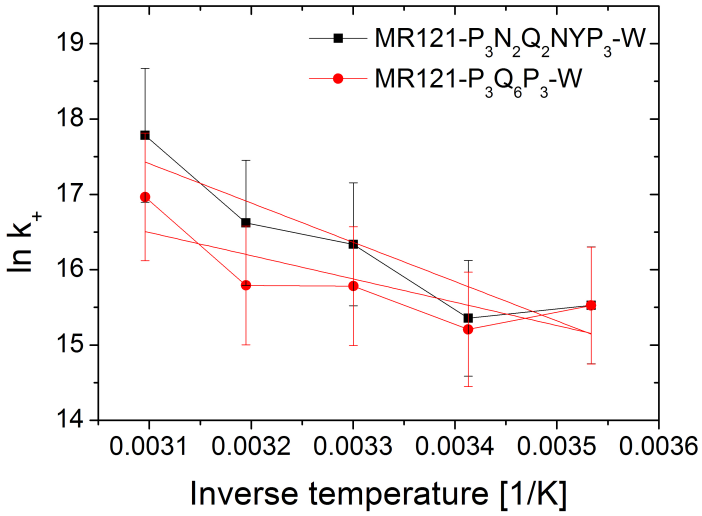

Figure 4.11: This figure shows the logarithm of the loop closure rate k_+ in dependence of the inverse temperature for both glutaminerich peptides. The error bars origin from the fitting of the FCS data. This are Arrhenius plots that show a sufficient linearity to fit this data with a linear model to extract the Arrhenius activation enthalpy ΔH_a. As examples were chosen the data of both peptides without sucrose.

4.2.2 The activation enthalpy of glutaminerich peptides

In our model the loop closure is a two step process and accordingly there exists an energy barrier that has to be overcome. The Arrhenius plot consists of the logarithm of the loop closure rate k_+ or the dissociation rate k_- versus the inverse temperature. Figure (4.11) shows the Arrhenius plots for the loop closure rate for both glutaminerich peptides. As one can see both data sets are sufficiently linear.

Figure (4.12) shows the Arrhenius activation enthalpy ΔH_a of the loop closure process (See (2.3)) in dependence of the viscosity of the solvent (in units of sucrose content in weight per volume percentages) that was obtained by the respective Arrhenius plots as shown exemplary in figure (4.11). The error bars origin from the linear fits of the respective Arrhenius plots. One can clearly see that the activation enthalpy ΔH_a decreases linearly with increasing sucrose con-

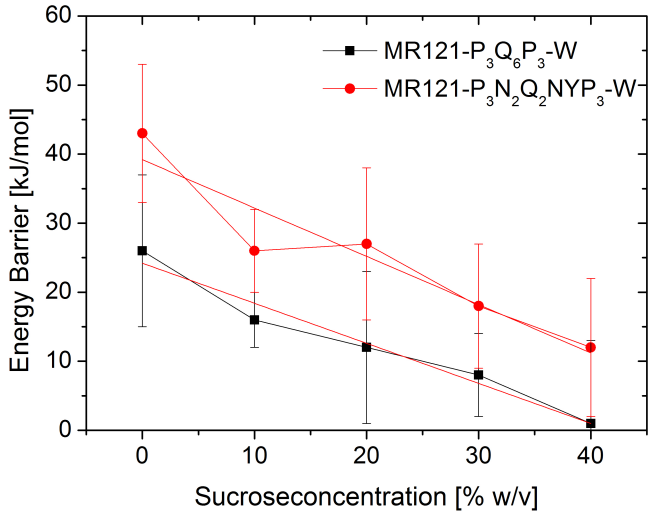

Figure 4.12: This figure shows the Arrhenius activation enthalpy ΔH_a of the loop closure rate k_+ in dependence of the sucrose concentration of the solvent in percentages of weight per volume. The error bars origin from the linear fit of the Arrhenius plots (see (2.3)).

centrations. At 40 % sucrose (w/v) the energy barrier to overcome loop formation is lowered for both cases by approximately 25 kJ/mol. Additionally the energy barrier is significantly higher for the MR121-$P_3N_2Q_2NYP_3$-W as for the MR121-$P_3Q_6P_3$-W peptide despite having a similar structure. This finding is somewhat counterintuitive because one may think that sucrose makes loop formation slower and the energy barrier higher. Indeed, loop formation is slower for high sucrose concentrations what can be seen in figures (4.6) and (4.7). This leads to the conclusion that sucrose slows down the loop closure rate by the change in viscosity but also lowers the activation enthalpy of the loop closure by interacting with the glutaminerich peptides. Another possibility for this behavior is that the internal friction of the loop closure is viscosity dependent.

As can be seen in figure (4.13) the energy barrier of the dissociation process is largely unaffected by sucrose for both peptides. This might indicate that the source of the internal friction is different from the loop closure.

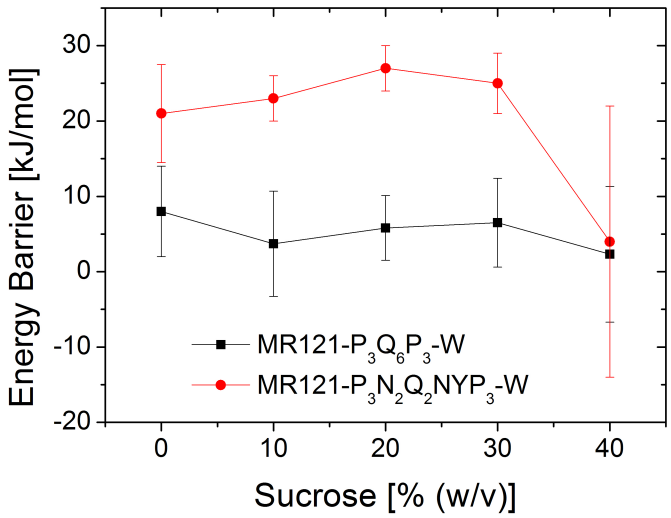

Figure 4.13: As in figure (4.12) one can see here the Arrhenius activation enthalpy ΔH_a, but here from the dissociation process k_- in dependence of the viscosity of the solvent in percentages of sucrose (w/v). The errorbars origin from the linear fits of the Arrhenius plots.

4.2.3 Thermodynamic evaluation of peptides

One can now further evaluate the data by van´t Hoff analysis (see section (2.3.2), [vH84]). This means that one looks at the equilibrium constant of the two state process and looks at the temperature dependence of it. More exactly the natural logarithm of the equilibrium constant is plotted against the inverse temperature. If it is temperature independent one obtains a linear behavior which can be fitted. For the MR121 tryptophan pair this values are known [DNS05] from ensemble measurements. In this bimolecular case the entropic contribution to the Gibbs Free Energy is $\Delta S = (3.2 \pm 0.1) \cdot 10^{-2} \frac{kJ}{K \cdot mol}$ and the enthalpic contribution is $\Delta H = (-20.8 \pm 0.2) \frac{kJ}{mol}$. So the Gibbs Free Energy results in $\Delta G = (-29.5 \pm 0.4) \frac{kJ}{mol}$. Note that the entropic contribution has a positive sign and the enthalpic contribution a negative sign which leads to a negative Gibbs energy. This means that in the microscopic level the solvent is the driving mechanism in the loop closure dynamic by Brownian motion and collisions of the solvent molecules, so the solvent does work on the system. The van´t Hoff analysis for the MR121-

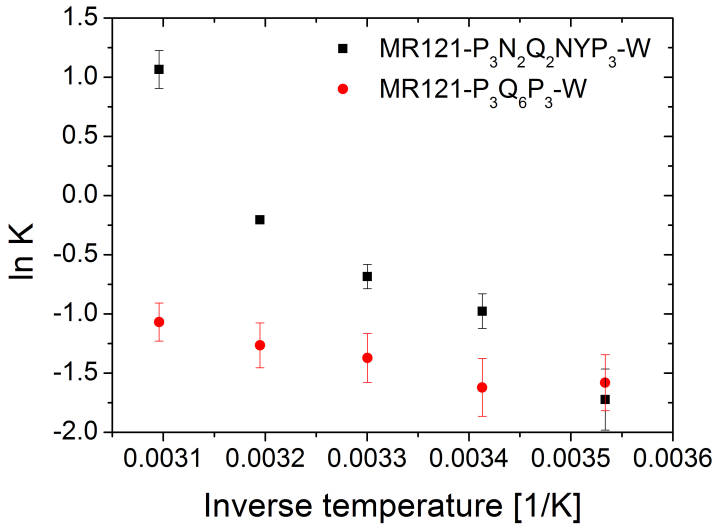

Figure 4.14: This figure shows the logarithm of the equilibrium constant plotted versus the inverse temperature in Kelvin. An exemplary data set from each glutaminerich peptide is shown. The errors origin from the fitting of the FCS curve. Both plots show a linear behavior which is due to the independency of the equilibrium constant from the temperature.

$P_3Q_6P_3$-W and the MR121-$P_3N_2Q_2NYP_3$-W were done in several concentrations of sucrose (0 % to 40 % (w/v)). The equilibrium constant was obtained from FCS measurements (see 3.3). Figure (4.14) shows the logarithm of the equilibrium constant versus the inverse temperature, so a van´t Hoff plot. An exemplary data set is shown for both glutaminerich peptides. One can see that both curves show a sufficient linearity that shows that the equilibrium constant is temperature independent and so enables us to determine the thermodynamic values from the slope and the Y-intercept of a linear fit (see (2.3.2)).

The values of the van´t Hoff analysis of these measurements can be seen in tables (4.1) and (4.2). One can see that for both peptides the signs of the values for the ΔS, ΔH and ΔG are reciprocal to the values for the bimolecular measurements of MR121 and tryptophan. But the ΔG is in the same order of magnitude. The reversal of the sign of the enthalpic and entropic contributions is an interesting fact. But one does not know if the reason for this lies in the labeling of the dye to a peptide per se or if the glutaminerich peptides are some-

Sucrose percentage	ΔS	ΔH	ΔG
% (w/v)	$kJ/mol \cdot K$	kJ/mol	kJ/mol
0	-0.154	47.8	94.0
10	-0.021	7.9	14.2
20	-0.088	27.5	53.9
30	-0.058	19.1	36.5
40	-0.074	25.6	47.8

Table 4.1: The thermodynamic values for the MR121-$P_3N_2Q_2NYP_3$-W peptide in sucrose

Sucrose percentage	ΔS	ΔH	ΔG
% (w/v)	$kJ/mol \cdot K$	kJ/mol	kJ/mol
0	-0.008	5.8	8.2
10	-0.026	10.6	18.4
20	-0.023	10.4	17.3
30	-0.002	4.2	4.8
40	+0.016	-8.1	12.9

Table 4.2: The thermodynamic values for the MR121-$P_3Q_6P_3$-W peptide in sucrose

Number of (GS) repeats	ΔS	ΔH	ΔG
	$kJ/mol \cdot K$	kJ/mol	kJ/mol
5	0.042	-13.7	-26.3
7	0.035	-11.4	-21.9
9	0.061	-18.4	-36.7
12	0.052	-15.4	-31.0
15	0.075	-19.2	-41.7

Table 4.3: The thermodynamic values for the MR121-$(GS)_x$-W peptides for x=5,7,9,12 and 15.

how special. Therefore we did van´t Hoff analyses for Glycine-serine peptides of lengths ranging from 11 amino acids to 31 amino acids analogical to the glutaminerich peptides. Table 4.3 shows the results of these measurements. One can see that the signs of the enthalpic and entropic contributions are the same as in the bimolecular case. For the Glycine-serine peptides the order of magnitude is the same. But the ΔS values, and therefore the ΔG values are larger than in the bimolecular case. This implies, that the labeling of the dye to the Glycine-serine peptides does not alter the complex building considerably and it shows again that the loop closure of Glycine-serine peptides is not hindered by the side groups of the amino acids.

The next step is to determine if the elongation of the peptides with the three proline residues changes the thermodynamic values. We saw above that the internal friction of the MR121-$P_3(GS)_3P_3$ is not changed by the proline elongation. The Arrhenius activation enthalpy was investigated and it was found a value of $\Delta H_a = (16 \pm 0.4)\frac{kJ}{mol}$ without a correction to the viscosity for fitting reasons. This is in good agreement with the not elongated Glycine-Serine peptides that show the same value. It is the value that has its origin in the molecular diffusion in water and shows that the loop closure dynamic is purely viscosity driven. The evaluation of the van´t Hoff data shows the following values for the proline elongated peptide: $\Delta S = -0.047\frac{kJ}{mol \cdot K}$ and $\Delta H = 12.2\frac{kJ}{mol}$ which leads to a Gibbs free energy of $\Delta G = 26.4\frac{kJ}{mol}$. This shows that the changes in the thermodynamic values stem from the elongation of the peptides with the proline residues. So in

conclusion, the elongation of peptides with three proline residues does not alter the internal friction behavior or the Arrhenius activation enthalpy but the thermodynamic values are changed significantly and this means that the equilibrium is shifted from the favorable loop closure to the favorable dissociation by the proline elongation.
One further observation is that the Gibbs free energy is bigger for almost all sucrose percentages for the MR121-$P_3N_2Q_2NYP_3$-W than for the MR121-$P_3Q_6P_3$-W. This is true for the Arrhenius activation enthalpy too. So the energy landscape for the MR121-$P_3N_2Q_2NYP_3$-W is rougher than for the MR121-$P_3Q_6P_3$-W.

These results show that it is possible to determine the energy landscape of short peptides with the presented measurement methods. The energy landscape meant here is composed from the Gibbs free energy and the Arrhenius activation enthalpy. With this information it is possible to draw a picture of a kramerslike two state model with the Arrhenius activation enthalpy as the hill to overcome in between the initial and end states that are energetically separated by the Gibbs free energy. Furthermore it shows that glutaminerich peptides behave significantly different than Glycine-serine peptides. They show internal friction and have a higher Arrhenius activation enthalpy than the Glycine-Serine peptides. Furthermore the change from a pure glutamine peptide to a peptide with asparagine residues changes the energy landscape of the loop closure dynamic considerably albeit a similar structure of glutamine and asparagine.
Lapidus et al investigated polyglutamine peptides with their tryptophan/cysteine contact quenching technique. Furthermore they simulated the measurement with a Monte Carlo algorithm. The model for the peptide was a wormlike chain model. They measured polyglutamines with different lengths and found for the one with 7 glutamine residues a loop closure rate of $2.45 \cdot 10^6 \frac{1}{s}$. This is in good agreement with our findings that yielded a loop closure rate of $4.4 \cdot 10^6 \frac{1}{s}$. Additionally they found a persistence length of $\approx 13.0\,\mathring{A}$ which is a large value compared to other peptides. They conclude that polyglutamine peptides are stiff molecules. This stiffness could be the reason for the high Arrhenius activation enthalpy and the internal friction that we found with our method.

4.2.4 Characterization of protein turns

So called beta turns are an important part of proteins that can have a great influence on the folding characteristics. As can be seen in section 4.2 we are able to investigate fast end to end contact dynamics for short peptides. Protein turns are usually in the order of only a few amino acids and therefore the end to end contact formation can be very fast. Our method is suited to investigate this. This can be seen in figure (4.15) where examples of FCS curves are depicted. The first difference to the other FCS data is, is that this curves were recorded without the DPC-230 correlator card. Therefore the time resolution is smaller. One can see that the diffusion time is shifted to longer diffusion times due to the higher viscosity of the solvent. The yellow lines denote the fits that were made as explained in section (3.3) but without the antibunching term. One can see the influence of the sucrose on the amplitude and relaxation time of the loop closure dynamics.

As mentioned in section 2.8 the turn sequence DDATKT is an important part of the immunoglobulin binding protein G from streptococcus [SZO$^+$09]. We modified it in the following way to be able to monitor the end to end contact formation dynamics for this turn. The N-terminus was modified with MR121 and at the C-terminus was a tryptophan residue added. Furthermore the second aspartic acid was changed to a proline residue. So the peptides were in detail the MR121-DDATKT-W and MR121-DPATKT-W. We did the same thermodynamic measurements as in the case of the glutaminerich peptides. From these we obtained the Arrhenius activation enthalpy ΔH_a for the end to end contact formation rate k_+ and from the van´t Hoff analysis were the Gibbs free energy ΔG obtained additionally to the entropic (ΔS) and enthalpic (ΔH) contributions. Furthermore the turns were investigated in regards of internal friction (see 2.6).

At first we looked at the viscosity dependence of the loop formation rate k_+ to investigate the internal friction of the turns. Figure (4.16) shows $1/k_+$ versus the viscosity of the solvent. As a solute to increase the viscosity sucrose was added up to a rate of 40 % (w/v). The data set shows a good linearity which enables us to fit a linear model to the data. The Y-intercept then yields the internal friction. Figure (4.16) is an example data set that shows the measurability of

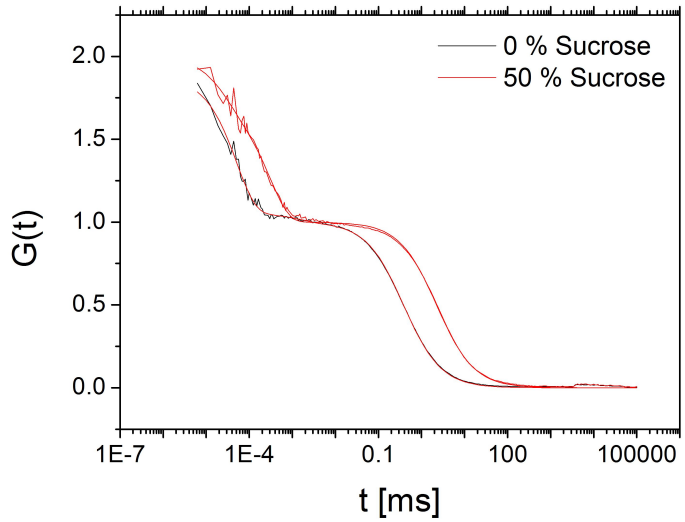

Figure 4.15: This figure shows examples of FCS curves of the DDATKT turn sequence measured in different sucrose concentrations. The measurements were done without the DPC-230 correlator card which limits the time resolution. The yellow lines denote the fits that were made as explained in section (3.3) but without the antibunching term.

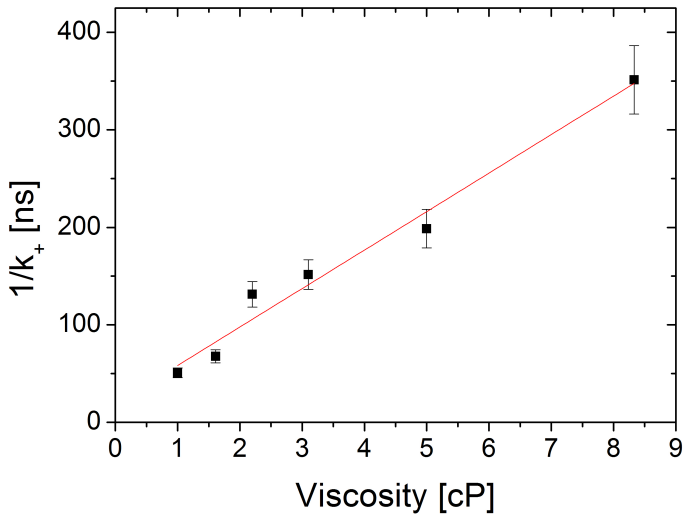

Figure 4.16: This figure shows the inverse loop formation rate $1/k_+$ versus the viscosity. The data set shows a good linearity that enables the fitting of the data with a linear model. The Y-intercept of the linear curve represents the internal friction.

internal friction with the turn sequences.

It was found that both turn sequences show a significant internal friction contribution. The MR121-DDATKT-W has a Y-intercept at $(1.7 \pm 0.3) \cdot 10^{-8}$ s and the MR121-DPATKT-W even showed a Y-Intercept of $(2.3 \pm 0.4) \cdot 10^{-8}$ s measured at 20°C. This is a significant internal friction contribution but it is one order of magnitude smaller than in the case of the glutaminerich peptides.

After investigating the viscosity dependence Arrhenius plots were made to determine the activation enthalpy ΔH_a of the loop closure dynamic of the turns. Figure (4.17) shows a sample data set that demonstrates a good linearity of the Arrhenius plots and indicates that the activation enthalpy is not temperature dependent (see 2.3.1).

The Arrhenius activation enthalpy ΔH_a supports the view that both turns have some barrier to cross in addition to the solvent viscosity because they have a viscosity corrected value of $(27 \pm 6.6) \frac{kJ}{mol}$ for the original turn and $(9.7 \pm 4.2) \frac{kJ}{mol}$ for the mutated turn measured in the standard buffer solution without sucrose.

Figure (4.18) shows that, like the previous figures, the van´t Hoff plots show a

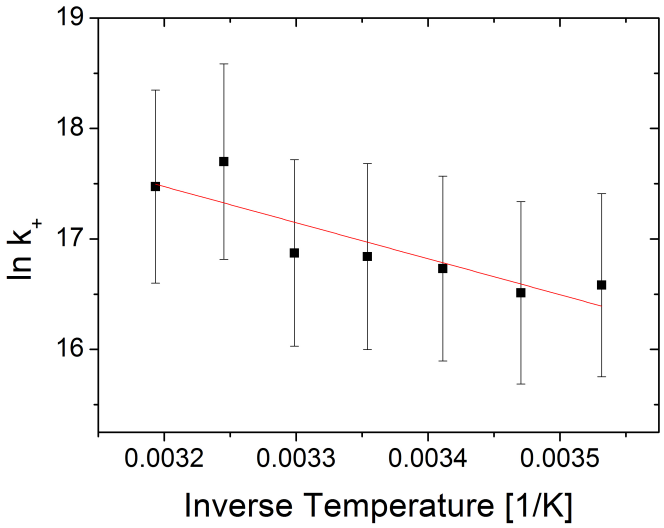

Figure 4.17: This figure shows the Arrhenius plot of the MR121-DDATKT-W turn. The data set shows enough linearity to fit a linear model to the data and extract the activation enthalpy ΔH_a from the slope of the fit.

good linearity too and enable us to extract the thermodynamic values from the data (see 2.3.2). After evaluating the data via the van´t Hoff analysis the following values have been obtained. The original turn has an entropic contribution ΔS of $(-0.006 \pm 0.017)\frac{kJ}{K \cdot mol}$ and an enthalpic contribution ΔH of $(0.3 \pm 5.2)\frac{kJ}{mol}$. This results in a Gibbs free energy ΔG of $(2.1 \pm 10.3)\frac{kJ}{mol}$. This value is a small value and has a positive sign, like the glutaminerich peptides ($\Delta G = 94\frac{kJ}{mol}$ and $\Delta G' = 8.2\frac{kJ}{mol}$ respectively). This could imply that parts of the turn sequence are stiff like the proline elongation in the MR121-$P_3(GS)_3P_3$-W. The mutant with the proline residue behaves more like an intrinsically unstructured fully flexible peptide because it shows a negative Gibbs free energy of $(-17.6 \pm 3.1)\frac{kJ}{mol}$ which consists of a ΔS of $(0.028 \pm 0.005)\frac{kJ}{K \cdot mol}$ and a ΔH of $(-9.2 \pm 1.6)\frac{kJ}{mol}$ ($\Delta G = -26.3\frac{kJ}{mol}$ for the MR121-$(GS)_5$-W peptide). These values are both smaller than the values for the Glycine-serine peptides. This implies that the mutant is not as flexible as them but comes close to this. Additionally it shows, that the proline residue considerably changes the end to end contact behavior of the turn sequence. This result shows that the original turn structure is not just a random sequence but is important for building of the secondary structure of the B3 domain of the im-

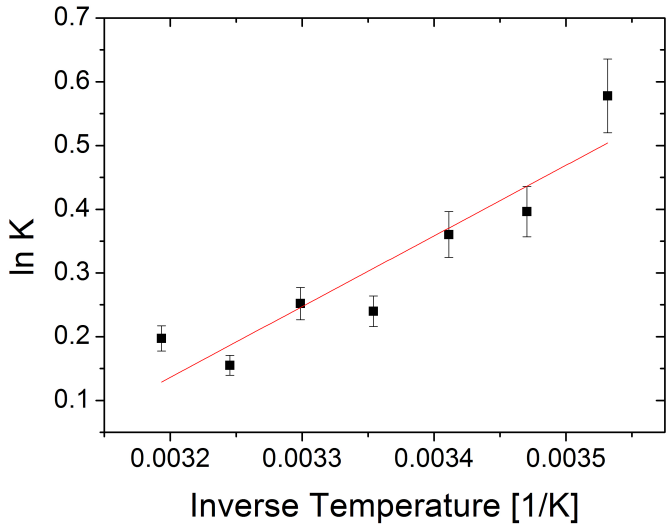

Figure 4.18: This figure shows the logarithm of the equilibrium constant K plotted versus the inverse temperature, so a van´t Hoff plot. Like above the linearity of the data is good and it enables us to extract the thermodynamic values by fitting the data with a linear model.

munoglobulin binding protein G. Maybe it introduces a kink in the protein chain which makes building of a β-sheet faster. Furthermore this result shows how important β-turns are for the structure of a protein and that minor mutations might alter the folding behavior of a given protein considerably. Additionally we were able to show that our method can report on the loop closure dynamics of turns.

4.3 The influence of the salt bridge on Tryptophan Cage folding

The Tryptophan Cage (TC) miniprotein presents an ideal model system to study folding pathways [NDS05] . This is because it is short (20 amino acids) and folds rapidly ($\approx \mu$s). It shows secondary structures and a salt bridge between two of these structures (α-helix and Polyproline helix). Theoretical studies could not draw a comprehensive picture of the influence of the salt bridge (see section

(2.7)). The goal of this work was to shed light on this issue and measure the influence of the salt bridge.

4.3.1 Does the label destabilize the TC?

It is essential to make sure that the changes that are introduced to the TC do not change the folding behavior significantly. It would be possible that the dye with which the TC is labeled stabilizes or destabilizes the folding by sterically hindering the motion of the amino acid chain or building complexes with amino acid side groups.

The first step was to determine the melting temperature of unlabeled TC as a benchmark for the stability of the miniprotein in its unperturbed form. To achieve this a CD spectrum was recorded as described in section (3.4). The sample concentration was approximately 0.4 mg/ml of the unlabeled TC and of the TCR16Q mutant. The spectra were measured in a temperature range from 10°C to 60°C in increments of 5°C. At every temperature the Θ_{221} value was determined from the respective CD spectrum, which is the Θ-value at a wavelength of 221 nm. This value is a measure for the α-helical contribution to the ensemble of states in the measurement and shows the folded fraction of TC in the solution. Figure (4.19) shows the Θ_{221} value in dependency of the temperature for both molecules. The values are normalized to the value at 60°C where almost all of the molecules are in the unfolded state. The inlay shows examples of respective CD spectra where the ellipticity Θ is plotted versus the wavelength. These curves were fitted with a sigmoidal model to determine the melting temperature of the molecules. For the TC a temperature of 36°C was seen. The TCR16Q mutant is a great deal less stable and exhibits a melting temperature of 8°C. This is a first strong hint, that the salt bridge, that is not present in the TCR16Q mutant, has a great influence on the stability of this miniprotein.

The next step was to determine the melting temperature of both molecules with the label. Unfortunately, the absorption of the dye in the UV range is high which would most probably overshadow the CD absorption. This stopped us from trying

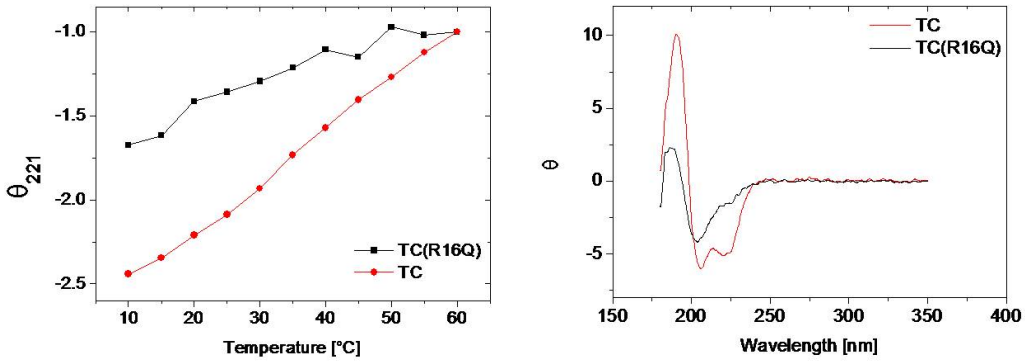

Figure 4.19: This figure shows on the left hand side the Θ_{221} value of the TC (blue) and the TCR16Q mutant (black) in dependency of the temperature. This value is a measure of the fraction of folded molecules in the solution. The melting temperatures are 36°C for the TC and 8°C for the TCR16Q. The right hand side shows examples of CD spectra for both molecules where the ellipticity Θ is plotted versus the wavelength.

this approach. Therefore fluorescence spectroscopy on the ensemble level was used (see (3.5 and 3.3)). To determine upper and lower borders for this measurements and to examine the influence of the temperature on the dye two more samples were measured at the same time as the TC and the TCR16Q (see (3.7)). The temperature range is from 5°C to 80°C. The fluorescence signal was normalized to the respective maximum of MR121 absorption to eliminate the influence of the sample concentration. This is equivalent to the respective quantum yield (QY, see(2.1.4)) of the dye that is attached to the respective molecule. Furthermore, the QY was then normalized to the TCW6F mutant that has no tryptophan residue and therefore does not quench the MR121 fluorescence. This was done to eliminate the influence of the temperature on the dye fluorescence. Figure (4.20) shows the result of this measurement: If one fits these curves with a sigmoidal growth model the melting temperature for the TC exhibits to be 35°C and for the TCR16Q mutant 14°C respectively. These values are in good agreement to the values that were measured in the CD measurements (36°C and 8°C respectively). This shows, that the label does not bear a significant influence on the folding characteristics of the TC and TCR16Q molecule.

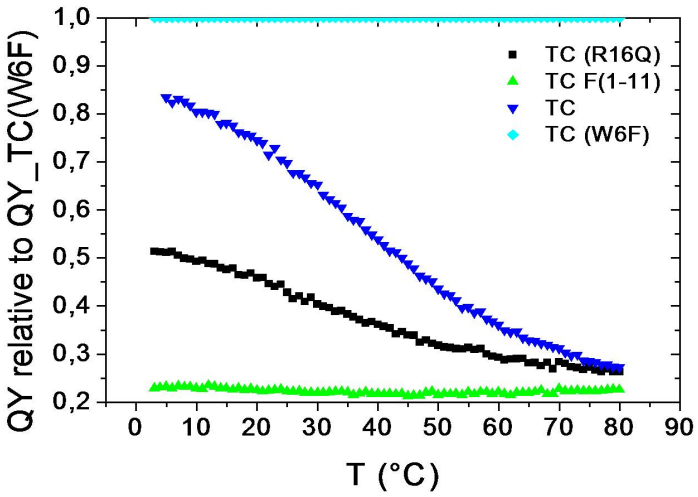

Figure 4.20: Ensemble measurement of the TC and the TCR16Q mutant. The signal was normalized to the fluorescence of the TCW6F mutant to eliminate the influence of the temperature on the MR121 fluorescence. The TC F(1-11) fragment does not exhibit a folded structure and so the tryptophan is always able to quench the MR121 fluorescence which strongly reduces its QY. Fitted to a sigmoidal model the melting temperatures are 35°C for the TC and 14°C for the TCR16Q mutant.

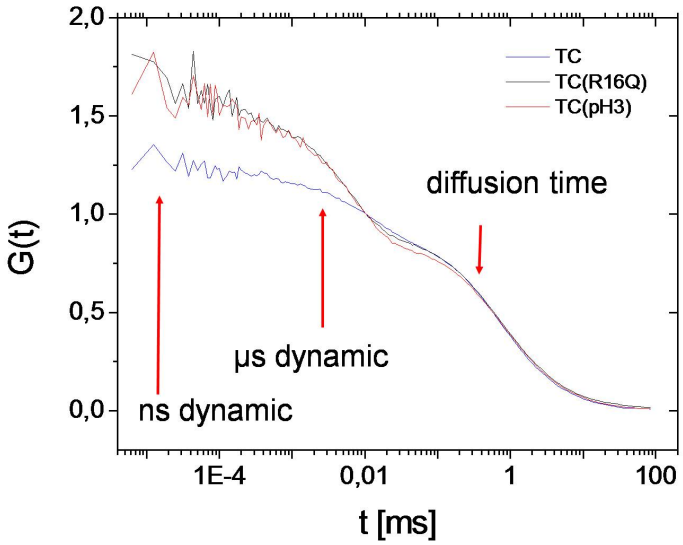

Figure 4.21: A typical FCS curve of the TC, TCR16Q and TC at pH of 3. The measurement was done without the DPC-230 correlator card which explains the comparatively poor time resolution. The arrows show where the typical time constants are for the respective dynamics of the TC and its mutant. The μs dynamic origins from the folding and unfolding and the ns dynamic is generated by the amino acid chain dynamics that lead to a quenching of the dye.

4.3.2 Measurement of folding dynamics of the TC

The next step was to determine the folding and unfolding times of the TC and his mutants (τ_f and τ_u respectively). This can be done by the PET-FCS technique (see (3.3)) because the folding and unfolding of the TC induces fluctuations in the fluorescence of MR121. In figure (4.21) typical FCS curves of the TC and TCR16Q are shown. Furthermore a curve is shown where TC was measured at a pH of 3. Both the TCR16Q and the measurement at a pH of 3 effectively remove the salt bridge from the miniprotein. The arrows in the picture show where the respective dynamics can be spotted in a FCS curve. The μs dynamic origins from the folding and unfolding of the TC and the ns dynamic is generated by the amino acid chain dynamics that leads to a quenching of the MR121 by the tryptophan residue. Figure (4.21) shows qualitatively that the folding dynamics of the TCR16Q and TC at pH 3 behave similar. Furthermore one can observe that

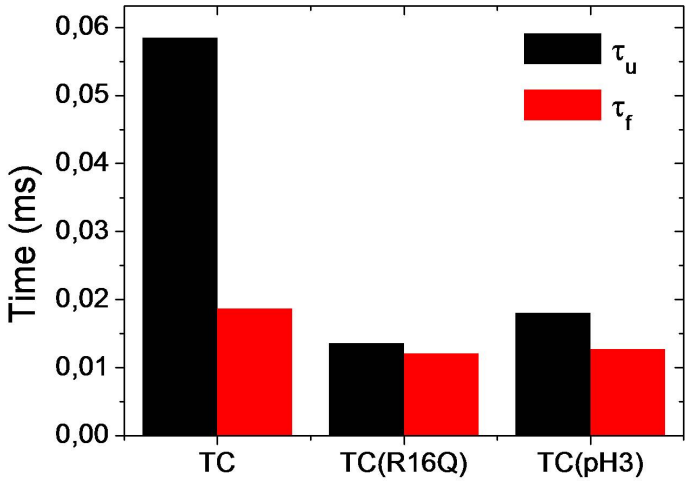

Figure 4.22: This figure shows the folding τ_f and unfolding τ_u times of the TC, TCR16Q and TC at pH3 respectively. One can clearly see that the removal of the salt bridge in the TC(R16Q) mutant and the TC at a pH of 3 reduce the unfolding time significantly and in the same order of magnitude. This shows that the salt bridge is essential for the stability of the TC.

the folding rate has to be smaller in comparison to the TC because the amplitude $K = \frac{k_u}{k_f}$ is bigger. One can now fit these curves and extract the folding times of dynamic in the way shown in section (3.3). To get the folding and unfolding times (τ_f and τ_u) one has simply to look at the inverse of the folding and unfolding rates (k_f,k_u). In figure (4.22) the result of this analysis are depicted. One can see, that the folding times are similar for all depicted proteins. This indicates, that the salt bridge does not influence the folding of the protein. If one now looks at the unfolding times it is obvious, that the removal of the salt bridge speeds up the unfolding of the protein tremendously. The unfolding occurs faster by a factor of 5 approximately. This indicates that the protein structure is largely destabilized by the removal of the salt bridge. Furthermore, the data shows that the source of the removal of the salt bridge is irrelevant and that the mutant accomplishes exactly that. So the salt bridge does not speed up the folding of the TC but it is essential for the high stability of the miniprotein.

4.4 Osmolyte influence on polymer dynamics and protein folding

Protein folding is in principle a spontaneous transfer from the unfolded amino acid chain to the folded configuration and structure. The driving force of this transition is the Gibbs free energy. To make life possible as we know it nature had to develop means to influence this transition. This is essential in order to be able to react to external stresses that influence the transition like heat, pressure or denaturants to name but a few. One answer to these stresses are organic osmolytes. These are small uncharged molecules that are able to regulate the cell volume and the solvent quality. The last point is the critical one for protein folding because the solvent quality plays a major role for the unfolded $\Leftrightarrow$ folded transition.

4.4.1 Unstructured peptides in osmolyte solutions

This section looks at the influence that organic osmolytes have on the loop closure dynamics of short unstructured peptides (see (2.9)). Therefore we have used the MR121-$(GS)_x$-W peptides because they are understood well [KFB$^+$03] [NLDS07] [Hud01] [LEH00].

At first we looked if TMAO exhibits an influence on the fluorescence of the dye MR121. Measurements of it at different temperatures and TMAO concentrations clearly showed no influence on the dye bar the change in solvent viscosity.

The next step was to look if TMAO has an effect on the MR121 tryptophan complex. Therefore bimolecular measurements were done in several concentrations of TMAO. The temperature was 20°C and the buffer solution was the standard measurement buffer (see (3.6)). To deduct the influence of viscosity changes, the contact formation and dissociation rates were compared to the diffusion time of the dye. It is directly linked to the viscosity of the solution. To compare the rates to the diffusion time all values have been normalized to the first value in the measurement row. Figure (4.23) shows the results of this measurement. As one can see, the rates are all only viscosity controlled and the TMAO does not have an additional influence on the complex formation of the reporter system.

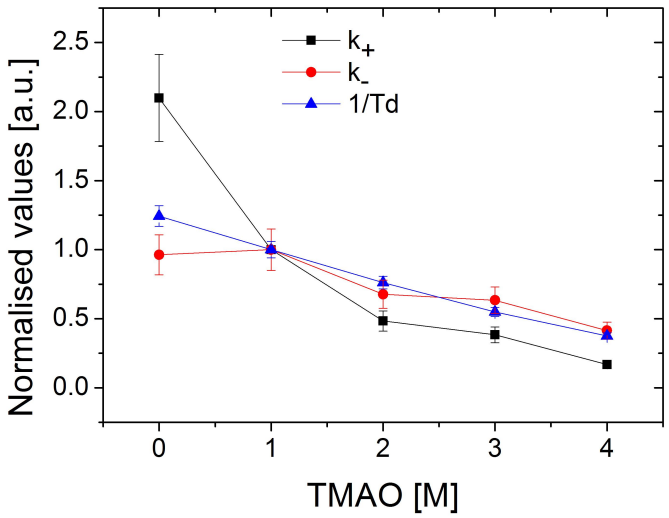

Figure 4.23: Bimolecular measurement of MR121 and tryptophan in the organic osmolyte TMAO normalized to the first value in the measurement row for easier comparison. In this instance k_+ denotes the formation rate of the MR121-tryptophan complex and k_- stands for the dissociation rate of the complex. T_d stands for the diffusion time of the dye through the detection volume.

Then we had a look at the MR121-$(GS)_9$-W peptide at different temperatures in a solution of 2 M TMAO. The temperature range was from 10°C to 40°C. One can see example FCS curves of the MR121-$(GS)_9$-W peptide at different temperatures in figure (4.24). The diffusion term is changed at different temperatures because of the change in viscosity. Both the amplitude and the relaxation time change which can clearly be seen. The FCS curves were fitted as explained in section (3.3). Additionally one can see in figure (4.25) the influence of TMAO on the FCS curves. The changes on the amplitude and the relaxation time are small compared to figure (4.24). The diffusion term is shifted because of the change in viscosity due to the addition of TMAO.

To fully characterize the influence of TMAO on the loop closure kinetics both the loop formation and the dissociation rate without and with 2 M TMAO were investigated. As one can see in figure (4.26) all rates are unaffected by TMAO over the whole temperature range.

One can now look at the MR121-$(GS)_9$-W at different TMAO concentrations

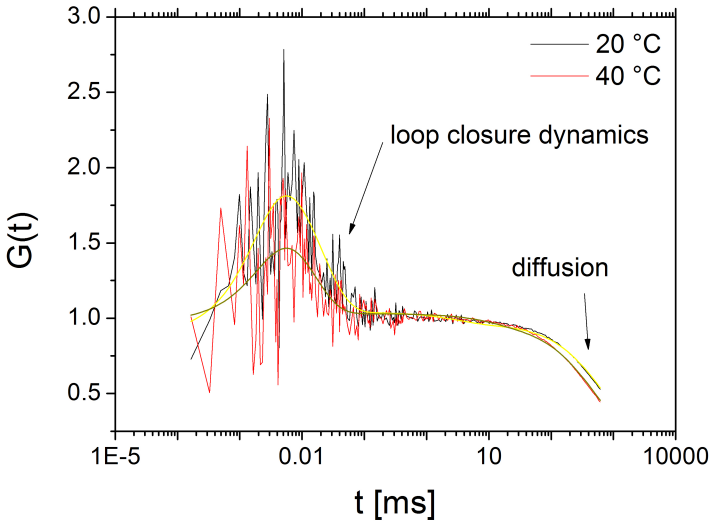

Figure 4.24: This figure shows examples of FCS curves of the MR121-$(GS)_9$-W for two temperatures. The yellow lines denote the fits that were made as explained in section (3.3).

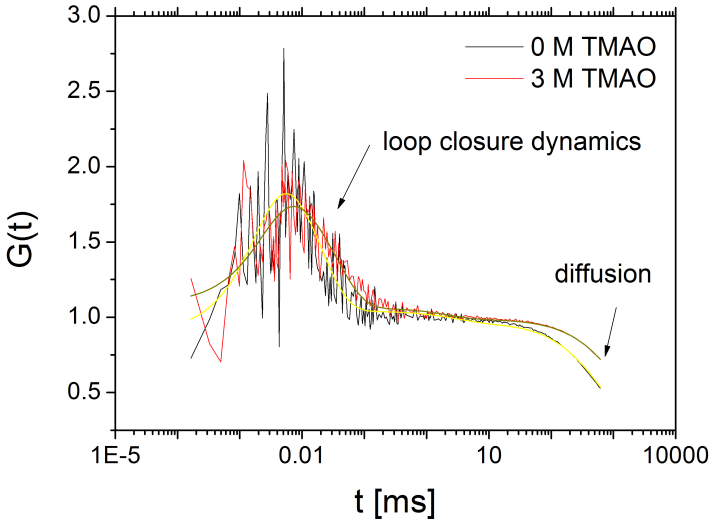

Figure 4.25: The topic of this figure are examples of FCS curves of the MR121-$(GS)_9$-W in two different TMAO concentrations. The yellow lines denote the fits that were made as explained in section (3.3).

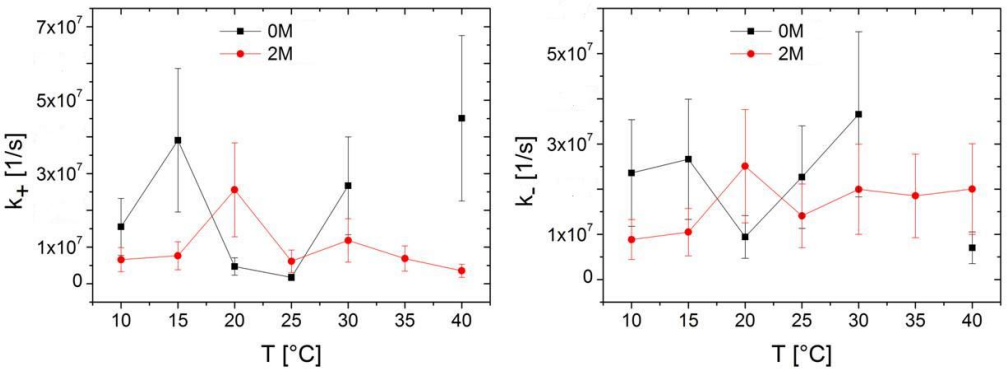

Figure 4.26: Loop closure k_+ and dissociation rates k_- of the MR121-$(GS)_9$-W peptide at different temperatures and in a concentration of 0 M and 2 M TMAO. The rates at all temperatures are unaffected by TMAO.

and compare it to the behavior in several sucrose solutions. Figure (4.27) shows these measurements and one can clearly see that TMAO does not have any additional effect on unstructured peptides besides the change in viscosity. The next step was now to see if this is true for peptides of different lengths. Therefore measurements were done in 0 M to 3 M TMAO with MR121-$(GS)_x$-W peptides where $x = 1, 3, 5, 9$ and 12. Figure (4.28) shows that loop closure k_+ and dissociation rates k_- are largely unaffected by the addition of TMAO to the solvent for all peptides of different lengths.
To finish the examination of the influence of osmolytes on unstructured fully flexible peptides we did the same measurements shown in figure (4.28) with 0 M to 3 M of GdHCl solutions. The results of these measurements are shown in figure (4.29). As in figure (4.28) one can see in figure (4.29) that the organic osmolyte GdHCl does not influence the loop closure dynamic of unstructured fully flexible peptides of various lengths.

To summarize all findings one can say, that organic osmolytes including denaturants and protecting osmolytes do not influence the reporter system and that they also have no impact on fully flexible unstructured peptides. This is a hint to the conclusion that organic osmolytes do not interact with the backbone of the peptide and so that the interaction of them with proteins is due to an inter-

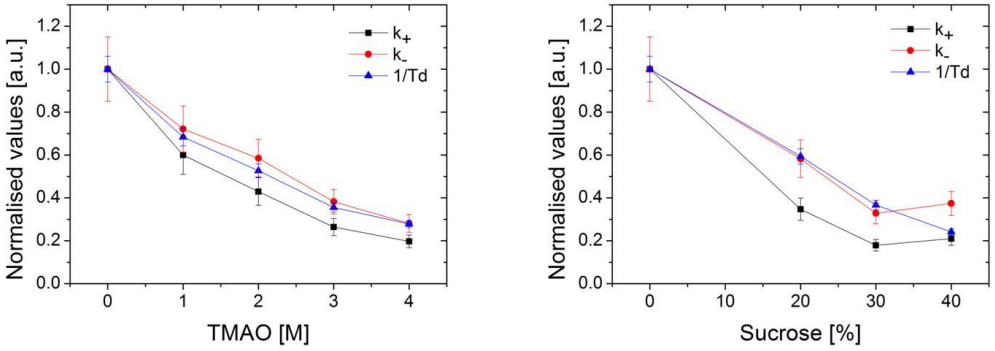

Figure 4.27: The left graph shows the MR121-$(GS)_9$-W in a solution of up to 4M TMAO. The loop closure k_+ and dissociation rate k_- are compared to the inverse diffusion time $1/Td$ that is directly linked to the viscosity of the solution. All values are normalized to the first measurement point (only measurement buffer solution). The right graph shows the same measurement variables for the MR121-$(GS)_9$-W in sucrose.

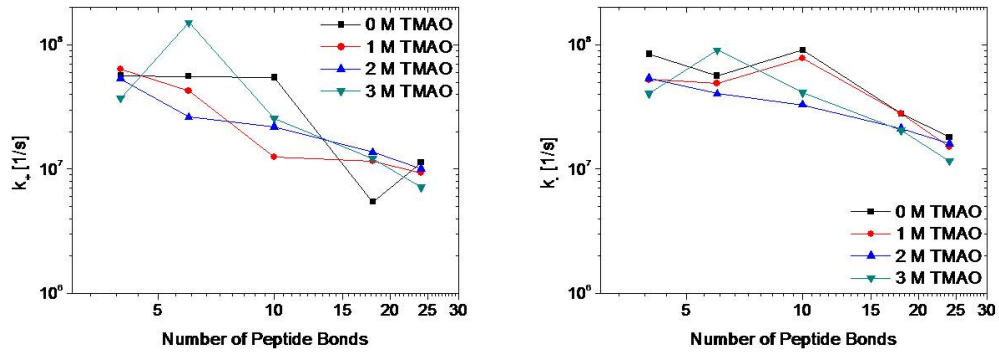

Figure 4.28: This figure shows the loop closure (k_+) and dissociation rates (k_-) of the MR121-$(GS)_x$-W with $x = 1, 3, 5, 9$ and 12. The measurements were done in concentrations of TMAO of 0M to 3M respectively.

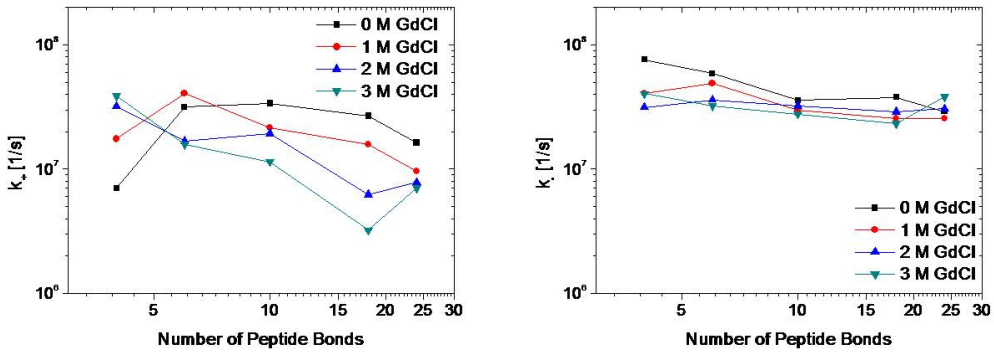

Figure 4.29: Depicted are the loop closure k_+ and dissociation rates k_- of MR121-$(GS)_x$-W peptides with $x = 1, 3, 5, 9$ and 12. The solution contained 0 M to 3 M of GdHCl.

action with the amino acid side groups of the protein. This is in contradiction to literature because it is assumed that osmolytes interact with the backbone considerably [BR08]. A possibility might be that the osmolytes show no effect on the Glycine-Serine peptides because they are intrinsically unstructured and behave like a fully flexible chain. Osmolytes change the solvent quality but for a fully flexible, unstructured chain the solvent quality seems to be unimportant regarding the loop closure dynamic.

4.4.2 Glutaminerich peptides in osmolyte solutions

As stated in section (4.4.1) organic osmolytes do not have an additional influence on the loop closure kinetic of unstructured peptides besides changing the viscosity of the solvent. This section discusses the influence of organic osmolytes on glutaminerich peptides. As an example peptide the MR121-$P_3N_2Q_2NYP_3$-W was measured in GdHCl and TMAO (see (2.9) and(3.7)). To distinguish the effects of the osmolytes from the simple change in viscosity the peptides were additionally measured in a sucrose solution of the same viscosity. As reference the MR121-$(GS)_9$-W was used. Figure (4.30) shows the loop closure k_+ and dissociation rates k_- for both chosen peptides. They are directly compared to the respective rates in a sucrose solution with the same viscosity to distinguish the osmolyte effect from the change in viscosity. The columns in the diagram that are

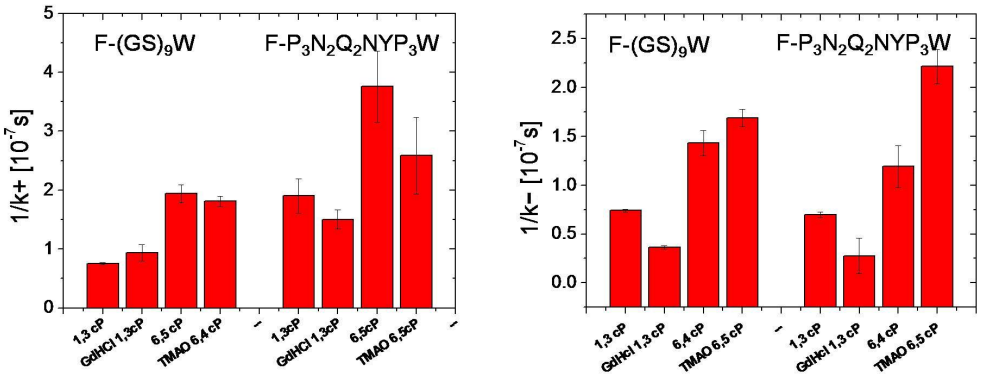

Figure 4.30: This figure shows the loop closure k_+ and dissociation rates k_- of the MR121-$P_3N_2Q_2NYP_3$-W and the MR121-$(GS)_9$-W peptides in different solutions. In both diagrams the left four columns show the MR121-$(GS)_9$-W peptide and the right columns the MR121-$P_3N_2Q_2NYP_3$-W. Then two columns directly compare the value of the measurement in sucrose to the one in GdHCl or TMAO respectively. Additionally the respective viscosity value is given. The error bars origin from the standard deviation of three independent measurements. The F in the description of the diagrams stands for fluorophore and corresponds to MR121 in this case.

only named with the appropriate viscosity value correspond to the measurements done in sucrose. In both diagrams the left four columns show the influence of the osmolytes on the unstructured MR121-$(GS)_9$-W peptide. One can see that the loop closure time $1/k_+$ of it is not influenced by the organic osmolytes significantly whereas the dissociation time $1/k_-$ is slightly reduced for the GdHCl and stays the same for TMAO. One can now compare this osmolyte fingerprint of the MR121-$(GS)_9$-W peptide to the one of the MR121-$P_3N_2Q_2NYP_3$-W peptide. It shows, that it behaves like the MR121-$(GS)_9$-W peptide in regards to the GdHCl. But TMAO changes both the loop closure time and the dissociation time of the MR121-$P_3N_2Q_2NYP_3$-W significantly. The loop closure is accelerated and the dissociation is decelerated.
This indicates that TMAO is able to stabilize a loop or hairpin like structure for a glutaminerich peptide as opposed to no influence on the loop formation kinetics of unstructured, fully flexible peptides.

4.4.3 Tryptophancage in osmolyte solutions

This section describes the effects that TMAO possesses on the folding of the tryptophan cage (TC) miniprotein. Therefore the TC was studied on the ensemble level and by FCS.
The first measurements were done in the ensemble level. Melting curves were recorded for the TC and the TC(R16Q) mutant in several TMAO concentrations. As can be seen in section (4.3) the removal of the salt bridge by the mutation destabilizes the Tryptophan Cage considerably. The measurements that can be seen in figure (4.31) were done in a temperature range of 5°C to 50°C. The concentration of TMAO was 0M, 1M and 3M respectively. The quantum yield (QY) is directly proportional to the fraction folded of the protein because in the folded conformation the dye is not quenched by the tryptophan (see section (2.7)). One can clearly see that the TMAO significantly stabilizes the folding of the TC. The stability loss by removing the salt bridge is countered by the TMAO that stabilizes the TC.
Figure (4.32) shows the melting curves of the TC for several TMAO concentrations in the ensemble level. The temperature range is from 10°C to 70°C and

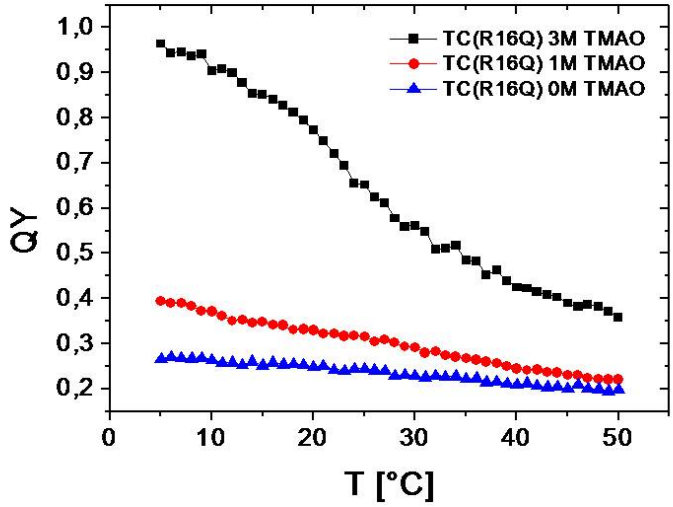

Figure 4.31: Ensemble level measurements of the TC(R16Q) mutant in a temperature range of 5°C to 50°C. The TMAO concentration was 0M, 1M and 3M respectively. The quantum yield (QY) is directly proportional to the fraction folded of the protein because in the folded conformation the dye is not quenched by the tryptophan (see section (2.7)).

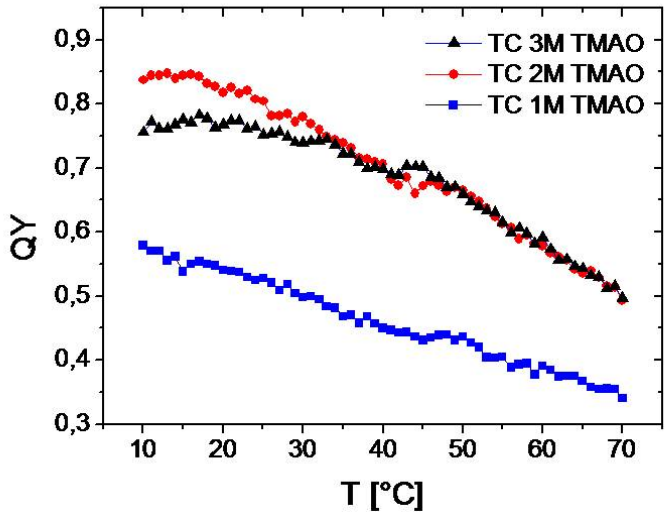

Figure 4.32: Measurement of the melting curve of the TC in TMAO (1M,2M,3M TMAO solution) for a temperature range of 10°C to 70°C. As in figure (4.31) the quantum yield is directly proportional to the fraction of folded proteins.

the TMAO concentration was 1M, 2M and 3M. One can see that TMAO also stabilizes the TC. But in contrast to the TC(R16Q) mutant the 3 M solution of TMAO does not yield a further stabilizing effect.

With FCS it is possible to determine the fraction of folded molecules F_f directly from the equilibrium constant K via $F_f = \frac{1}{1+K}$ (see (3.3)). Measurements of this value can be done in various different solvent conditions and temperatures. By this it is possible to determine melting temperatures of the TC in different TMAO concentrations. As can be seen in the examples FCS curves of the TC the folding dynamic is in a time range where the triplet dynamic is located too. Furthermore the triplet dynamic is influenced by TMAO and the triplet amplitude rises with increasing TMAO concentration. But the fits show that the triplet dynamic is separated enough from the folding dynamics so that it does not influence the fitting as can be seen in section (4.1).
The control samples were the TC F1 (Amino acids 1 to 11) and TC(W6F) fragment (see (3.7)). They were measured from 10°C to 40°C in solutions of 0M, 1M, 2M and 3M TMAO. Figure (4.33) shows a typical FCS curve of the TCF1. The

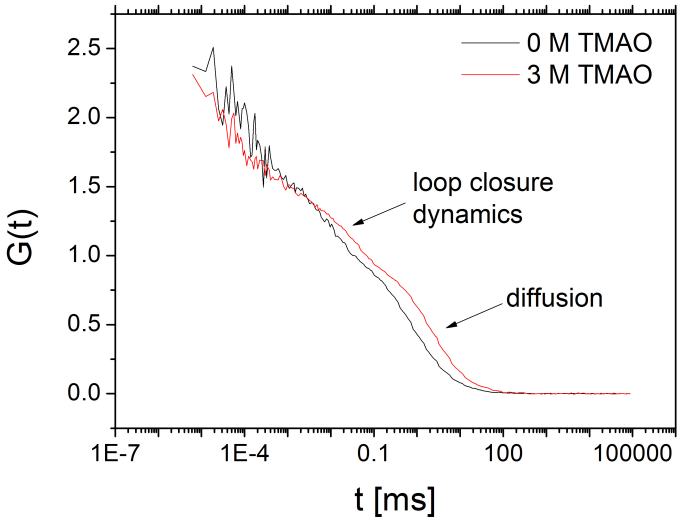

Figure 4.33: This figure shows examples of FCS curves of the TCF1 at a temperature of 20°C. The arrows indicate the typical timescales of the respective decays.

arrows indicate the typical timescales of the respective decays. One can see in figure (4.34) that the F_f rises over temperature without TMAO. This finding is in agreement with the measurements done for the MR121-$(GS)_7$-W peptides and it proves that the TCF1 behaves like an unstructured polypeptide chain. This can be seen in figure (4.35) where the fraction folded of the MR121-$(GS)_7$-W is depicted for different temperatures. Note, that the fraction folded also rises in this case. The reason for the rise of this parameter is, that with rising temperature the dissociation rate gets faster and so the equilibrium constant K gets smaller. This now leads to the rise of the fraction folded at higher temperatures. In this regard the name of this parameter is misleading. The rise of the fraction folded for the TCF1 is countered by TMAO what can be seen in figure (4.34).
If one now looks at the TC(W6F) in TMAO one can see a strange behavior. Normally, without a tryptophan residue, the dye should not be quenched and should not be significantly influenced neither by temperature nor by TMAO. But figure (4.36) shows that from a concentration of 2 M TMAO the F_f decreases which is unexpected. This means that the loop formation rate k_+ somehow increases. So the dye is quenched by some unknown mechanism. As can be seen in figure (4.37)

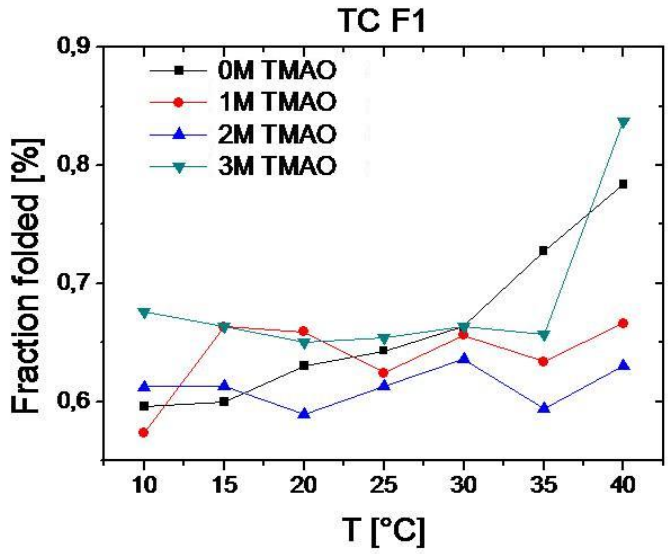

Figure 4.34: The TCF1 fragment melting curves for a temperature range from 10°C to 40°C. The fraction of folded molecules was determined from FCS measurements at three different TMAO concentrations (see (3.3)).

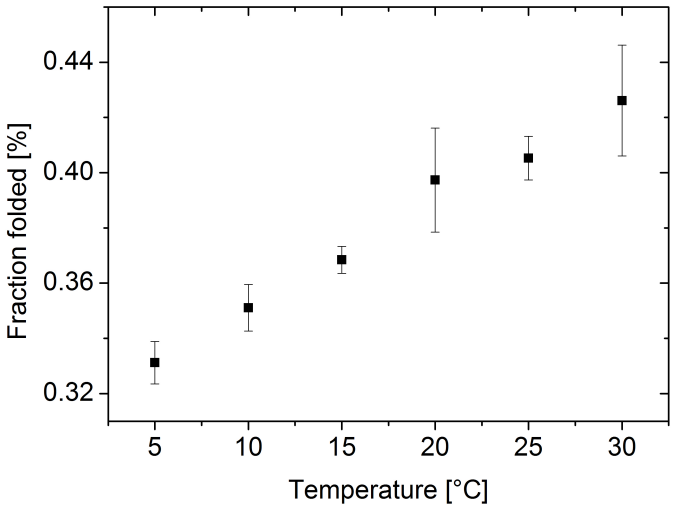

Figure 4.35: This figure shows the fraction folded for the MR121-$(GS)_7$-W at different temperatures. The errorbars origin from three independent measurements.

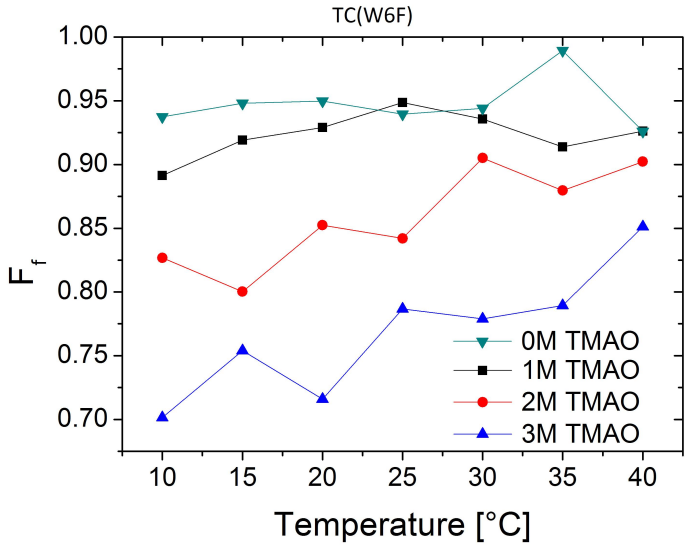

Figure 4.36: This figure shows the fraction folded F_f of the TC(W6F) versus the temperature for three different TMAO concentrations. From this curves the melting temperature can be determined by a sigmoidal fit.

the FCS curves also show that the TMAO significantly influence the TC(W6F). After the control samples the TC(R16Q) mutant will be discussed. Figure (4.38) shows the FCS curves of this mutant at a temperature of 20°C and for two different TMAO concentrations. One can clearly observe the change of the decay that corresponds to the folding transition. Figure (4.39) shows the TC(R16Q) mutant in TMAO. Depicted is the fraction of folded molecules F_f versus the temperature. One can see, that the TC(R16Q) without TMAO behaves like an unstructured polypeptide because the fraction of folded molecules rises with temperature which is also the case for the $(GS)_x$-W peptides. The reason for this behavior is that with rising temperature the dissociation rate of the complex rises faster than the loop closure rate. These are directly connected to the amplitude K via equation (3.2) and thus to the F_f value. The addition of TMAO changes this picture and the TC(R16Q) mutant behaves more like a folded protein which can be seen by the fact, that the fraction of folded molecules decreases which corresponds to a melting curve behavior of proteins. Furthermore the fraction of folded molecules significantly rises. This shows that TMAO is able to change the stability of the TC(R16Q) significantly.

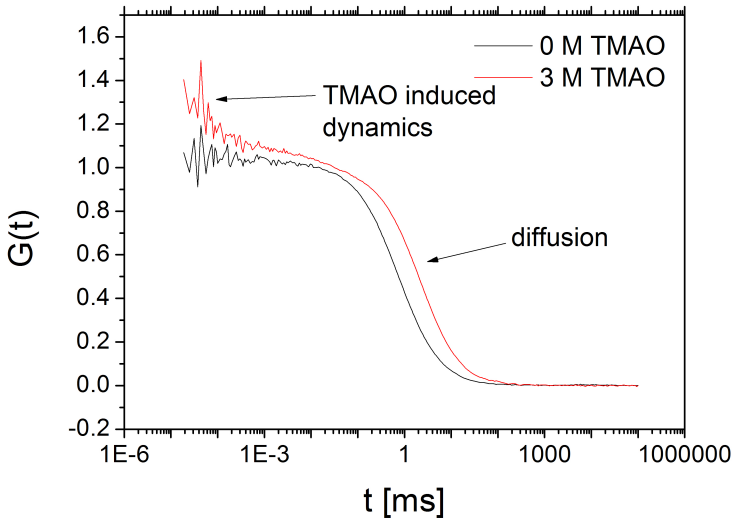

Figure 4.37: This figure shows examples of FCS curves of the TC(W6F) at 20°C and different TMAO concentrations. The arrows indicate the respective typical timescales of the decay.

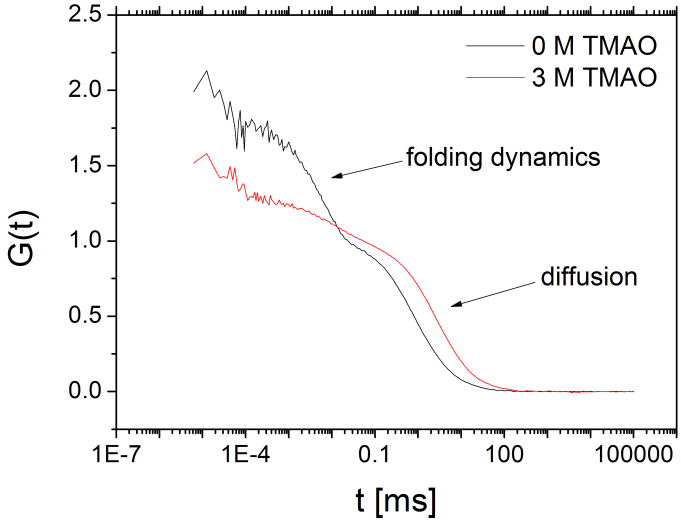

Figure 4.38: This figure shows examples of FCS curves of the TC(R16Q) at a temperature of 20°C and two TMAO concentrations. The arrows indicate the respective typical timescales of the decay.

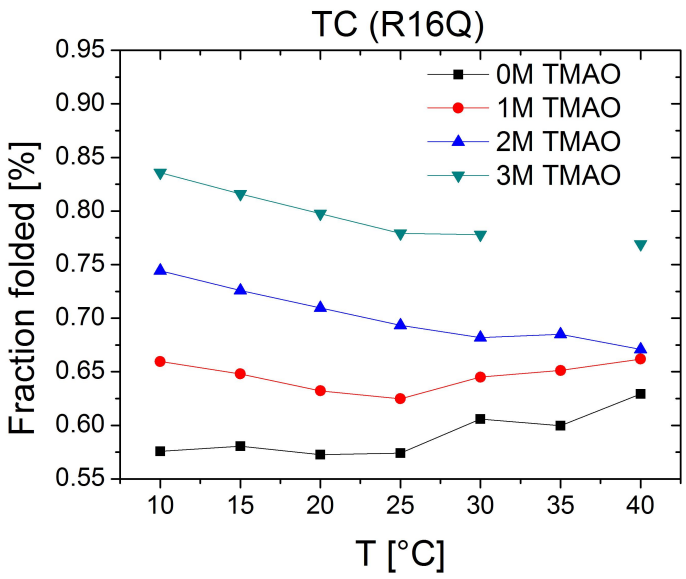

Figure 4.39: The fraction of folded molecules versus the temperature of the TC(R16Q) molecule determined by FCS for different temperatures. From these curves it is possible to determine the melting temperature by a sigmoidal fit.

We now look at the same measurement for the TC in figure (4.40). One can see here that the TMAO clearly stabilizes the TC and rises the fraction of folded molecules significantly close to a value of one for 10°C and 4 M TMAO. This can also be seen in the FCS curves directly as can be seen in figure (4.41). The decay that corresponds to the folding dynamics is significantly influenced by TMAO. In comparison to the TC(R16Q) one can see that at 3 M TMAO the TC(R16Q) is as stable as the not mutated TC, so TMAO is able to fully compensate for the loss of the salt bridge. By looking at the melting temperatures for the TC one gets the following numbers from sigmoidal fits. Without TMAO the melting temperature from this fits is 16°C. In TMAO solutions the melting temperature rises to 39°C, 57°C and 58°C in 1 M, 2 M and 3 M TMAO respectively. This shows that TMAO significantly increases the stability of the TC. Furthermore there seems to be an upper limit for the increase in stability because the melting temperature for 3 M TMAO does not increase that much as from 1 M to 2 M TMAO for example.

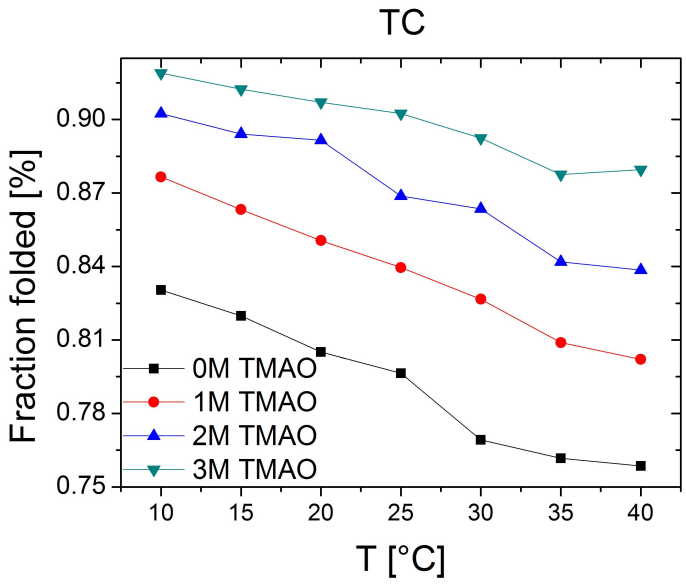

Figure 4.40: This figure shows the fraction of folded molecules of the TC in TMAO at different temperatures measured by FCS. From these curves it is possible to determine the melting temperature by a sigmoidal fit.

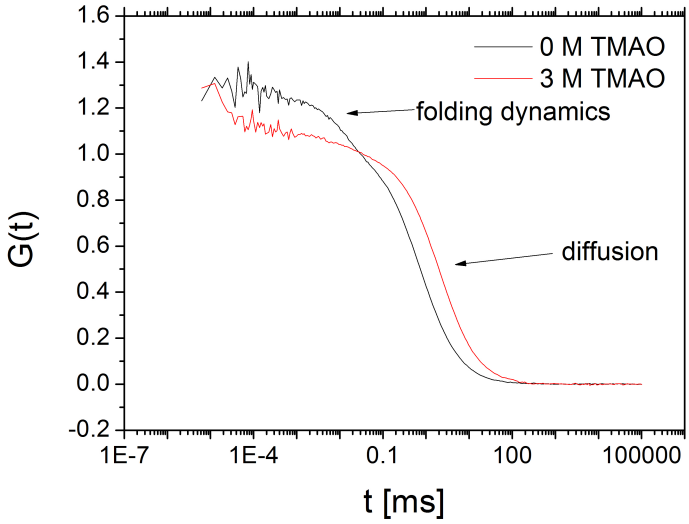

Figure 4.41: This figure shows examples of FCS curves for the TC at a temperature of 20°C and for two concentrations of TMAO. The arrows indicate the respective typical timescales of the decay.

Chapter 5

Conclusions

The topic of this work is to shed light on the initial steps of protein folding and the factors that influence it.
At first we fully characterized the reporter system to see if it introduces artifacts that could be mistaken as signal. Furthermore it has to be shown that the additions, which were made to the solvent, do not interact with the reporter system. As can be seen in sections (3.7) and (4.1) the reporter system is able to do the investigations at hand even in several different additions to the solution like sucrose, TMAO or GdHCl. The measurement still works in a solution with high viscosity or amounts of cosolutes. Additionally, the enhancement of the fluorescence correlation spectroscopy setup with the DPC230 correlation card works well and the antibunching of the dye is now the time limiting factor (see(3.2)). Furthermore we are now able to determine even fast loop closure dynamics of short peptides with good accuracy.
As the loop closure of a peptide is an important step in the protein folding pathway we first looked at the energy landscape of this dynamic process. We investigated the influences of the internal friction on glutamine rich peptides and the energy landscape of the loop closure dynamic. It is assumed that glutamine rich peptides are quite stiff [SL08]. The loop formation is slow compared to fully flexible, unstructured peptides. Additionally it was found that a considerable internal friction contribution is present in these peptides and that the Arrhenius activation enthalpy is high. This could be a hint to the cause of the aggregation of glutaminerich proteins and peptides that is the reason for neurodegenerative

diseases like Huntingtons or Alzheimer's. We could show that our method is able to determine the energy landscape of the loop closure dynamic of peptides (see (4.2)).

An important feature of most proteins are the so called β turns. They enable the protein to adopt the mostly globular form and are the connecting feature of β-strands. Furthermore they are a part of β-hairpins. We investigated Gibbs Free Energy and internal friction of a turn of the immunoglobulin binding protein G from streptococcus and a mutant of it. We found that the native turn structure has a similar Gibbs Free Energy as the glutaminerich peptides and also shows internal friction. The introduction of one point mutation changed the whole picture significantly. These measurements show that turns are important for the protein folding dynamics and are not only some random sequence that connects parts of the protein.

The folding dynamics of the tryptophan cage (TC) miniprotein is not fully understood yet. There are three different theoretical studies that predicted very different influences of the salt bridge of the TC on the stability of it [Zho03] [PNG07] [JB06]. We could show that the salt bridge is important for the stability of the TC with different methods. Additionally it was found that our reporter system does not destabilize the TC significantly (see (4.3)). This makes it possible to utilize our reporter system for studies of small, fast folding proteins.

The last step was to investigate the influence of organic osmolytes on the loop closure dynamic of peptides and the folding of TC. Unstructured fully flexible peptides of Glycine-serine residues are understood well [Buc05] [NLDS07]. It is known, that they do not show an internal friction contribution. We could show, that neither GdHCl as a denaturant nor TMAO as protecting osmolyte influence the fully flexible unstructured peptides besides the change of viscosity of the solvent (see (4.4.1)).

A very interesting investigation was to look at the influence of the protecting osmolyte TMAO on the folding of the TC miniprotein as a model system. Furthermore the comparatively unstable mutant without the salt bridge was investigated in TMAO. We were able to show that TMAO considerably stabilizes the TC and that the melting temperature rises by adding it to the solvent. The mutant without salt bridge shows to be as stable as the normal TC without TMAO

in a solution of 4 M TMAO. This shows that TMAO is able to counter the effects of destabilizing circumstances and how sharks might be able to counter the destabilizing effect of urea with high amounts of TMAO (see (4.4)).
Furthermore we could measure the influence of organic osmolytes on glutaminerich peptides. It is known that they do not influence fully flexible, unstructured peptides. But glutaminerich peptides are considerably stabilized by TMAO (a protecting osmolyte) whereas GdHCl (a denaturant) does not show an influence on the glutaminerich peptides. This might be a hint that glutaminerich peptides might have a sort of secondary structure that is stabilized by TMAO. It also shows that TMAO interacts with the side groups of the peptides and not only with the peptide backbone (see (4.4.2)).

This work shows that the PET-FCS technique presented here is able to investigate the energy landscape of peptides and the influence of osmolytes on the protein folding. Future measurements should focus on the investigation of the influence on a variety of amino acid sequences which promises interesting insights. It might be possible to find peptide structures like hairpins that are influenced by organic osmolytes. A more technical direction of research should go in a direction to further improve the FCS setup. The measurements in this work required a long measurement time. But the setup is not stable enough to support measurements that are longer than several hours. An automation of the setup that allows measurements over days would be beneficial. Furthermore the labeling procedure was complex and required several HPLC runs. This fact has to be considered for further research of these topics.

List of Figures

Bibliography

[ACD09] Toronto ON Canada Advanced Chemistry Developement, Inc. Acd/chemsketch (freeware), version 12.01. www.acdlabs.com, 2009.

[AJH+92] A. Ansari, C. M. Jones, E. R. Henry, J. Hofrichter, and W. A. Eaton. The role of solvent viscosity in the dynamics of protein conformational changes. *Science*, 256(5065):1796–1798, Jun 1992.

[Arr89] S. Arrhenius. *Z. physikalische Chemie*, 4:226, 1889.

[Atk02] P.W. Atkins. *Physikalische Chemie*. Wiley-VCH, 2002.

[BR08] D. Wayne Bolen and George D Rose. Structure and energetics of the hydrogen-bonded backbone in protein folding. *Annu Rev Biochem*, 77:339–362, 2008.

[Buc05] T. Buchner, J.; Kiefhaber. *Protein Folding Handbook*. Wiley-VCH, 2005.

[Can80] P.R.; Freeman Fasman Cantor, C.R.; Schimmel. *Biophysical Chemistry*. 1980.

[CNJ05] Chiranjib Chakraborty, Shyam Nandi, and Snehasis Jana. Prion disease: a deadly disease for protein misfolding. *Curr Pharm Biotechnol*, 6(2):167–177, Apr 2005.

[DNS05] Sören Doose, Hannes Neuweiler, and Markus Sauer. A close look at fluorescence quenching of organic dyes by tryptophan. *Chemphyschem*, 6(11):2277–2285, Nov 2005.

[EMH+00] W. A. Eaton, V. Muñoz, S. J. Hagen, G. S. Jas, L. J. Lapidus, E. R. Henry, and J. Hofrichter. Fast kinetics and mechanisms in protein folding. *Annu Rev Biophys Biomol Struct*, 29:327–359, 2000.

[HA61] E. HABER and C. B. ANFINSEN. Regeneration of enzyme activity by air oxidation of reduced subtilisin-modified ribonuclease. *J Biol Chem*, 236:422–424, Feb 1961.

[Ha01] T. Ha. Single-molecule fluorescence resonance energy transfer. *Methods*, 25(1):78–86, Sep 2001.

[Hag05] L.; Pabit S.A. Hagen, S.J.; Qiu. Diffusional limits to the speed of protein folding: fact or friction? *Journal of Physics: Condensed Matter*, 17:1503 – 1514, 2005.

[Hoo78] J.J. Hood. *Philos. Mag.*, 6:371, 1878.

[Hud01] F.; Gramlich G.; Nau W.M. Hudgins, R.R.; Hunag. A fluorescence-based method for direct measurement of submicrosecond intramolecular contact formation in biopolymers: an exploratory study with polypeptides. *JACS*, 124:556 – 564, 2001.

[JB06] J. Juraszek and P. G. Bolhuis. Sampling the multiple folding mechanisms of trp-cage in explicit solvent. *Proc Natl Acad Sci U S A*, 103(43):15859–15864, Oct 2006.

[KB02] O. Krichevsky and G. Bonnet. Fluorescence correlation spectroscopy: the technique and its applications. *REPORTS ON PROGRESS IN PHYSICS*, 65:251 – 297, 2002.

[KFB+03] Florian Krieger, Beat Fierz, Oliver Bieri, Mario Drewello, and Thomas Kiefhaber. Dynamics of unfolded polypeptide chains as model for the earliest steps in protein folding. *J Mol Biol*, 332(1):265–274, Sep 2003.

[Kli97] D. Klimov, D.K.; Thirumalai. Viscosity dependence of the folding rates of proteins. *Physical Review Letters: condensed Matter*, 1997.

[KLL+04] Achillefs N Kapanidis, Nam Ki Lee, Ted A Laurence, Sören Doose, Emmanuel Margeat, and Shimon Weiss. Fluorescence-aided molecule sorting: analysis of structure and interactions by alternating-laser excitation of single molecules. *Proc Natl Acad Sci U S A*, 101(24):8936–8941, Jun 2004.

[Kra40] H.A. Kramers. Brownian motion in a field of force and the diffuison model of chemical reactions. *Physica VII*, 4:284 – 304, 1940.

[Lak06] J.R. Lakowicz. *Principles Of Fluorescence Spectroscopy*. Springer, 2006.

[LEH00] L. J. Lapidus, W. A. Eaton, and J. Hofrichter. Measuring the rate of intramolecular contact formation in polypeptides. *Proc Natl Acad Sci U S A*, 97(13):7220–7225, Jun 2000.

[lM96] Rudolf Rigler Ülo Mets, Jerker Widengren. Application of the anti-bunching in dye fluoresence: measuring the excitation rates in solution. *Chemical Physics*, 218:191 – 198, 1996.

[Man85] M.C. Manke, C.W.; Williams. Internal viscosity of polymers and the role of solvent resistance. *Macromolecules*, 18:2045 – 2051, 1985.

[Mar93] R.A. Marcus. Elektronentransferreaktionen in der chemie - theorie und experiment (nobel- vortrag). *Angew. Chem.*, 105:1161 – 1172, 1993.

[Men69] R. Menziger, M.; Wolfgang. The meaning and use of the arrhenius activation energy. *Angew. Chem.*, 8:438 – 444, 1969.

[MEW74] D. Magde, E. L. Elson, and W. W. Webb. Fluorescence correlation spectroscopy. ii. an experimental realization. *Biopolymers*, 13(1):29–61, Jan 1974.

[MG08] Anna Marie C Marcelino and Lila M Gierasch. Roles of beta-turns in protein folding: from peptide models to protein engineering. *Biopolymers*, 89(5):380–391, May 2008.

[MKK05] Andreas Möglich, Florian Krieger, and Thomas Kiefhaber. Molecular basis for the effect of urea and guanidinium chloride on the dynamics of unfolded polypeptide chains. *J Mol Biol*, 345(1):153–162, Jan 2005.

[NDS05] Hannes Neuweiler, Sören Doose, and Markus Sauer. A microscopic view of miniprotein folding: enhanced folding efficiency through formation of an intermediate. *Proc Natl Acad Sci U S A*, 102(46):16650–16655, Nov 2005.

[Neu02] H. Neuweiler. *(Synthesis, Spectroscopic Characterization, and Molecular Dynamics Simulation of Fluorescently Labeled Peptides for Single-Molecule Detection of p53 Antibodies).* PhD thesis, Naturwissenschaftlich-Mathematischen Gesamtfakultät der Ruprecht-Karls-Universität Heidelberg, 2002.

[NFA02] Jonathan W Neidigh, R. Matthew Fesinmeyer, and Niels H Andersen. Designing a 20-residue protein. *Nat Struct Biol*, 9(6):425–430, Jun 2002.

[NLDS07] Hannes Neuweiler, Marc Löllmann, Sören Doose, and Markus Sauer. Dynamics of unfolded polypeptide chains in crowded environment studied by fluorescence correlation spectroscopy. *J Mol Biol*, 365(3):856–869, Jan 2007.

[PNG07] Dietmar Paschek, Hugh Nymeyer, and Angel E García. Replica exchange simulation of reversible folding/unfolding of the trp-cage miniprotein in explicit solvent: on the structure and possible role of internal water. *J Struct Biol*, 157(3):524–533, Mar 2007.

[RFBM06] George D Rose, Patrick J Fleming, Jayanth R Banavar, and Amos Maritan. A backbone-based theory of protein folding. *Proc Natl Acad Sci U S A*, 103(45):16623–16633, Nov 2006.

[RK93] Ü. Mets1 J. Widengren Rigler, R and P. Kask. Fluorescence correlation spectroscopy with high count rate and low background: analysis of translational diffusion. *European Biophysics Journal*, 22(3):159, 1993.

[SL08] Vijay R Singh and Lisa J Lapidus. The intrinsic stiffness of polyglutamine peptides. *J Phys Chem B*, 112(42):13172–13176, Oct 2008.

[SSS+99] E. Scherzinger, A. Sittler, K. Schweiger, V. Heiser, R. Lurz, R. Hasenbank, G. P. Bates, H. Lehrach, and E. E. Wanker. Self-assembly of polyglutamine-containing huntingtin fragments into amyloid-like fibrils: implications for huntington's disease pathology. *Proc Natl Acad Sci U S A*, 96(8):4604–4609, Apr 1999.

[Sza80] Schulten K. Schulten Z. Szabo, A. First passage time approach to diffusion controlled reactions. *J. Chem. Phys.*, 72:4350 – 4357, 1980.

[SZO+09] Agnieszka Skwierawska, Wioletta Zmudzi?ska, Stanis?aw O?dziej, Adam Liwo, and Harold A Scheraga. Mechanism of formation of the c-terminal beta-hairpin of the b3 domain of the immunoglobulin binding protein g from streptococcus. ii. interplay of local backbone conformational dynamics and long-range hydrophobic interactions in hairpin formation. *Proteins*, 76(3):637–654, Aug 2009.

[TWV+02] Philip Tinnefeld, Kenneth D Weston, Tom Vosch, Mircea Cotlet, Tanja Weil, Johan Hofkens, Klaus Müllen, Frans C De Schryver, and Markus Sauer. Antibunching in the emission of a single tetrachromophoric dendritic system. *J Am Chem Soc*, 124(48):14310–14311, Dec 2002.

[vH84] J.H. van´t Hoff. Etudes de thermodynamique chemique. *F.Muller and Co.*, 1884.

[Was88] M. R. Wasielewski. "distance dependence of electron transfer reactions" in photoinduced electron transfer part a. *Elsevier*, pages 161 – 208, 1988.

[Wei99] S. Weiss. Fluorescence spectroscopy of single biomolecules. *Science*, 283(5408):1676–1683, Mar 1999.

[Zho03] Ruhong Zhou. Trp-cage: folding free energy landscape in explicit water. *Proc Natl Acad Sci U S A*, 100(23):13280–13285, Nov 2003.

Acknowledgement

I thank all people that helped me to make this work possible and supported me on the path to do so.
I am very grateful to Prof. Dr. Markus Sauer for the opportunity to work in his workgroup and for the interesting subject that I worked on. Many thanks to Dr. Hannes Neuweiler for introducing me to this topic and showing me how its done in the lab. Furthermore I want to thank Dr. Sören Doose for the great support he gave me.
Prof. Dr. Drexhage was of great help by providing us with the dye MR121. Many thanks.
I acknowledge the DFG for paying me.
The working atmosphere in this workgroup was outstanding and I enjoyed it very much every day. Thanks to Dr. Achim Donnermayer, Dr. Ralf Brune, Michael Schwering, Idir Yahiatène and last but not least André Lampe as great bureau partners that taught me a lot and helped me whenever I needed help. Furthermore I want to thank Simon Hennig, Tobias Klamp and Fabian Humpert for a also great comradeship during my time in this workgroup. We laughed a lot. Furthermore I want to thank the guys that went to lunch with me every day. I will miss the soap operas and political discussions very much.
I want to thank all my friends who did a great job in spending my freetime with me.
Finally I want to thank my family for their great support they gave me. Thank you!

”Hiermit erkläre ich an Eides Statt, dass ich die vorliegende Arbeit selbstständig und ohne unerlaubte Hilfsmittel durchgeführt habe.”

Bielefeld, im Mai 2010

Marc Löllmann